Development of a Computer-Controlled Inverted Pendulum

A Thesis Submitted
in Partial Fulfilment of the Requirements
for the Degree of
Master of Technology

by

N. Kasi Reddy

to the

Department of Electrical Engineering
Indian Institute of Technology, Kanpur

APRIL, 1990

Dedicated to

- *My Grand Parents*
- *Mother*
- *Brothers, Krishna and Srinivas*
- *Ravi* and
- *My Teachers*

ACKNOWLEDGEMENTS

I express my deep sense of gratitude and sincere thanks to my Guides Dr A. Ghosh and Dr. R N. Biswas for their excellent guidance and invaluable suggestions without which this work would not have been completed. Thanks once again, to Dr Ghosh for allowing me to use his PERSONAL computer and to Dr R N Biswas for arranging scholarship in the later stages of the work.

I am indebted to Dr. S S. Prabhu, Dr A Joshi and Dr. A K. Mallik for the useful discussions, I had at various stages of this work I would also like to thank Dr K E Hole, Dr Govind Sharma, Dr. A K Raina ,Dr B. Sarkar, Dr. R.N. Biswas and Dr A Ghosh for introducing me to useful courses in my M.Tech program.

I am grateful to the following amiable friends - Hari, Ganesan, Ravindra, Seshadri, Rajpal, Subba Rao, Arun, Dixi, Mathur and **F-Top gang** (A.V., Indrajit Dutt, Gun, Nitin etc.), who shared my feelings on-line and off-line through out my career at I I T.K.

Finally, I shall thank Mr Tiwari, I/C, ACES Work-shop for his extended cooperation in fabricating the experimental set-up.

- Kasi

CERTIFICATE

This is to certify that the work contained in this thesis entitled ***Development of a Computer-Controlled Inverted Pendulum*** has been carried out by Mr N Kasi Reddy under our supervision and that the same has not been submitted elsewhere for a degree

(ARINDAM GHOSH)
Asst Professor

(R.N Biswas)
Professor

Department of Electrical Engineering
Indian Institute of Technology
Kanpur 208 016

ABSTRACT

This thesis discusses the development of a computer-controlled inverted pendulum which automatically balances itself The thesis is divided into two different parts In the first part, the theoretical development of the inverted pendulum, its control and the simulation results are presented Again the DC motor which is used for balancing the pendulum has its own friction which might be detrimental for the balancing system It will be more desirable to compensate for this motor friction In the first part itself, various friction compensation schemes are discussed which also include a proposed self-tuning friction compensator

The second part contains the hardware development and experimantal results of a rail-mounted vehicle-pendulum system The DC motor used for the balancing system is of a separately excited type which has a voltage rating of 240 volts. For driving this high voltage motor, a power amplifier (Four-Quadrant Chopper) is designed and developed The system is interfaced with an IBM compatible PC/XT through which the performance of the proposed controllers are tested.

CONTENTS

Chapter 1	Introduction	1
	1 1 Description of the system of study	4
	1 2 Applications of the Inverted Pendulum model	5
	1 2 1 Source of confidence	5
	1 2 2 Analogy with a launching rocket	6
	1 2 3 In the study of legged machines	7
	1 3 Organization of thesis	12
Chapter 2	Friction compensation of DC Motor	14
	2 1 Mathematical models	14
	2 1.1 Concept of friction compensation	16
	2 1 2 Investigation of friction behavior	18
	2 2 Control design	20
	2 3 Adaptive Friction compensation	21
	2 4 Parameter estimation	23
	2 4 1 Recursive Least Squares Algorithm	23
	2 4 2 Application of RLS algorithm for friction compensation	25
	2 5 Self-Tuning Regulators	26
	2 5 1 Self-Tuning Regulators based on pole-zero placement design	26
	2.6 Self-Tuning Regulator for the friction compensation	30
	2 7 Simulation Results	32
	2 8 Conclusions	34
Chapter 3	Inverted Pendulum model and control	42
	3 1 Mathematical modeling of an Inverted Pendulum	43
	3 2 Design of servo-control system	51
	3 3 Design of the observer	56
	3 4 Digital Computer simulation	57
	3 5 Conclusions	61
Chapter 4	Experimental Set-up	67
	4 1 Experimental setup of the Cart-Pendulum system	67
	4 2 Switching schemes	70
	4.3 Functional Block diagram of the motor-drive circuit	75
	4 4 Chopper and control circuits	78

4 4 1 Chopper circuit 78
4 4 2 Driver circuit 80
4 4 3 Pulse Width Modulator 81
4 4 4 Current Reversing Controller 83
4 4 5 Current Sensor 83
4 4 6 Current Limiting Controller 84
4 4 7 Logic circuit 85
4 4.8 Tacho-generator circuit 85
4 5 Conclusions 85
Chapter 5 Experimental Results and Conclusions 86
5 1 Computer control 86
5 2 Speed control of DC Motor 87
5.3 Control of the Inverted Pendulum 94
5 4 Conclusions and Scope for Future work 99

References 101

Chapter 1
Introduction

It has been the practice of a Control Engineer, or for that matter any engineer, to predict the dynamic behavior of systems not yet built. This is called *dynamic analysis*. To perform this, he imagines and then studies a simple *model* whose behavior will closely match the behavior of the actual system This is because numerous situations arise in which it is virtually impossible to make direct studies on the system under consideration, but where much valuable information can be gained form the study of a model of the system. Here the word *model*, as generally used in scientific work, connotes a miniature replica of a device used for the demonstration of ideas and methods[28] In spite of the diversity of models, every representation of a group of ideas seems to belong to the categories of Direct analogs and Mathematics. These terms are explained below

Direct Analogs: The most direct analogs, are scaled replicas of the systems being modeled. The concept of scale models together with other equivalent or analogous forms of representation has facilitated the performance of many engineering tasks. A typical example is the use of scale models in the study of the effectiveness of dams in controlling the run-off in a watershed area.

Network analyzers are a form of direct analog that is not a scale model. In this type of model, an electrical power system, including generators, transmission lines, and electrical loads, and thus consisting of both lumped-parameter and distributed parameter portions, is represented by means of a collection of lumped resistances, inductances, and capacitances Voltages representing the generators are impressed on the analyzer, and currents and

voltages are measured at other points in the network as they would be measured in the system being studied

It is not necessary to find a replica of every individual element of the original system, but only those which contribute much to the system This can be done if the performance of the original system can be formulated mathematically If such a formulation is possible, the model can reproduce the mathematical operations implicit in the mathematical formulation of the original system, regardless of the actual nature or elements of that system Models formed thus are indirect analogs Their formulation is based on the mathematical similarities existing between the laws governing the performance of many different physical systems. Example of this analogy is illustrated in fig 1.1

The mathematical equations describing the mechanical system shown in fig 1 1(a) can be written as

$$f(t) = M\frac{dv}{dt} + Bv + K\int v\,dt \qquad \text{.....} \qquad 1.0.1$$

where,

f(t) is the force applied between the frame of reference and the mass, M

B is the coefficient of friction

$v(t) = \frac{ds}{dt}$ with s(t) being the position of mass with respect to the reference frame

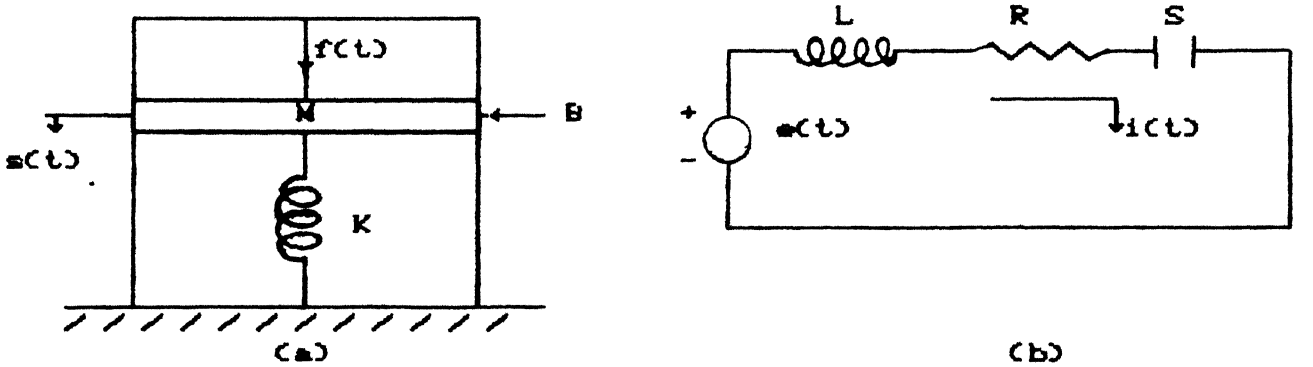

Fig. 1.1. Analogous mechanical and electrical systems

Similarly, the relations describing the electrical system shown in fig 1.1(b) is

$$e(t) = L\frac{di}{dt} + Ri + S\int i\,dt \qquad \ldots\ldots \qquad 1.0.2$$

where,

e(t) is the voltage applied to the network

i(t) is the current flowing in the circuit

L is the inductance

R is the resistance

S is the elastance which is the inverse of capacitance

Comparison of eqns 1.0.1 and 1.0.2 shows that they are identical in form and, consequently, will have identical mathematical solutions. Therefore, if voltage is made analogous to force, current is analogous to velocity, inductance is analogous to mass, resistance is analogous to viscous friction, and elastance is analogous to stiffness. Thus, the simple electrical network shown in fig. 1.1(b) can be used to study the dynamic performance of mechanical system shown in fig. 1.1(a).

Mathematical Models: The model structure that has found the most extensive and celebrated application in scientific and engineering problems is the so called **mathematical model** Here, of course, the person who is to make effective use of mathematical models in the study of systems must be aware of the laws governing the relationships between various process variables and must be able to employ the techniques for the simplification and study of them. Once we have a mathematical model of the system, the next step immediately is to turn our attention to the techniques that we might use to study the model, i.e., study the dynamic behavior of the mathematical model by solving the differential equations. This task, with the present day availability of Digital Computers, has

become much simpler In control engineering studies, any complicated control task is first analyzed using this mathematical model before it is actually implemented To this prototype, we add the neglected features, to realize the actual *physical system*

The work done for this thesis, *"development of computer controlled Inverted Pendulum"*, can be fitted into the category "indirect analog" because this model is used as an idealized system in the study of legged machines, rocket launching problems, and in many other unstable mechanical systems. Some of these aspects are discussed in the following sections The control of inverted pendulum is achieved after selecting an optimum controller by studying it's mathematical model and simulating the same on a digital computer.

1.1 Description of the system of study

The system of study of this thesis is shown in fig 1.2 As far as the study of dynamic machines that balance actively are concerned, the first machines that balanced actively were automatically controlled Inverted Pendulums [27]. Every one knows that a human can balance a broom or stick on his finger with relative ease Why not use automatic control to build a broom that can balance itself? Probably this might have been the motivation behind the person who first built

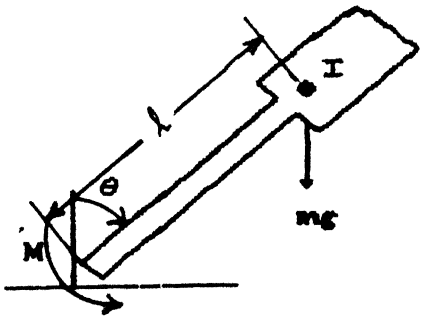

Fig. 1.2. The simple inverted pendulum

this machine What ever might have been the reason, this control system is an excellent tool for studying feedback control system - uncomplicated, yet covers many fundamental aspects of modern control theory.

In the system shown in fig. 1.2, the pendulum is free to fall over about it's pivot axis. The mathematical equations describing this system is given by

$$(ml^2 + I)\ddot{\theta} - mgl\,\mathrm{Sin}\theta = M \qquad \ldots \qquad 1.1.1$$

where,

θ is the angle of the inverted pendulum with the vertical

l is the distance from the pivot point to the center of gravity of mass

I is the moment of intertia of the pendulum about its center of mass

g is the gravitational accelaration

M is the externally applied torque

The control object is to keep the pendulum in the vertical position This can be achieved by manipulating the control torque, M.

1.2 Applications of the inverted pendulum model

In this section "some" of the applications of the inverted pendulum model are discussed.

1.2.1 Source of Confidence.

Does controlling an inverted pendulum act as a source of confidence(!) for a layman of the state space theory? The answer is yes because this system represents a useful laboratory idealization of unstable mechanical systems (or plants) which are encountered by (of course) control engineer from time to time. Many of the state space theory approaches like controller design, observer design (Kalman filter or observer design if some noise is present in the system) etc. can be studied using this system which is inherently unstable.

1.2.2 Analogy with a launching rocket[9]

Designing a stabilizing controller for the inverted pendulum has got good analogy to the design of a controller for launching a rocket

The balancing of a pendulum on top of a finger is possible by moving the finger rapidly in a horizontal plane, thus applying horizontal forces on the lower support. Here one has to notice that in this balancing phenomena our sensory systems like eye, nervous system etc are providing the feed back and the controller (our brain) is sending the control signal. This system now can more practically be interpreted in terms of launching a rocket, which must be balanced on it's own thrust vector by rotating the engine after monitoring its positions, velocity etc using a RADAR (fig 1.3)

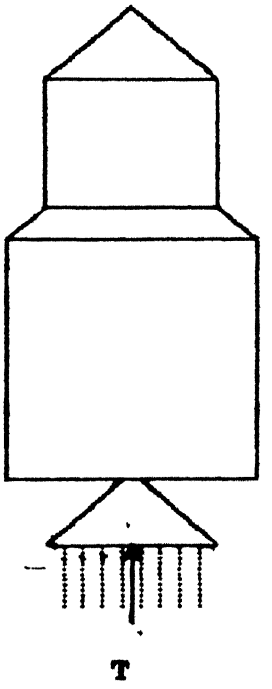

Fig 1.3. Booster vehicle balanced on top of thruster engine

By gimbaling the entire engine assembly (or by "secondary-injection" techniques), the thrust vector T can be given small horizontal components which have the same effect on the rocket as the torque M has on the pendulum system. Therefore, it is possible to develop a system which will be capable of balancing the pendulum, and analogous approaches can be taken to the booster control problem It should be noted that there exists a basic difference between the systems of figs 1.2 and 1.3 The pendulum in fig 1.2 is restricted to perform dynamics in only one vertical plane, where as the rocket may fall (and often does) in any direction However, it can be shown that if attention is limited to small angular deviations, the dynamics in the paper plane or the pitch plane is decoupled from the dynamics in the yaw plane i.e the vertical plane perpendicular to the pitch plane. This means, in effect, that we shall have to find some transformation which will decouple the pitch and yaw dynamics separately As a matter of fact, the constraints on pendulum of fig 1.1 are also removed and studied in literature[21].

1.2.3 In the study of Legged Machines

Legged machines are dynamic machines that **"balance"** themselves actively[27]. The reasons for studying these machines is to understand human and animal locomotion. The interest in understanding biped locomotion, is not only from a desire to build biped robots to perform tasks which are dangerous or degrading to humans, but also to improve prosthetic devices for humans, that have either partially or completely lost lower limb control. The interest in bipeds and other legged locomotion vehicles as alternatives to wheeled and tracked vehicles arises from the recognized mobility advantages of human and animals over rough terrains. The control simplicity and high-speed mobility advantages of wheeled vehicles are lost where smooth level roadways cannot be provided. In fact, the

simple but practical staircase is a recognized curse to wheel chair bound paraplegics If a simple-to-control and highly mobile set of robotic legs can be constructed, the mobility of normal humans could conceivably be provided for paraplegics The present inability to construct highly mobile legged locomotion vehicles stems from the lack of a solid mathematical description of legged locomotion and the result of which is, a deficiency in understanding the associated control problem

The main problems associated with these machines is their balancing and transition from one place to other place These aspects are discussed in the following

Inverted pendulum model for postural control[24]

Mathematical models capable of explaining the observed behavior of man and animals during locomotion and while manipulating objects are not clearly understood. This might be because

(i) Human musculo-skeletal system involves great dynamical complexity.

(ii) Even greatly simplified differential equation models for human motion are highly nonlinear and so are difficult to solve.

(iii) Measurement techniques necessary for testing such models against physical observations have been inadequate.

The simplest possible dynamical model for human motion is one which idealizes the entire body to a single rigid mass. The resulting model because of this simplification is the simple inverted pendulum illustrated in fig 1.4. The analogies of the quantities of this model with humans are as follows.

Torque M, represents the total moment produced at the two ankles of a human subject during quiet standing.

Two forces, F_x and F_y, represent the horizontal and vertical components of ground,

respectively

θ may be thought of as ankle angle (which is the single degree of freedom of this system)

g represents the gravitational accelaration

I moment of inertia of the subject's entire body

M corresponding mass

and

l is the distance from the ankle joint to the center of gravity of this mass

The equations of motion of this model will be similar to 1.1.1. For maintaining erect posture four different sensing modalities are considered and the following feedback law is obtained

$$M = K_1\theta + K_2\dot{\theta} + K_3\dot{\theta}_{sc} + K_4\theta_o \quad \ldots\ldots \quad 1.2.1$$

where,

θ and $\dot{\theta}$ are ankle angle and ankle angle rates as shown (fig 1.4)

θ_{sc} is an approximation to the angular rate information sensed by the semicircular canals

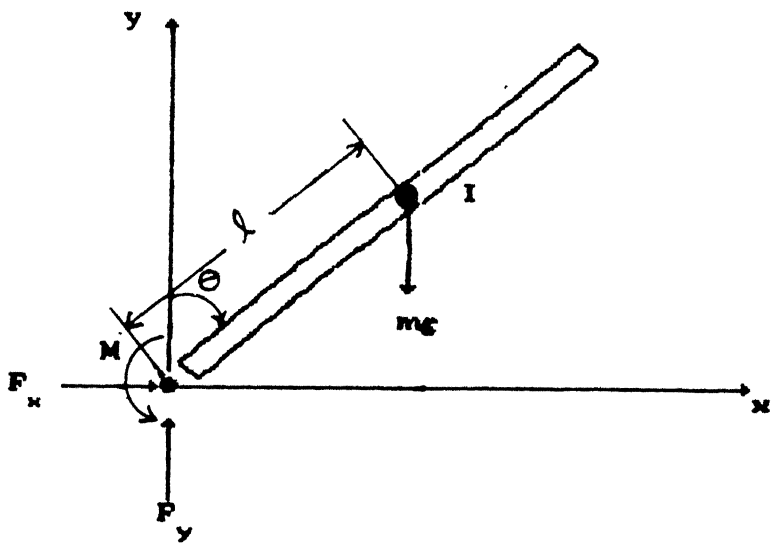

Fig. 1.4. Inverted Pendulum Model for Postural Control

θ_o is the angular position sensed by the otolith system

While a normal human being is able to use all this information (in addition to visual sensing), an individual with sensory impairment may lack some inputs, corresponding to zero coefficients in some of the terms in eqn 1.2.1. Some specific cases corresponding to this are considered in [24] and not discussed here Here our motivation is not to discuss all of this in detail, but to show how a simple inverted pendulum model can account for many of the observed characteristics of body sway during quiet standing.

Aspects of Inverted Pendulum problem for Modeling of Locomotion Systems

The inverted pendulum can be used as one of the simplest models of a biped locomotion systems Locomotion in humans, robots and manipulators consists of periodic motion[19] Problems normally associated with periodic motion are generation, stabilization and trajectory following and changing. These problems are discussed with the help of inverted pendulum as the simplest model of a biped[20].

Practical locomotion controls for bipeds should be capable of producing locomotion gaits of any reasonable stride length and velocity, should be capable of stabilizing these gaits, and further more, should be capable of providing transitions from one periodic trajectory to another [20]. The equation governing the planar motion of a uniped is similar to that of an inverted pendulum of eqn. 1.1.1.

Many important aspects of human locomotion can be investigated through the study of the periodic motion of inverted pendulum, as explained below. Once a cycle of a periodic gait of a biped has been specified, locomotion is then a continuous repetition of that cycle. The cycle corresponds to swinging the body

on one foot, putting down the other foot and swinging the body forward again. Locomotion with the help of inverted pendulum can be imagined if we assume that the inverted pendulum has two arms pivoted at the center of gravity of mass. In the following analysis, these aspects are studied for a single inverted pendulum, the same can be extended to the pendulum which is working in tandem with the former These two motions can be combined properly to study the locomotion. To make the dynamic system stable, state feedback (described in detail in chapter 3) can be utilized The operation of the system can be explained with the help of block diagram shown in fig. 1.5

The input to the simple inverted pendulum is the applied torque, M. Assume that the measurement of θ and $\dot{\theta}$ are available. The torque M now should be able to

(i) stabilize the pendulum and

(ii) Generate periodic motion

This can be achieved if M is of the form

$$M = K_1\theta + K_2\dot{\theta} + G\,\phi(t) \qquad \ldots\ldots \qquad 1.2.2$$

In this equation K_1 and K_2 are feedback gains used to place the poles of the linearized system in appropriate locations in the left half of the complex plane, G is the gain of an amplifier, and $\phi(t)$ is the input periodic signal that the pendulum should ideally track The motion, thus obtained from control law 1.2.2 may be

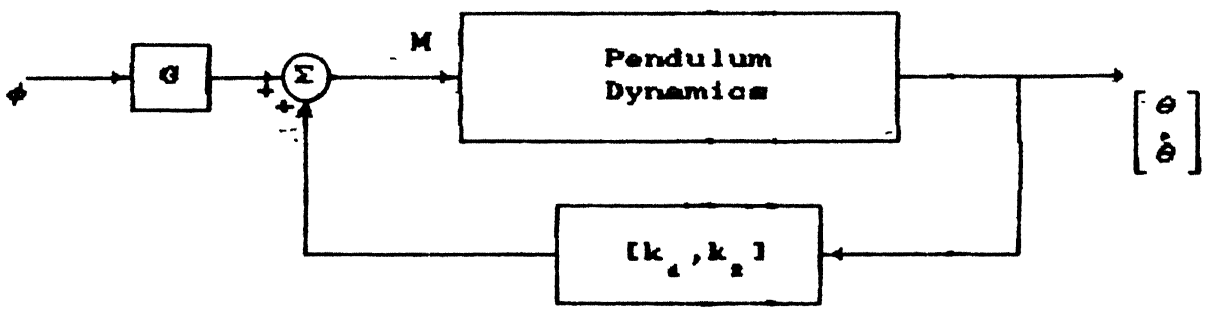

Fig. 1.5. Generation of periodic motion

termed stable mode periodic motion. Another way of achieving the periodic motion is by varying the control torque of eqn 1.1.1 as follows The variation is use the feedback gains to place the system poles on the imaginary axis of the complex plane and eliminate $\phi(t)$ The system will oscillate naturally after initial conditions are applied However, this motion is unstable in the sense of postural stability i.e. with this control postural stability can not be achieved when the system is motionless Note here that we are assuming M is continuously available.

One more way of generating a periodic motion, when the torque M is not available continuously is described in [20] This method assumes that the torque is available intermittently. These pulses must be applied periodically and must have sufficient strength to reverse the direction of motion of the pendulum mass. Such pulses may be analogous to thrusting of braking torque generated at the ankle of a biped during the foot liftoff or foot touchdown respectively. The concepts like trajectory stabilization and transition controls are studied in [20] and are not considered here

1.3 Organization of thesis

In this section we give an outline of the main contents of the chapters that follow.

The performance of high-quality servos used in robots and systems for tracking and pointing, which are largely described by linear models, is often limited by nonlinear phenomena such as friction and backlash. The possibilities of improving the performance of a servo by nonlinear compensation is discussed in chapter 2. Various friction models are also reviewed and controllers are described for variations of inertia and load torque. simulation results are also presented at the end of the chapter to show the performance of proposed controllers.

In chapter 3, the control of Inverted Pendulum is studied Mathematical models capable of explaining the observed behavior of man and higher animals during locomotion and while manipulating objects involve great complexity In this chapter some mathematical techniques are presented to provide some knowledge regarding the complex mathematical models for studying the dynamics and control. Important concepts like controller design, observer design etc. are also treated in the same Chapter. Finally, choosing an optimal controller is illustrated with the help of simulation results.

Chapter 4 is concerned with the implementation issues - development of cart-pendulum system and designing a driver for this system Controlling of an Inverted Pendulum requires a servo motor with quick respose and enough torquing capacity For driving high power motors a special hardware is required. These issues are dealt in Chapter 4.

The proposed ideas have been tested experimentally on the developed system. In chapter 5, results of some experiments are presented. Some conclusions and suggestions for further work are also given at the end of the chapter.

Chapter 2
Friction Compensation of DC Motor

In precision servos, which are used in robots and many sophisticated applications, Friction which is always present, to some degree, causes difficulties, gives rise to poor performance, and may even be a source of stabilization errors The better the quality of the servo the less is the friction For poorer quality motors it may be advisable to compensate for the friction Unfortunately, however, this friction is not directly measurable Thus to compensate for the friction an observer has to be designed which adaptively adjusts this friction into agreement with the actual friction behavior by processing inputs from conventional system sensors Measurements from these sensors cause on-line adjustment of model parameters, resulting in "adaptive" compensator action. This model's output is used to generate an addition to conventional stabilization subsystem commands The resulting additional motor torque is equal and opposed to the actual friction disturbance such that the residual torque, and hence stabilization errors, are a small fraction of those for an uncompensated system The model-referenced compensator thus operates in a predictive, adaptive, feedforward manner to pre-condition the stabilization subsystem, reducing the stabilization errors well below the levels which are achievable through conventional feedback operation alone

2.1 Mathematical Models

If a load is attached to the output shaft of a Direct Current Motor, then the torque developed at the motor shaft is equal to the sum of the torques dissipated by the motor and its load. That is,

$$\begin{bmatrix}\text{Torque From}\\ \text{motor}\\ \text{shaft}\end{bmatrix} = \begin{bmatrix}\text{Torque on}\\ \text{Motor}\end{bmatrix} + \begin{bmatrix}\text{Torque on load referred}\\ \text{to the}\\ \text{Motor shaft}\end{bmatrix} \quad \ldots 2.1.1$$

or, in equation form

$$T = J\frac{d\omega}{dt} + T_L \quad \ldots\ldots 2.1.2$$

where,

ω is the speed of the motor shaft in rad/sec

J is the total moment of inertia of the motor-load system referred to the motor shaft in $kg\text{-}m^2$

The load torque, T_L, can be further divided into the following components.

a) Friction Torque T_f : The friction will be present at the motor shaft and also in various parts of the load This friction torque is the equivalent value of various friction Torques referred to the motor shaft and is discussed in detail in the subsequent sections

b) Windage Torque T_W : When the motor runs, the wind generates a torque opposing the motion of the shaft This is known as windage torque.

c) Mechanical Torque T_m : This is the torque required to do useful mechanical work and depends on the type of the load connected to the motor shaft.

For a separately excited or permanent magnet motor, the field will be constant and the torque developed at the motor shaft, T, can be assumed to be proportional to the armature current, I_a i.e.,

$$T = K_a I_a \quad \ldots\ldots\ldots 2.1.3$$

where K_a is the current constant.

From the above discussion, with all the components, the eqn. 2.1.2 is modified in the form,

$$K_a I_a = T_f + T_W + T_m + J\frac{d\omega}{dt} \quad \ldots\ldots 2.1.4$$

Since in this chapter our main concentration is to do the friction compensation we shall not, intentionally, apply any load to the motor or in other words make $T_l = 0$ in the above equation Thus the eqn 2 1 4 reduces to

$$K_a I_a = T_f + T_W + J\frac{d\omega}{dt} \quad \ldots \quad 2\,1\,5$$

The windage torque T_W, which is proportional to the speed squared, is given by

$$T_W = c\omega^2$$

where c is a constant

In many applications this torque can be neglected and with this approximation, the eqn 2 1 5 can further be reduced to

$$K_a I_a = T_f + J\frac{d\omega}{dt} \quad \ldots \quad 2.1.6$$

This is the basic equation which is used for friction compensation presented in this chapter

2.1.1. Concept of friction compensation

As mentioned before, to overcome the errors due to the friction present it is essential to have the detailed knowledge about the friction behavior. The effects of the friction can be reduced by mounting torque sensors, which measure the friction levels, on the motor shaft and substituting in eqn. 2.1.6. Eqn. 2.1.6 is, however, nonlinear and a linear feedback cannot be used in a straight forward manner. To facilitate this, a linearized model of eqn. 2.1.6 is obtained. This is illustrated in fig 2.1.

The equation of the motor from eqn. 2.1.6 is given by

$$J\frac{d\omega}{dt} = K_a I_a - T_f \quad \ldots\ldots \quad 2.1.7$$

$$= K_a\left(I_a - \frac{T_f}{K_a}\right)$$

The above equation now suggests that if we introduce a new control variable, u, given by

$$u = I_a - \frac{T_f}{K_a} \quad \ldots . \quad 2.1.8$$

it can be reduced to

$$J\frac{d\omega}{dt} = K_a u(t) \qquad \ldots\ldots \qquad 2.1.9$$

Therefore, the system now obtained does not contain any friction terms, and thus the motor can be said to be friction less. Hence, the feedback given by eqn 2.1.8 can be called **friction compensation** It is clear, now, from 2.1.8, that to make the motor frictionless, one has to estimate the process variable T_f and system parameter K_a The control with the estimated variables is given by

$$u = I_a - \frac{\hat{T}_f}{\hat{K}_a} \qquad \ldots\ldots \qquad 2.1.10$$

where $\hat{T}_f$ is an estimate function of T_f and $\hat{K}_a$ is an estimate of the current constant K_a

The parameter k_a is the torque constant of the motor whose value can be found from the catalogues This can also be measured The other variable, namely Friction Torque, has to be estimated by some scheme.

The idea of measuring this torque, although it gives better results than by measuring it indirectly, by placing some torque sensors would be difficult because of the mounting problems involved in the process. In many applications where a motor is used as an actuator there would be transducers which are used to measure the variables like position, velocity etc., So it would be a good idea if we

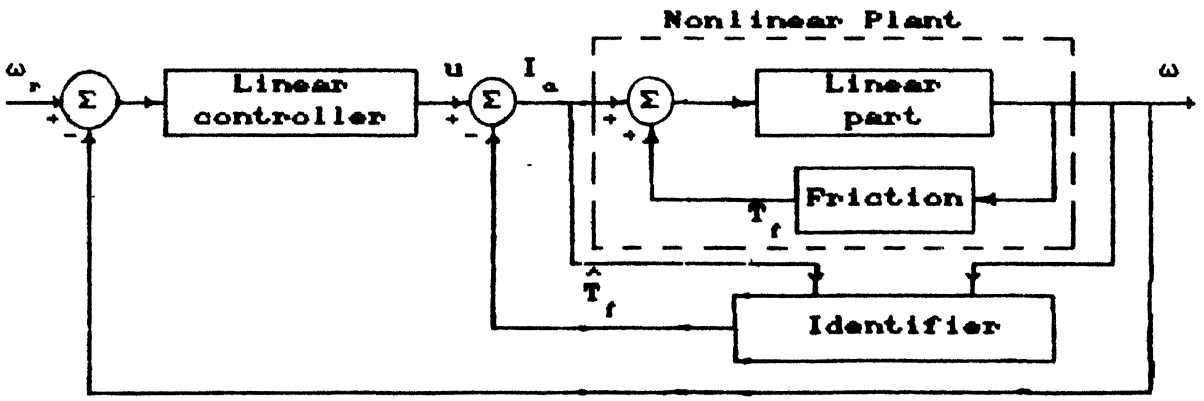

Fig 2.1. Block diagram of motor controller with adaptive friction compensation

make use of these measurements Once we get the velocity measurement we can make an estimation of the friction torque by knowing the relation between these two variables So, essentially, the estimation of torque depends on the shape of the function relating ω to T_f

2.1.2. *Investigation of Friction Behavior*

The detailed knowledge of friction behavior is necessary to achieve accurate real-time model This is particularly true concerning the transient behavior of friction caused by relative motion during polarity reversals of the motor-load system This polarity reversal is a frequent occur nce in the stabilization of an Inverted Pendulum

Characterization of friction by the classical *'Coulomb/stiction'* model has proven to be especially lacking in this regard[33] Fig.2.2(a) shows this friction characteristic

A different friction behaviour, presented in fig. 2.2(b) has been experimentally verified by Walrath [33]. There, the model was based on studies of a stabilized platform with ball bearings on the gimbals This friction behavior can be modeled by the following differential equation,

$$T_f(t) + a\frac{dT_f}{dt} = b\ \mathrm{sgn}(\omega) \qquad \ldots\ldots \qquad 2.1.11$$

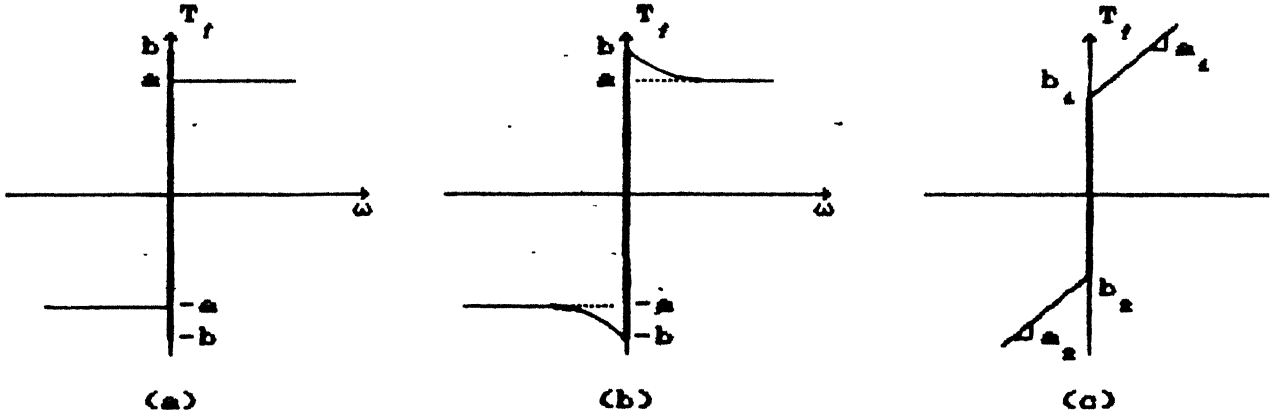

Fig 2.2. Different friction models

where,

b is the constant rolling friction Torque in N-m,

a is the exponential time constant in sec, which can be varied experimentally

$$sgn(w) = \begin{cases} 1 \text{ if } \omega > 0 \\ -1 \text{ if } \omega < 0 \end{cases}$$

But in [2], the authors have pointed that this model introduced additional dynamics and does not consider the breakaway friction or stiction characteristics The same authors have suggested another kind of friction model, which is shown in fig 2.2(c) This can be modeled by the equation,

$$T_f = \begin{cases} a_1\omega + b_1 & \text{if } \omega > 0 \\ a_2\omega + b_2 & \text{if } \omega < 0 \end{cases} \quad \ldots\ldots \quad 2.1.12$$

In our experiments we have used the functions of the form eqn 2.1.12 This simple model makes it possible to deal with variations and asymmetries of the friction torque which are not included in other two models.

In our experiments we have adjusted the parameters a_1, b_1, a_2, and b_2 to make the motor frictionless. But all these experiments revealed that these parameters are not constant and vary with time and various other factors like e.g., temperature, coupling of the load to the motor shaft etc., This motivates us to make the friction compensation adaptive. Once the system is linearized in the form of eqn. 2.1 9, one can always use the conventional controller design techniques for closed loop system stabilization.

The above discussion is based on the assumption that K_a is a constant and can be experimentally determined. If it is experimentally determined, the chances are that it might not give a proper value. In the next section it will be shown that the parameters identified depends on the Intertia also. The technique presented cannot take variations in inertia and other type of loads into account. In such a case also the adaptive compensation will result in a better performcance. This

would, however, introduce additional burden in the form of computations required for parameter estimation, and measurement of some more process variables like armature current This, infact, has motivated us to control the closed loop system using a **Self Tuning controller**, which is discussed in detail in the later stages of this Chapter

2.2 Control Design

In this section, a current controller design is presented which assumes that a perfect friction compensation is made The nonlinear plant, after linearization is given by eqn 2.1.9 Once the plant is linear, we can always make use of the design tools, which are already available for the design of the closed loop controller.

For this kind of a system, a simple Proportional plus Integral (PI) controller, which is unquestionably the most common controller in industry, can be used. The control law of a PI controller is given by

$$u(t) = K_p e(t) + \frac{1}{T_i}\int_0^t e(\tau)\, d\tau \qquad \ldots\ldots \qquad 2.2.1$$

where,

e(t) is the error between the reference signal ω_r and the output speed ω, i.e ,

$$e(t) = \omega_r(t) - \omega(t) \qquad \ldots\ldots \qquad 2.2.2$$

K_p is the proportional gain and T_i is the integral time constant which is assumed to be the inverse of integral gain.

The controller given by eqn. 2.2.1 for the system described by 2.1.9 will give a closed loop transfer function of the form,

$$\frac{\omega(s)}{\omega_r(s)} = G(s) = \frac{\omega_0^2}{s^2 + 2\zeta\omega_0 s + \omega_0^2} \qquad \ldots\ldots \qquad 2.2.3$$

where,

$\omega(s)$ and $\omega_r(s)$ are the Laplace Transforms of $\omega(t)$ and $\omega_r(t)$, respectively.In the above equation, the damping ratio (ζ) and natural undamped frequency (ω_0) are

given by

$$\zeta = \frac{K_a K_p}{2\omega_0 J} \quad \ldots\ldots \quad 2.2.4$$

and

$$\omega_0^2 = \frac{JT_i}{K_a} \quad \ldots\ldots \quad 2.2.5$$

These two quantities can be prespecified to obtain the desired closed-loop performance and based on the specification, we can compute the constants, K_p and T_i from eqns 2.2 4 and 2.2.5

For digital computer application, the control law needs to be discretized Using the rectangular rule integral of eqn 2.2 1 can be approximated as

$$\int_0^t e(\tau)\, d\tau = \sum_{i=0}^{k} e(i)\, h \quad \ldots\ldots \quad 2.2.6$$

where h is the sampling period and k is the sample number
Thus, the control law in the descretized form can be written as

$$u(k) = K_p e(k) + \frac{1}{T_i} \sum_{i=0}^{k} e(i)\, h \quad \ldots\ldots \quad 2.2.7$$

where,

$$e(i) = \omega_r(i) - \omega(i)$$

To compute control law from eqn. 2.2.7, we need to store the previous values of error, e, and this will cause severe memory and time limitation. It is more desirable to obtain u(k) through recursive computation This can easily be derived from eqn. 2.2.7 and is given as

$$u(k) = u(k-1) + (K_p + \frac{h}{T_i})(\omega_r(k) - \omega(k-1)) - K_p(\omega(k-1) - \omega(k-1)) \quad \ldots\ldots \quad 2.2.8$$

This is called Velocity Algorithm.

2.3 Adaptive Friction Compensation

In the previous sections we have discussed different friction models and the necessity to add a conventional feedback to evaluate the effectiveness of the friction compensation. In a typical servo application the moment of inertia and the current constant K_a may be treated as known parameters. To perform the friction compensation it is necessary to obtain the estimates of the friction torque

functions T_f. If we take the torque function given by eqn. 2.1.12 this problem reduces to estimation of the parameters a_i, b_i, i=1,2

Discretizing eqn 2.1.7 using rectangular rule, we obtain

$$\omega(k+1) = \omega(k) + \frac{h}{J}(K_a I_a(k) - a_i\omega(k) - b_i) \quad \ldots\ldots \quad 2.3.1$$

This approximation retains the number of parameters of the physical model. Many other alternatives such as zero-order hold model or tusting's rule etc., exist and can be chosen appropriately depending on the size of actual sampling period.

The subscript i can be eliminated from eqn 2.3.1 by introducing the following equation

$$\omega(k+1) = \omega(k) + \frac{h}{J}[K_a I_a(k) - m(k)(a_1\omega(k) + b_1) - (1-m(k))(a_2\omega(k)+b_2)] \quad 2.3.2$$

where

$$m(k) = \begin{cases} 1 & \text{if } \omega(k) > 0 \\ -1 & \text{if } \omega(k) < 0 \end{cases} \quad \ldots\ldots \quad 2.3.3$$

Eqn 2.3.2 then can be rewritten in a more compact form as

$$\omega(k+1) = A(q^{-1})\omega(k) + B(q^{-1})I_a(k) + g(k) \quad \ldots\ldots \quad 2.3.4$$

with

$$g(k) = m(k)g_1(k) + (1-m(k))g_2(k) \quad \ldots\ldots \quad 2.3.5$$

$$g_1(k) = \alpha_1\omega(k) + \beta_1 \quad \ldots\ldots \quad 2.3.6$$

$$g_2(k) = \alpha_2\omega(k) + \beta_2 \quad \ldots\ldots \quad 2.3.7$$

For our example model the values of the polynomials $A(q^{-1})$, $B(q^{-1})$, α_i, and β_i are

$$A(q^{-1}) = 1 \quad \ldots\ldots \quad 2.3.8$$

$$B(q^{-1}) = \frac{hK_a}{J} \quad \ldots\ldots \quad 2.3.9$$

$$\alpha_i = -\frac{ha_i}{J} \quad \ldots\ldots \quad 2.3.10$$

$$\beta_i = -\frac{hb_i}{J} \quad \ldots\ldots \quad 2.3.11$$

for i = 1,2.

By the arguments of section 2.2 the nonlinear model 2.3.4 can be linearized if the following control law is applied

$$u(k) = l_s(k) + \frac{g(k)}{B} \quad \ldots\ldots \quad 2.3.12$$

Applying the above control law in the process model 2.3.4, we obtain

$$\omega(k+1) = A(q^{-1})\omega(k) + B(q^{-1})u(k) \quad \ldots\ldots \quad 2.3.13$$

$$(1-A(q^{-1})q^{-1})\omega(k) = q^{-1}B(q^{-1})u(k) \quad \ldots\ldots \quad 2.3.14$$

$$\tilde{A}(q^{-1})w(k) = q^{-1}B(q^{-1})u(k) \quad \ldots\ldots \quad 2.3.15$$

with

$$\tilde{A}(q^{-1}) = 1 - A(q^{-1})q^{-1} \quad \ldots\ldots \quad 2.3.16$$

For this model, now, the control law given in section 2.2 can be applied to get the prescribed closed loop system performance

2.4 Parameter estimation:

For this thesis, a Recursive Leasts Squares parameter identification technique is used. This is discussed briefly below.

2.4.1 *Recursive Least Squares (RLS) Algorithm*[13]

To explain the RLS algorithm consider the process model given by

$$F(q^{-1})y(k) = q^{-n}G(q^{-1})u(k) \quad \ldots\ldots \quad 2.4.1$$

which can be represented explicitly by

$$y(k) + f_1y(k-1) + \ldots + f_{n_f}y(k-n_f) = g_0u(k-n) + g_1u(k-n-1) + \ldots + g_{n_g}u(k-n-n_g) \quad \ldots\ldots \quad 2.4.2$$

Now if we define the column vectors

$$\psi_k = [\,-y(k-1) \ldots\ldots -y(k-n_f)\ u(k-n) \ldots\ldots\ldots u(k-n-n_g)\,]^T \quad \ldots\ldots \quad 2.4.3$$

$$\theta = [\,f_1\ f_2 \ldots f_{n_f}\ g_0\ g_1 \ldots g_{n_g}\,]^T \quad \ldots\ldots \quad 2.4.4$$

the above model can be written as

$$y(k) = \psi_k^T\theta = \theta^T\psi_k \quad \ldots\ldots \quad 2.4.5$$

The vectors ψ_k and θ are usually known as regression vector and parameter

vectors, respectively. If we introduce a vector of parameter estimates

$$\hat{\theta} = [\ \hat{f}_1\ \hat{f}_2\ ..\ \hat{f}_{nf}\ \hat{g}_0\ \hat{g}_1\ ...\ \hat{g}_{ng}]^T \quad . \qquad 2.4.6$$

the output of the estimator is

$$\hat{y}(k) = \psi_k^T\hat{\theta} = \hat{\theta}^T\psi_k \quad ... \qquad 2.4.7$$

In Least squares algorithm the aim is to minimize a cost which is given by

$$J = \sum_0^n \varepsilon^2(k)$$

where

$$\varepsilon(k) = y(k) - \hat{y}(k) \quad .... \qquad 2.4.8$$

Minimizing this criterion, the following relationships for the estimation of parameters can be obtained

$$\left.\begin{aligned} \hat{\theta}_k &= \hat{\theta}_{k-1} + L_k\,[\ y(k) - \psi_k^T\hat{\theta}_{k-1}\ ] \\ L_k &= \frac{P_{k-1}\psi_k}{1 + \psi_k^T P_{k-1}\psi_k} \\ P_k &= P_{k-1} - L_k\psi_k^T P_{k-1} \end{aligned}\right\} \quad .... \qquad 2.4.9$$

The convergence of this algorithm depends on various factors. But critical are the initial values of the Covariance Matrix P_k and the initial parameters of the predictor Usually if some prior information about the process is available then one can use this data itself as the initial values for the Predictor. The covariance matrix in such a case is usually started with

$$P_0 = \frac{cov[\hat{\theta}_0]}{E[y_k^2]} \quad ..... \qquad 2.4.10$$

where $\hat{\theta}_0$ is the initial vector of the parameters for the adaptive predictor and $E[y_k^2]$ is the output variance. Square-root algorithms are useful if the problem is poorly conditioned. Fast algorithms can be used if computing time is crucial.

2.4.2. *Application of RLS algorithm for friction compensation*

The process model, for the DC motor with friction, from eqn 2.3.4 is given by

$$\omega(k+1) = A(q^{-1})\omega(k) + B(q^{-1})u(k) + g(k) \quad .. \quad 2.4.11$$

Since it is assumed that the parameters K_a and J are constant, an "efficient adaptive predictor model" then can be chosen as

$$\omega(k+1) = A(q^{-1})\omega(k) + B(q^{-1})u(k) + m(k)(\hat{\alpha}_1\omega(k)+\hat{\beta}_1) + (1-m(k))(\hat{\alpha}_2\omega(k)+\hat{\beta}_2) \quad .... \quad 2.4.12$$

The regression and parameter vectors for this model are

$$\hat{\psi}_k = [\ -m(k)\omega(k)\ -m(k)\ -(1-m(k))\omega(k)\ -(1-m(k))\ ]^T \quad .. \quad 2.4.13$$

$$\hat{\theta} = [\ \hat{\alpha}_1\ \hat{\beta}_1\ \ \hat{\alpha}_2\ \hat{\beta}_2\ ]^T \quad .. \quad 2.4.14$$

Now the parameter vector $\hat{\theta}$ can be updated using the RLS algorithm which is just stated above and the control can be computed from

$$I_a(k) = u(k) - \frac{\hat{g}(k)}{B(q^{-1})} \quad .. \quad 2.4.15$$

where

$$\hat{g}(k) = m(k)(\hat{\alpha}_1\omega(k) + \hat{\beta}_1) + (1 - m(k))(\hat{\alpha}_2\omega(k) + \hat{\beta}_2) \quad .. \quad 2.4.16$$

and u(k) is computed from the law given by eqn 2.2.10.

Before completing the discussion on adaptive friction compensation we can formulate the complete procedure used for this compensation, as follows.

step1: Take the measurement of the speed ω(k) of the motor.

step2: Update the parameters of the friction model 2.1.12 using the RLS algorithm given by the set of eqns. 2.2.7.

step3. Compute the control law from the eqn. 2.4.15.

This completes the discussion of the adaptive friction compensation. All these algorithms are verified by simulation. The results are described later in this chapter.

2.5 Self-Tuning Regulators

So far, in designing the controller we have assumed that the constants K_a and J are known and does not change with time. But in practice, this may not be true and may keep on changing with the operating conditions For example, in eqn 2.1.6 the parameter J is the total moment of inertia referred to the motor shaft whose constituents are the inertia of the motor as well as that of all external loads In many cases it may not be possible to obtain the exact measurement of inertia of all external loads The second cause is the change in the Torque constant K_a. This variation may be due to its dependability on the relative oscillation of the rotor and stator at high frequencies (ripple_torque)[2]. In the case of shunt motors, this may also change due to the fluctuations in the power supply voltage level, as K_a depends on the flux produced in the motor's field windings All these factors motivated us to use a self tuning regulator.

2.5.1 *Self tuning regulators based on pole-placement Design*[1]

A Self Tuning Regulator (STR) is based on the certainity equivalence principle of the adaptive control theory. If the plant parameters are poorly known a joint identifier and control scheme can be employed. In STRs design a control is coimputed assuming that the identified system parameters are true parameters The first STR which was proposed was based on minimum variance control theory which places all the closed-loop poles in the origin. This might not always be desirable as this could cause an excessive control magnitude. To avoid this problem, STRs based on pole-placement design have been discussed by many authors. A block diagram of a general STR is shown in fig. 2.3.

Problem formulation and Design procedure

Consider the process described by

$$G(q^{-1}) = \frac{q^{-n}B(q^{-1})}{A(q^{-1})} \qquad \ldots\ldots \qquad 2.5\,1$$

Assume that $n \geq 1$, A is monic and A and B are relatively coprime

It is desired to find a controller such that the closed loop is stable and that the transfer function from the reference signal u_c to the output is given by

$$G_m(q^{-1}) = \frac{q^{-n}B_m(q^{-1})}{A_m(q^{-1})} \qquad \ldots\ldots \qquad 2.5\,2$$

where A_m and B_m are coprime and A_m is monic

A general linear regulator can be described by

$$R(q^{-1})u(k) = T(q^{-1})u_c(k) - S(q^{-1})y(k) \qquad \ldots\ldots \qquad 2.5.3$$

here q^{-1} is the delay operator

The closed-loop transfer function relating y to u_c, with the control law 2.5.3 is given by

$$\frac{q^{-n}T(q^{-1})B(q^{-1})}{A(q^{-1})R(q^{-1}) + q^{-1}B(q^{-1})S(q^{-1})} = \frac{q^{-n}B_m(q^{-1})}{A_m(q^{-1})} \qquad \ldots\ldots \qquad 2.5.4$$

The design problem is thus equivalent to the algebraic problem of finding polynomials R, S and T such that the above equation holds. It follows from the

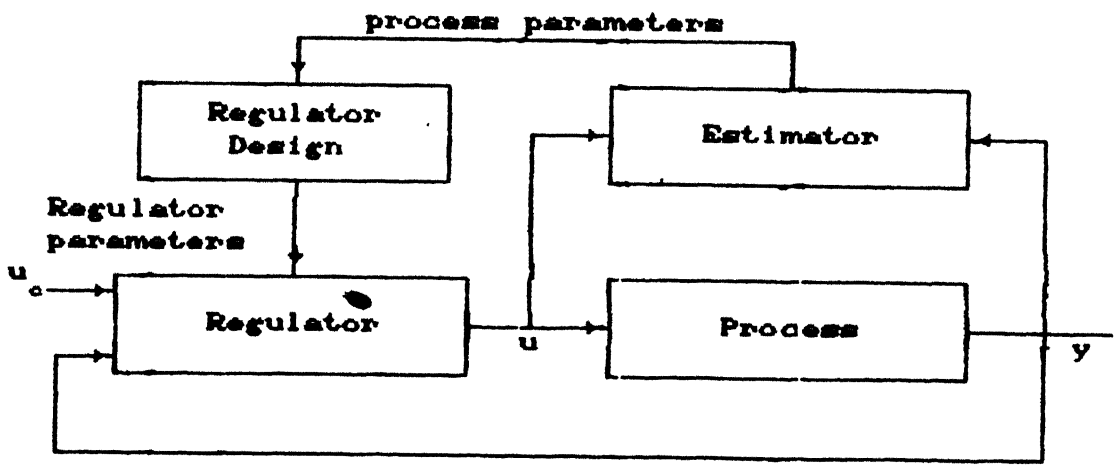

Fig. 2.3. Block diagram of a self-tuning regulator

above equation that factors of B which are not also factors of B_m must be factors of R. Since factors of B correspond to open-loop zeros it means that the open-loop zeros which are not the desired closed-loop zeros must be canceled

Factor B as $$B = B^+B^- \quad \ldots\ldots \quad 2.5.5$$

where all the zeros of B^+ are in the restricted stability region and all zeros of B^- are outside this region[1] Therefore, a necessary condition for solvability of the servo problem is that the specifications be such that

$$B_m = B_{m_1}B^- \quad \ldots \quad 2.5.6$$

A block diagram of the closed-loop system is shown if fig. 2.4 The design method is as follows

Given the process described by

$$A(q^{-1})y(k) = q^{-n}B(q^{-1})u(k) \quad \ldots \quad 2.5.7$$

and the prescribed closed loop performance described by

$$A_m(q^{-1})y(k) = q^{-n}B_m(q^{-1})u(k) \quad \ldots \quad 2.5.8$$

under the assumptions demanded by the eqns. 2.5.3 - 2.5.6.

step1 solve the equation

$$A(q^{-1})R_1(q^{-1}) + q^{-n}B^-(q^{-1})S(q^{-1}) = A_m(q^{-1}) \quad \ldots\ldots \quad 2.5.9$$

to get the polynomials $R_1(q^{-1})$ and $S(q^{-1})$.

step2 . The regulator which gives the desired closed loop response is given by eqn. 2.5.3, with

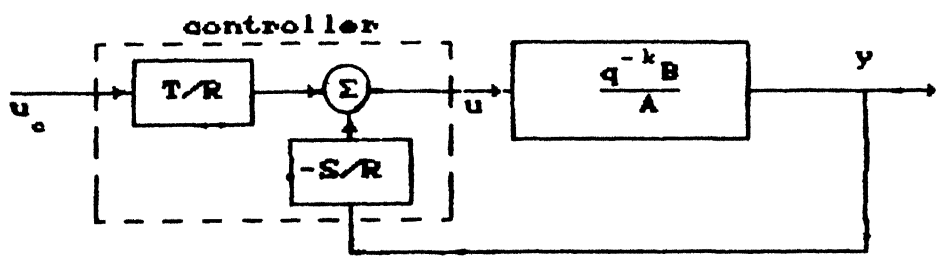

Fig 2.4 Block diagram of closed-loop system

$$R = R_1 B^+ \quad \ldots\ldots \quad 2.5.10$$

and $$T = B_{m_1}. \quad \ldots\ldots \quad 2.5.11$$

eqn 2.5.9 can always be solved for R_1 and S under the assumptions of Coprimeness between the polynomials A and B To perform the design, it is necessary to have procedures for decomposing the polynomial B into its factors B^+ and B^-, and for solving the linear polynomial in eqn 2.5.9. The decomposition is essentially a spectral factorization problem This can be solved by using Gauss's elimination or by using Euclid's Algorithm[3] In the adaptive algorithms, these calculations have to be performed in each step of the iteration, so the computation time will be more However, there are some special cases, where in one can simplify the calculations[1].

The Self-Tuning Regulator given in requires simple calculations and is explained below The basic idea is to rewrite the process model in such a way that the design step is trivial For minimum variance control, the process model can be rewritten so that the parameters of the minimum variance regulator are the parameters of the new model This procedure is said to be the **implicit identification** of a process model.

eqn. 2.5.9 gives

$$A_m(q^{-1})y(k) = A(q^{-1})R_1(q^{-1})y(k) + q^{-n}B^-(q^{-1})S(q^{-1})y(k) \quad \ldots\ldots \quad 2.5.12$$

Combination of this with 2.5.7 gives

$$A_m(q^{-1})y(k) = q^{-n}B^-(R(q^{-k})u(k) + S(q^{-k})y(k)) \quad \ldots\ldots \quad 2.5.13$$

If the control signal is chosen such that

$$Ru(k) = Tu_c(k) - sy(k)$$

where,

$T = B_{m_1}$ then we get the required closed loop transfer function. The algorithm can further be reduced to the following if all the process zeros are canceled or B^- is a constant. The algorithm can now be formalized by the

following

Deterministic direct Self-Tuning Algorithm:

Given the closed loop transfer function in the form of polynomial $A_m(q^{-1})$ with zeros in the restricted stability region and

$$B_{m_1} = K = A_m(1) \quad \ldots \quad 2.5.14$$

step1 Estimate the coefficients of the polynomials S, R and T in the model of

$$A_m(q^{-1})y(k) = q^{-n}B^{-}(R(q^{-1})u(k) + S(q^{-1})y(k)) \quad \ldots\ldots \quad 2.5.15$$

using the recursive estimation method

step2 Calculate the control signal from

$$Ru(k) = Tu_c(k) - sy(k) \quad \ldots \quad 2.5.16$$

step3 Repeat steps 1 and 2 at each sampling period

The properties of this algorithm are discussed extensively in [1] . With this introduction about Self-Tuning Regulators we are now ready to apply the algorithm for the friction compensation

2.6 Self-Tuning Regulator for the friction compensation

The idea of compensation using Self-Tuning Regulators is shown in fig. 2.5. The linearized model of the process, from eqn. 2.3.15, is

$$\omega(k+1) = A(q^{-1})\omega(k) + B(q^{-1})u(k) \quad \ldots\ldots \quad 2.6.1$$

with the control law u(k) given by

$$I_s(k) = u(k) - \frac{\hat{g}(k)}{B(q^{-1})} \quad \ldots\ldots \quad 2.6.2$$

$$= u(k) + \frac{1}{B}(m(k)\hat{\alpha}_1\omega(k) + \hat{\beta}_1) + (1-m(k))(\hat{\alpha}_2\omega(k) + \hat{\beta}_2))$$

Choose the regulator polynomials as

$$R(q^{-1}) = r_0 \quad \ldots\ldots \quad 2.6.3$$

$$S(q^{-1}) = s_0 + s_1q^{-1} \quad \ldots\ldots \quad 2.6.4$$

Now we can readily apply the procedure explained above.

Step1, therefore, now is to identify the parameters of the model,

$$A_m(q^{-1})y(k) = q^{-1}B^{-}(R(q^{-1})u(k) + S(q^{-1})y(k) \quad \ldots \quad 2.6.5$$

that is,

$$\omega(k) = [f(1)\omega(k-1) + f(2)\omega(k-2) + f(3)I_a(k-1) + m(k)(f(4)\omega(k-1) + f(5)) + (1-m(k))(f(6)\omega(k-1) + f(7))] \quad 2.6.6$$

with

$$A_m(q^{-1}) = 1 + a_{m_1}q^{-1} + a_{m_2}q^{-2}$$

$$f(1) = s_0 - a_{m_1}$$

$$f(2) = s_1 - a_{m_2}$$

$$f(3) = r_0$$

$$f(4) = \frac{r_0\hat{a}_1}{B}$$

$$f(5) = \frac{r_0\hat{b}_1}{B}$$

$$f(6) = \frac{r_0\hat{a}_2}{B}$$

$$f(7) = \frac{r_0\hat{b}_2}{B}$$

From the above set of equations, it is straight forward to obtain the parameters of the regulator as well as the parameters of the friction model.

Step2, is compute the control law from

$$Ru(k) = T\omega_r(k) - S\omega(k)$$

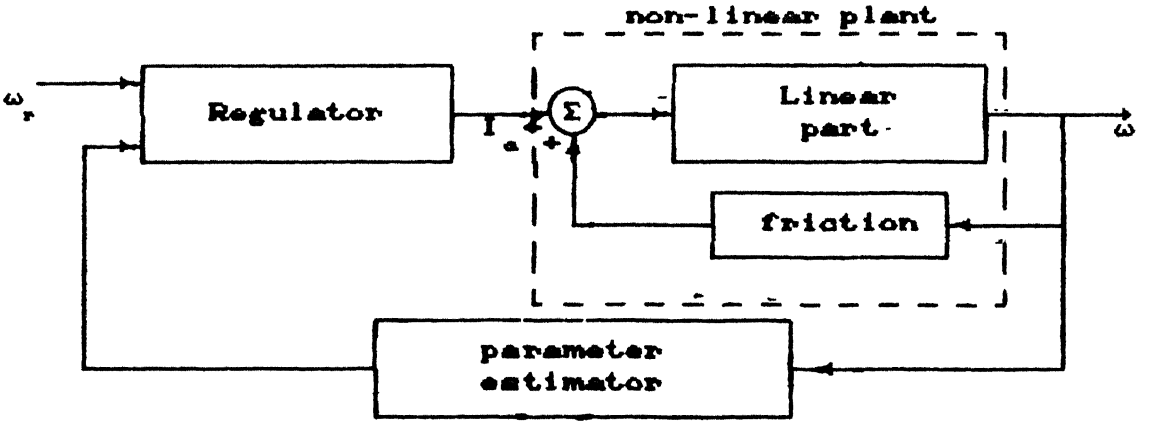

Fig. 2.5. Adaptive friction compensation using Self-Tuning Regulator

and

$$I_a(k) = u(k) + \frac{\hat{g}(k)}{B}$$

Polynomial T from eqn 2.5.14 is given by

$$T = A_m(1) = 1 + a_{m_1} + a_{m_2}$$

With this we come to the end on the discussion of friction compensation using Self-Tuning Regulator The results are described in the next section

2.7 Simulation Results

In this section we are going to describe the simulation results obtained using all the proposed controllers and merits and demerits of each are also discussed

In order to evaluate the performance of the proposed "adaptive Friction Compensators" it is essential to study how the system behaves with the conventional controller alone The parameters of the DC motor-load system used in simulation are listed in Table 2 1

Table. 2 1 Parameters used in simulations

Parameter		value
Current Constant	K_a	0.9508
Inertia	J	0.0014
Damping Constant	ζ	0.7109
natural frequency	ω_0	11.9760
Friction torque parameters		
	a_1	0.0114
	b_1	0.1000
	a_2	0.0150
	b_2	-0.1400
Sampling period	h	0.0300

Performance of three controllers, including the two controllers discussed in the above sections and a conventional PI Controller, is evaluated. This is done just to elucidate the merits and demerits of the controllers that were discussed In these experiments the control goal is to make the closed-loop system transfer function as

$$G_m(s) = \frac{51.63}{s^2+10.22s+51.63} \qquad \ldots\ldots \qquad 27.1$$

or, its counterpart in the discrete form,

$$G_m(q^{-1}) = \frac{0.1q^{-1}}{q^{-2}-1.5q^{-1}+0.6} \qquad \ldots\ldots \qquad 27.2$$

All the three controllers were tested for a total time of 350 samples The control was bounded to lie in the range [-0.8,0.8] amperes. This is chosen so, keeping the maximum current carrying capacity of the DC motor used in the experiments in mind. In all the experiments a command signal, $\omega_r(k)$, in the range [-10,10] rad/sec is used.

The first test shown in fig. 2.6(a) had as its control law the PI regulator descibed in section 2.2

As can be seen, the steady state error is going to zero, due to the integral action. The PI regulator performance is rather poor when there is a step change in the command signal. Figs. 2.6(b) and 2.6(c) shows the responses of the PI regulator with "non-adaptive" friction compensation. Here, these plots show, how the performance of the PI controller is improved if we introduce the compensation control. In these plots, although there is a difference in the parameters that are estimated, the process output is much better and smoother than that observed without this action. Here, the motor speed is changed smoothly during the transition from one direction to the other. Though, there are some more drawbacks in these controllers, atleast they give us the concept of friction compensation.

Figs 2.7(a) and 2.7(b) show results using PI regulator, now, with Adaptive Compensation In fig 2.7(a) it is assumed that the torque constant K_a and the inertia are constants and does not change with operating conditions This figure shows clearly that there is a substantial improvement in the dynamic response of the system with adaptive friction compensation The response is good already in the second transient Coming to the case when there is a change in the perameters K_a and J_a, one can see from fig 2.7(b) that there is certain degradation in the performance This clearly is due to the drawback of the Constant gain regulator used in the closed-loop system Figs 2.8(a) and 2.8(b) show the variation of the friction parameters with time. It can be easily be observed that when there are no changes in torque constant and load inertia, the parameters have converged within 1.5 seconds. On the otherhand, when there are changes in K_a and J the parameter convergence is very poor

From fig 2.9 we can see that the Self-Tuner has considerably better performance than a "Constant Gain Adaptive Compensator", in these circumstances This figure shows clearly that the Self-Tuner can easily cope with the parameter variations Finally, fig. 2.10 shows the variation of parameters with respect to time.

2.8 Conclusions

This chapter has described the approaches taken to the friction compensation of the DC-motor under various operating conditions and the simulation results of some algorithms. Different ways to estimate the parameters of the coefficients of the friction model have also been studied. The adaptive friction compensators have been found to superior as the friction depends on the operating conditions. It is seen that under conditions, where there is no variation in load inertia and current constant a friction compensator with

constant gain regulator is sufficient

In all these studies, it has been assumed that friction model considered is adequate The availability of a friction model with appropriate structure is crucial for the better performance of the adaptive friction compensation The simulation results obtained in this chapter will be compared with the experimental ones in chapter 5

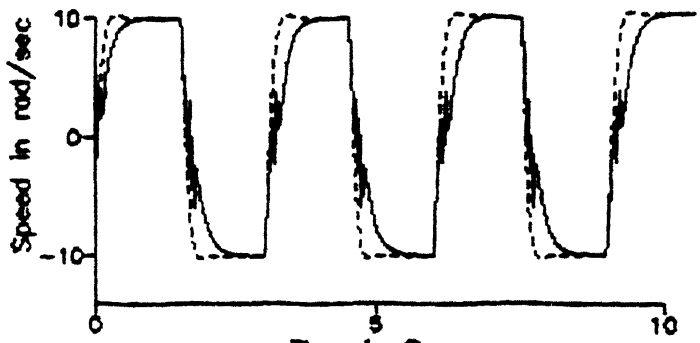

(a) no friction compensation

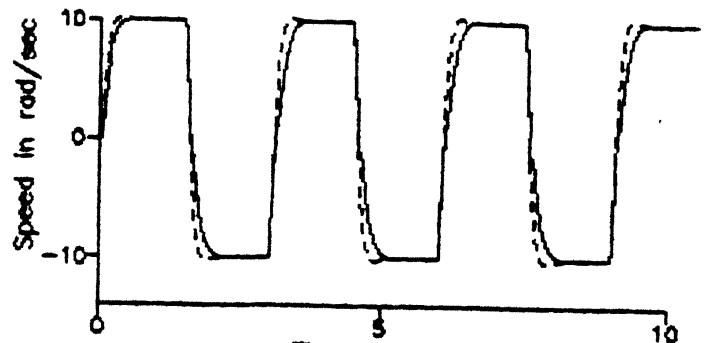

(b) compensation with under estimation of levels

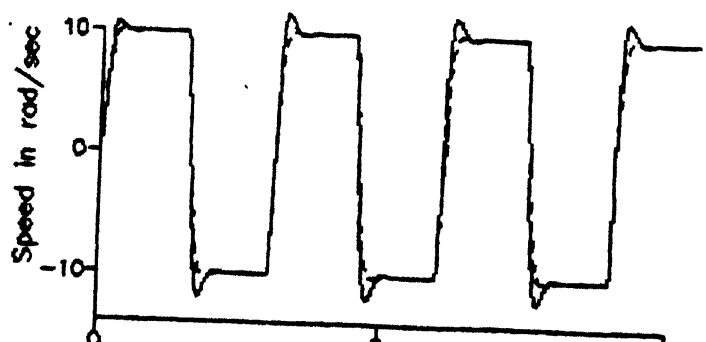

(c) Compenation with over estimation of levels

Fig 2.6. PI REGULATOR WITH NON-ADAPTIVE FRICTION COMPENSATION

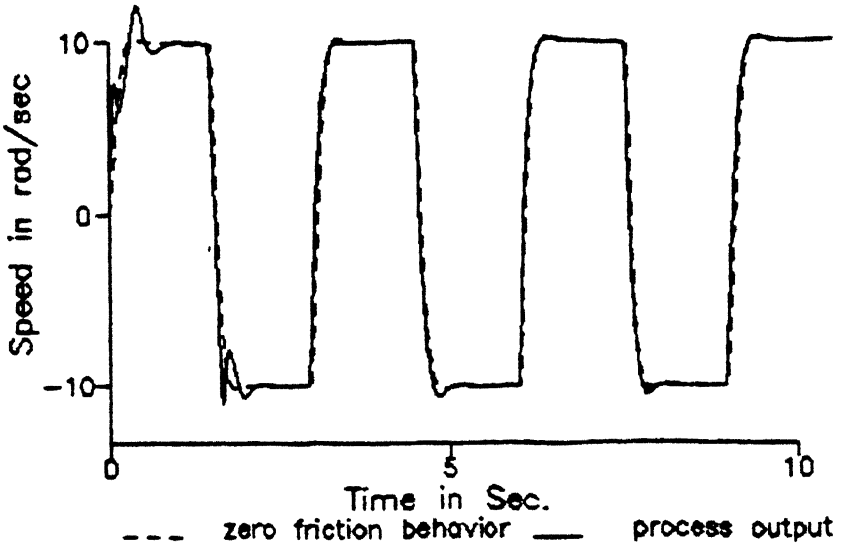

(a) compensation without any change in inertia and K_a

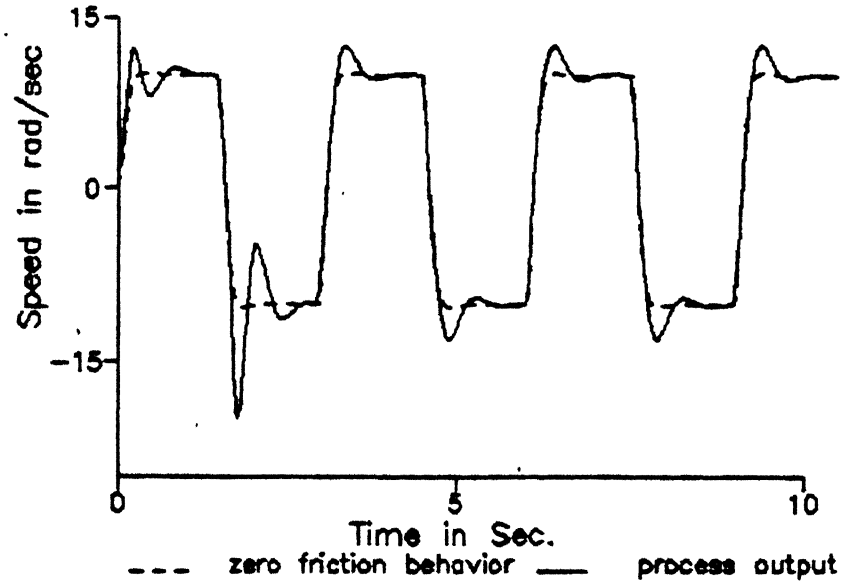

(b) compensation with changes in inertia and K_a

Fig 2.7 ADAPTIVE FRICTION COMPENSATION WITH PI-REGULATOR

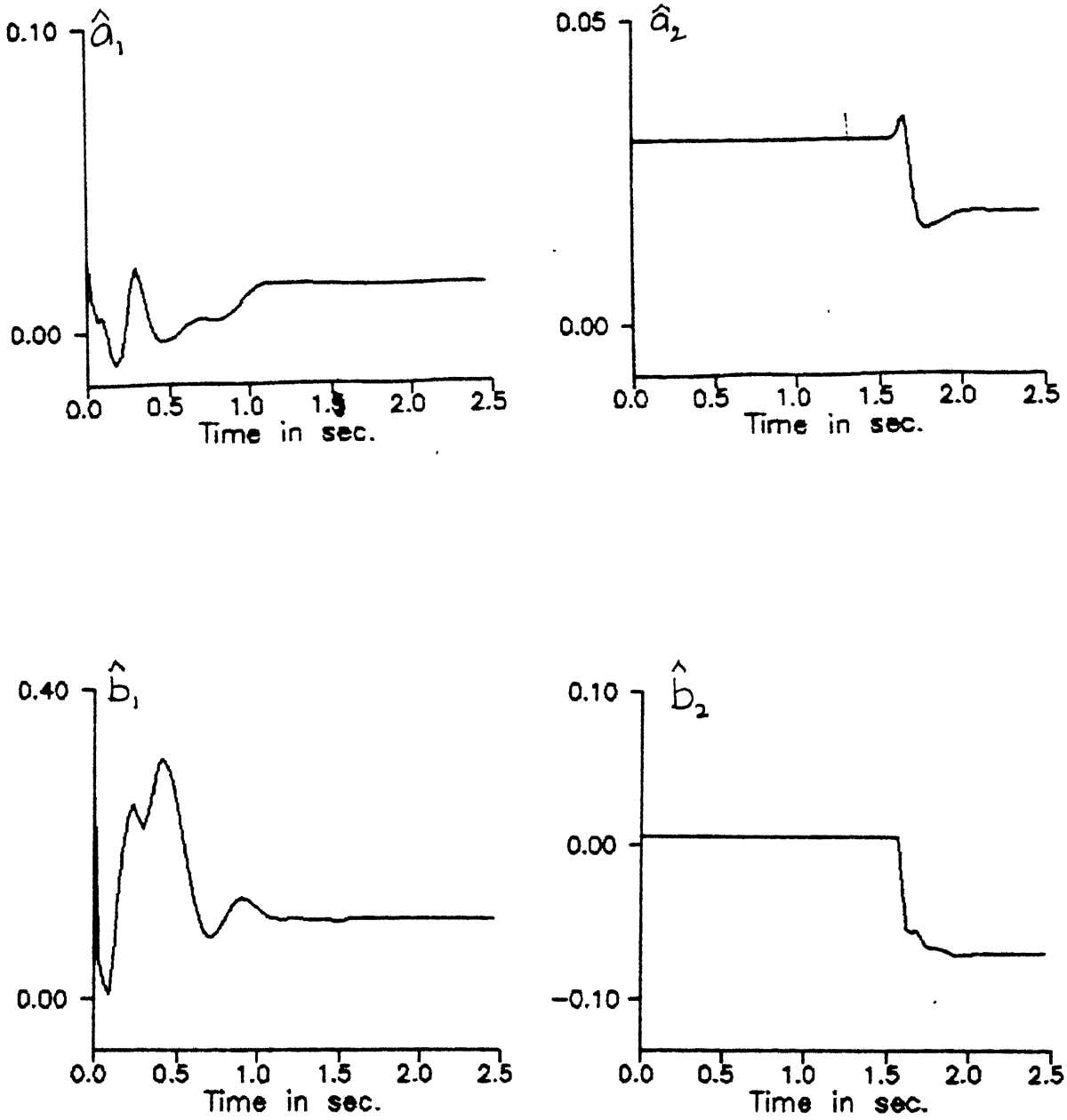

Fig 2.8 (a) TIME HISTORY OF PARAMETERS WITH CONSTANT GAIN REGULATOR WHEN THERE IS NO CHANGE IN INERTIA AND K_a

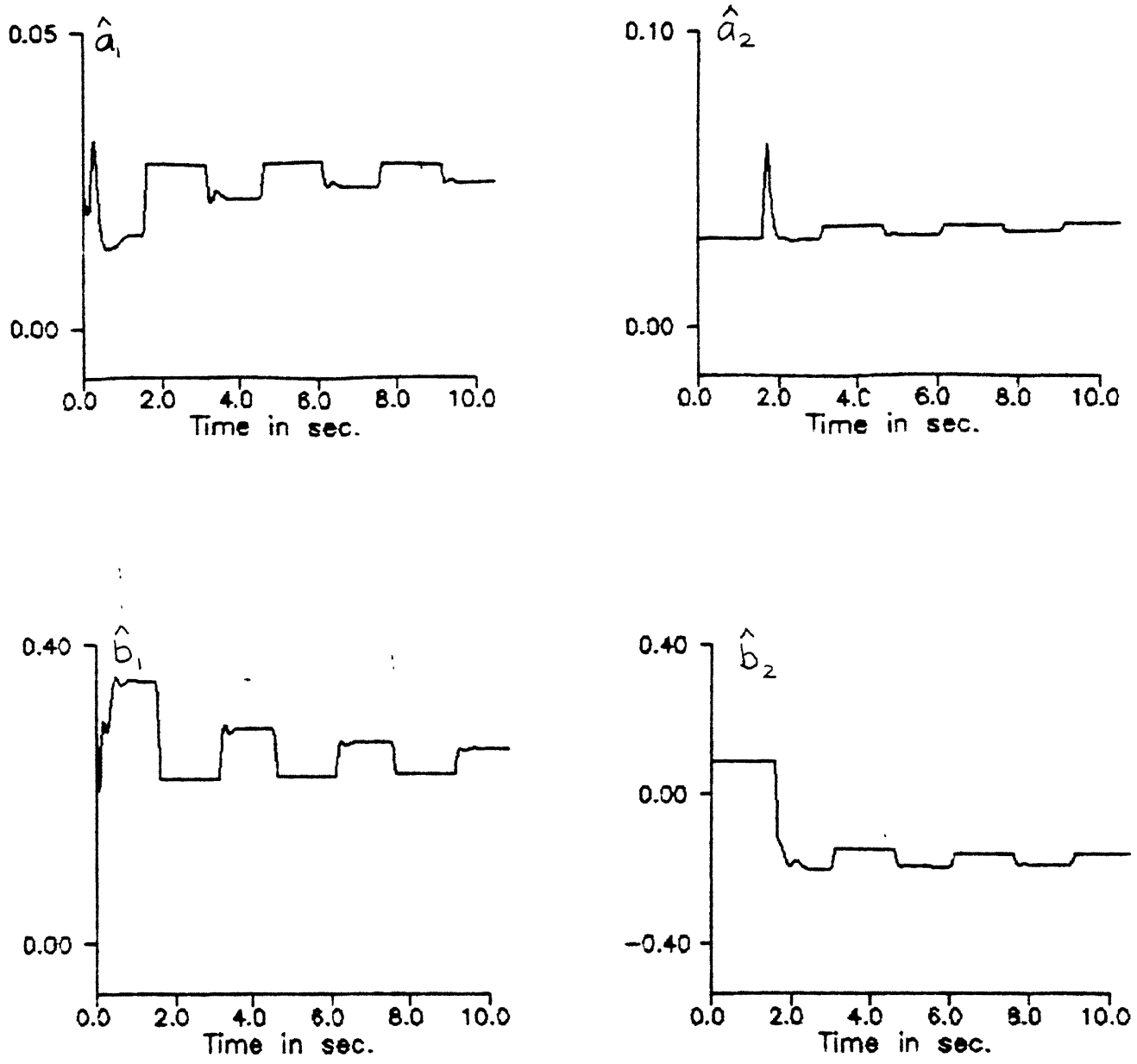

Fig. 2.8 (b) TIME HISTORY OF PARAMETERS WITH CONSTANT GAIN REGULATOR WHEN THERE IS CHANGE IN INERTIA AND K_a

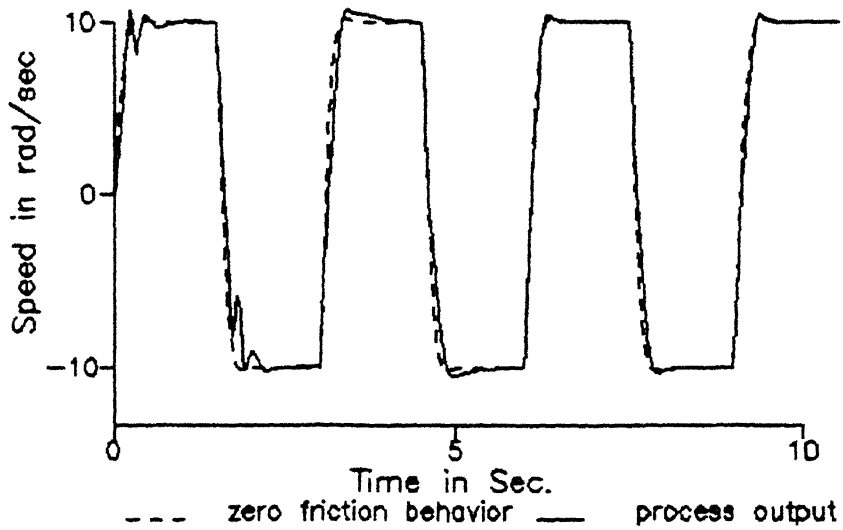

Fig.2.9. Adaptive friction compensation using Self-Tuner

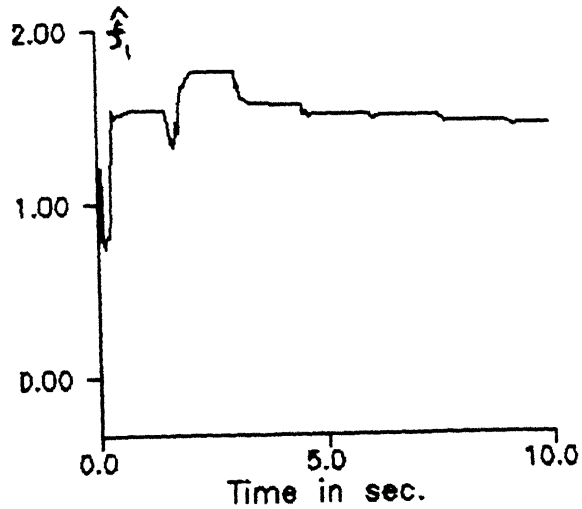

Fig 2.10 TIME HISTORY OF PARAMETERS WITH SELF-TUNER (CONTD.)

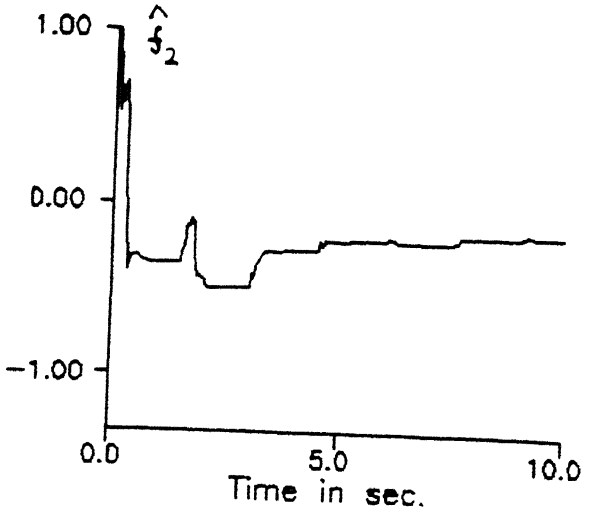

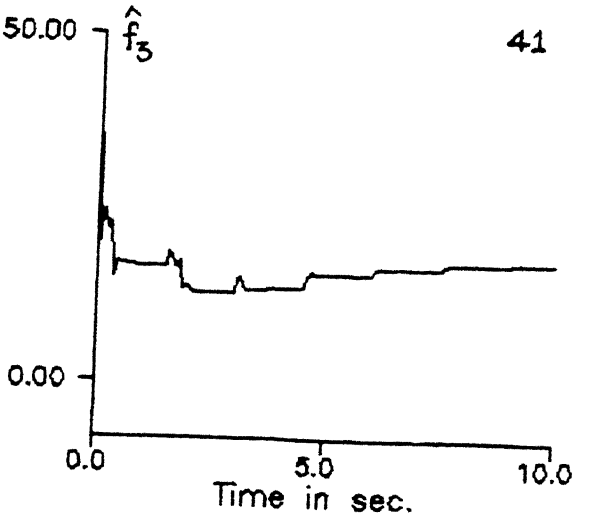

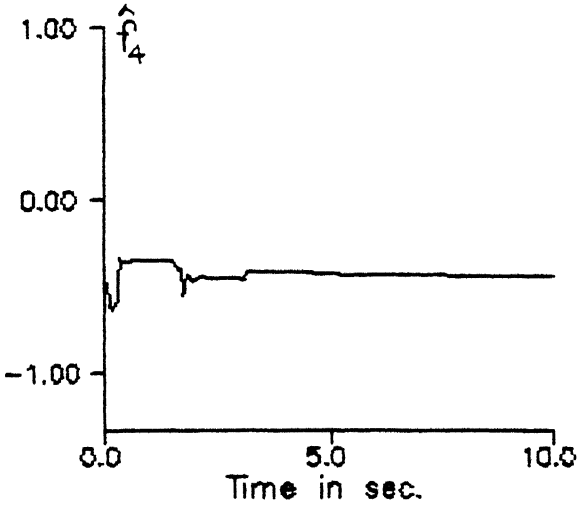

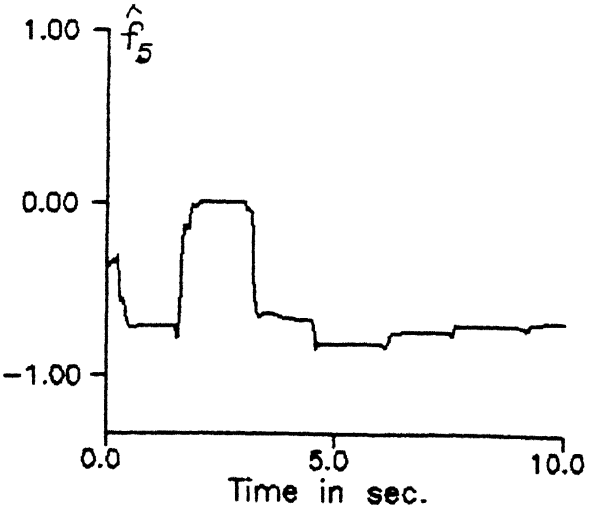

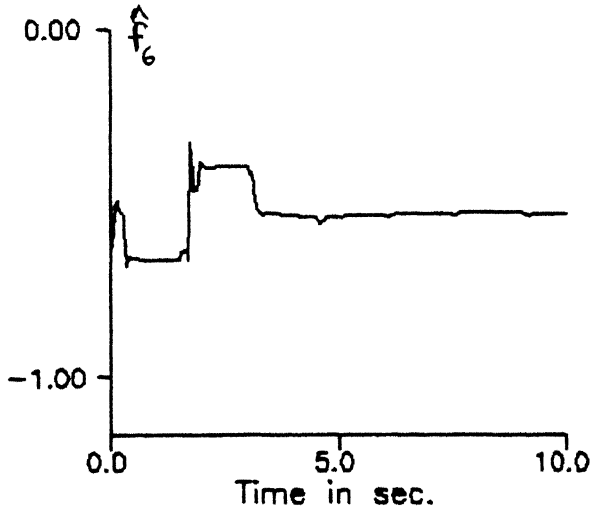

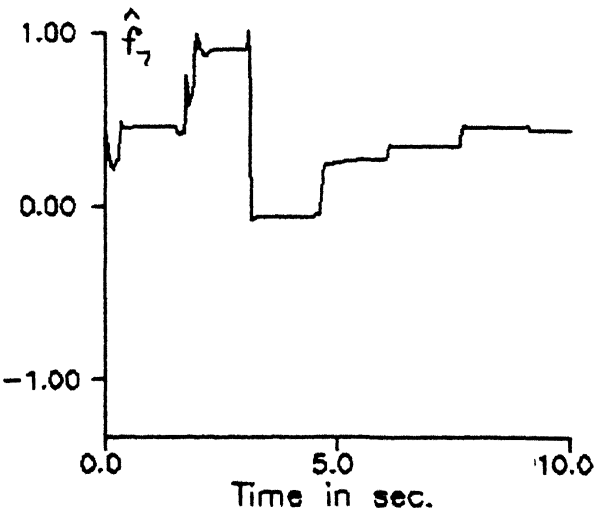

Fig. 2.10 TIME HISTORY OF PARAMETERS WITH SELF-TUNER

Chapter 3
Inverted Pendulum Model and Control

In this chapter mathematical modeling of the Inverted Pendulum and its dynamic behavior are discussed Devising adequate mathematical description of complex physical systems is in general a highly subjective and often an iterative task It requires a large measure of intuition, i e , an ability to determine which physical variables and descriptions are negligible and which are crucial for the accuracy of the model The mathematical techniques are presented because this

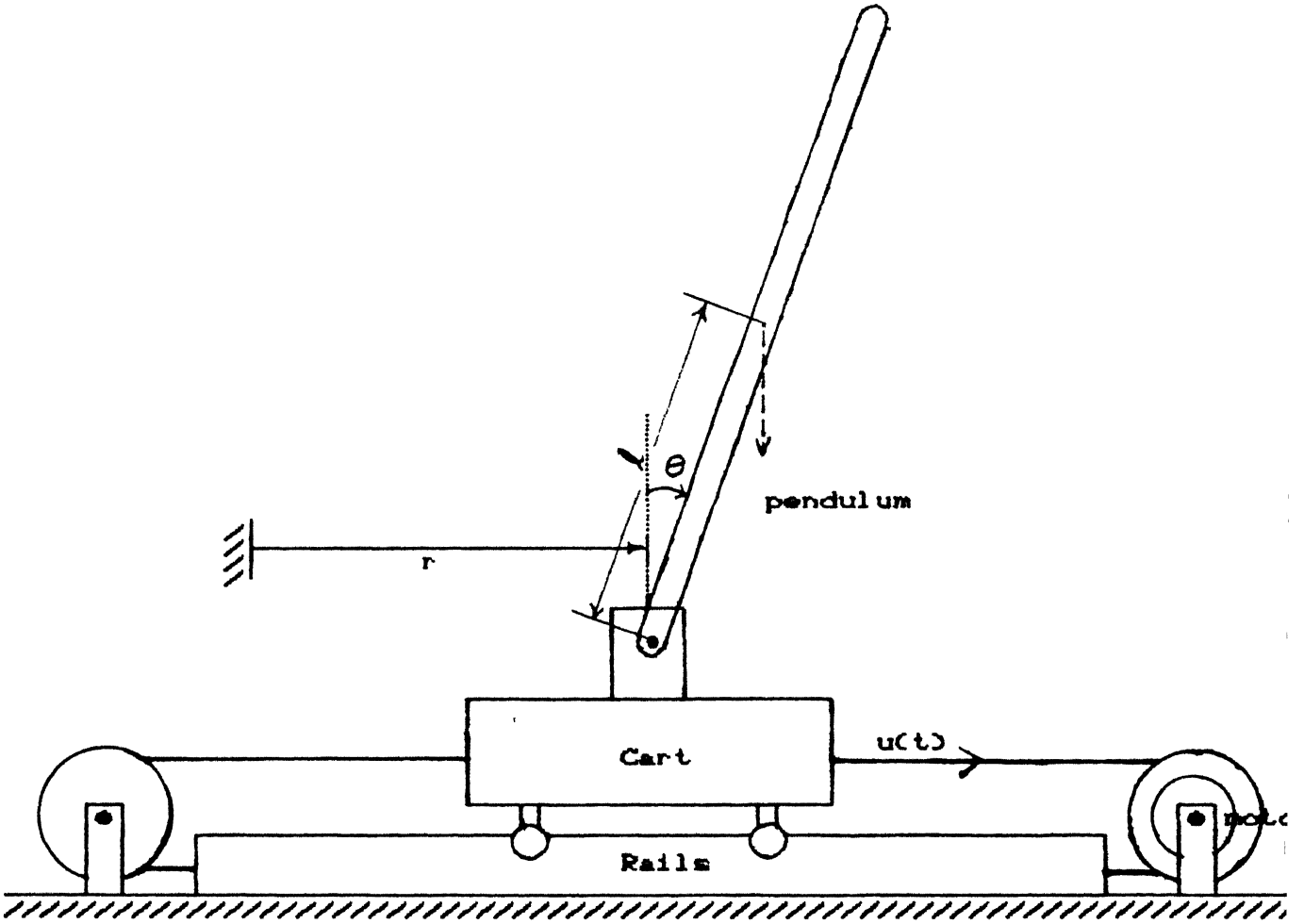

Fig. 3.1. Cart - Pendulum System

model, i.e., model of inverted pendulum, is considered, by many research groups, as simplified model of musculo-skeletal system, modeling of which is quite difficult because of the complexities involved Mathematical modeling of General Anthropomorphic Systems and its analogy with the inverted pendulum has been dealt extensively in [24] and [32]

3.1 Mathematical Modeling of an Inverted Pendulum

Consider the system shown in fig 3.1 It consists of a motor-driven cart on which a pendulum is mounted such that it rotates in the plane containing the line of motion of cart and vertical axis For obtaining differential equations governing the motion of this system, there are a sizable number of different approaches, each with its advantages and disadvantages The two methods most often used in mathematical modeling of Mechanical Systems are illustrated in the following analysis [24] The notations used in the following expressions can be followed from the Table 3 1

Method I : *Free body method*[7]

The method can be divided into the following steps.

1 **Geometry**: Picture the system in an arbitrary configuration (with respect to a reference configuration), then define coordinates and their positive directions. Note geometric identities; Note relations implied by geometric constraints

2. **Force equilibrium**. Write force balance relations.

   (i) Draw free-body diagram.

   (ii) Write equations of all the forces acting on the free body.

3. **Physical force-geometry relations**: Write these for the individual elements.

Here, in this procedure, one has to write as many independent equations as there are unknowns.

The procedure stated above is used in the following way to obtain the equations of motion of the inverted pendulum In the first analysis, for the sake of simplicity we assume that the pivot is friction less and no friction exists between the rails and wheels of the cart Then we have, from,

1 Geometry The system is shown in an arbitrary position in fig. 3.2 a and coordinates x and θ are defined Accelaration of the cart is given by

$$a_c = i_x \ddot{r} \qquad .. \qquad 3.1.1$$

here, a_c denotes the accelaration of the point C and i_x denotes the unit vector in the x-direction

To obtain the accelaration of the pendulum, define the position of pendulum's mass center, Q, in the fixed coordinate frame xy as shown in fig 3.2(a). The center of mass of the pendulum is then given by

$$s_Q = i_x r + (i_x l \, \mathrm{Sin}\theta + i_y l \, \mathrm{Cos}\theta) \qquad .. \qquad 3.1.2$$

where s_Q is the position of Q in the xy-frame

From eqn 3.1.2 we obtain the accelaration of the center of mass of the pendulum

Table 3.1 Parameters of cart-pendulum system

	parameter	symbol	value
Cart	Mass	m_c	0.411 kg
	Friction Constant	F	*
	Region of cart movement	r_o	$\pm$ 0.3 m
Pendulum	Mass	m	0.068 kg
	Length between the axis and c.g. (c.g. is the centre of gravity)	l	0.173 m
	Moment of Inertia about the c.g.	J	0.00012kgm^2
	Friction constant	C	0.0045kgm^2/s
	Accelaration due to gravity	g	9.8 m/s^2

* if perfect friction compensation is made then this variable can be treated as zero

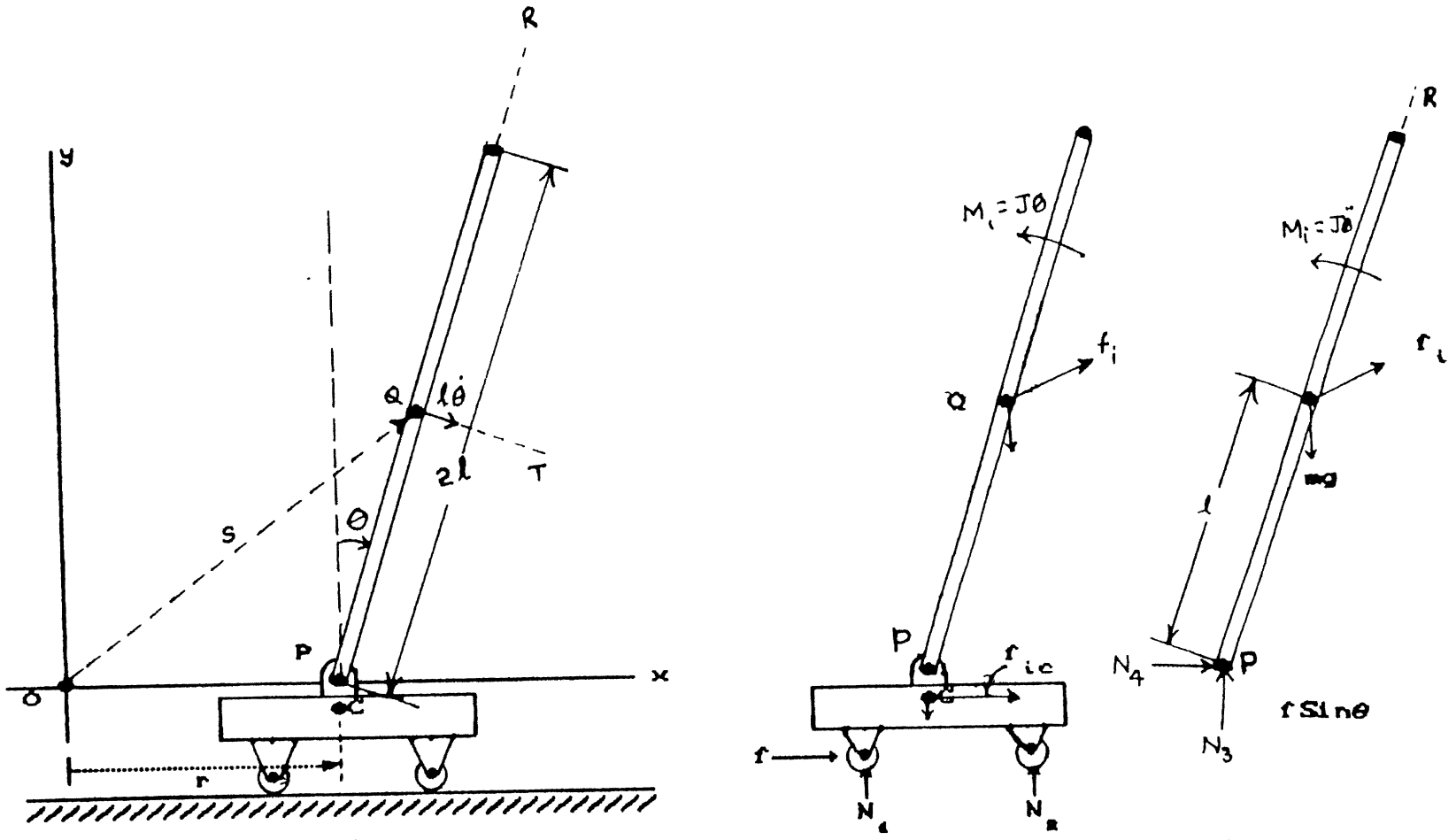

Fig 3.2. System for deriving the mathematical model

as

$$a_Q = i_x(\ddot{r} + l\ddot{\theta}\,\mathrm{Cos}\theta - l\dot{\theta}^2\,\mathrm{Sin}\theta) + i_y(-l\ddot{\theta}\,\mathrm{Sin}\theta - l\dot{\theta}^2\,\mathrm{Cos}\theta) \quad \ldots\ldots \quad 3.1.3$$

here i_y denotes the unit vector in the y-direction

2 Force equilibrium The two free-body diagrams of the system are shown in fig 3.2(b) D'Alembert's principle can be used to obtain the equation of motion, as follows Force u is the traction force, due to the motor, between the drive wheel and the rails Using Newton's second law of motion, we can write, from the first free body diagram

$$\sum f_x = 0 = (f_{ic})_x + (f_i)_x + u \quad \ldots\ldots \quad 3.1.4$$

here suffix x indicates the x-direction

In the second free-body diagram if we take moments about pivot point, P, of the pendulum i e , the z-axis which is out of paper, we obtain

$$\sum M_p = 0 = M_i - [i_R l \times f_i]_z - mgl\,\mathrm{Sin}\theta \quad \ldots\ldots \quad 3.1.5$$

where X signifies the vector cross product and i_R is the unit vector in the R-direction.

3 Physical Force-Geometry relations: We can write the following straight forward relations.

$$f_{ic} = -m_c\ddot{r}$$

$$M_i = J\ddot{\theta}$$

$$f_i = -ma_Q = -m[i_x(\ddot{r} + l\ddot{\theta}\,\mathrm{Cos}\theta - l\dot{\theta}^2\,\mathrm{Sin}\theta) + i_y(-l\ddot{\theta}\,\mathrm{Sin}\theta - l\dot{\theta}^2\,\mathrm{Cos}\theta)] \quad \ldots\ldots \quad 3.1.6$$

$$(f_i)_x = -m(a_Q)_x = -m[\ddot{r} + l\ddot{\theta}\,\mathrm{Cos}\theta - l\dot{\theta}^2\,\mathrm{Sin}\theta]$$

$$-[i_R l \times f_i]_z = lm[\ddot{r}\,\mathrm{Cos}\theta + l\ddot{\theta}]$$

substituting these relations into 3.1.4 and 3.1.5, and rearranging we obtain

$$\begin{aligned} m_c\ddot{r} + m\ddot{r} + ml\ddot{\theta}\,\mathrm{Cos}\theta - ml\dot{\theta}^2\,\mathrm{Sin}\theta &= u \\ J\ddot{\theta} + ml(\ddot{r}\,\mathrm{Cos}\theta + l\ddot{\theta}) - mgl\,\mathrm{Sin}\theta &= 0 \end{aligned} \quad \ldots\ldots \quad 3.1.7$$

The assumptions made above about friction will now be relaxed to some extent. The effects of friction then are introduced under the assumptions

(i) the friction of the cart is proportional only to the velocity $\dot{r}$ and

(ii) the friction generating the pivot axis is proportional to the velocity of the pendulum.

With this the above eqns 3.1.7 can be modified to the following form,

$$\left.\begin{aligned}(m + m_c)\ddot{r} + ml\dot{\theta}\,\mathrm{Cos}\theta &= -F\dot{r} + ml\dot{\theta}^2\,\mathrm{Sin}\theta + u \\ ml\ddot{r}\,\mathrm{Cos}\theta + (J + ml^2)\ddot{\theta} &= -C\theta + mlg\,\mathrm{Sin}\theta\end{aligned}\right\} \quad \ldots \quad 3.1.8$$

Method II : ***Generalized Coordinates***

If expressions for the total system kinetic energy and potential energy can be found in terms of independent joint position coordinates (generalized coordinates), then a number of classical approaches including the Lagrangian and Hamiltonian methods can, at least in principle, be brought to bear on the problem of deriving the system differential equations. The kinetic energy, potential energy and dissipation energy for the pendulum and cart are as follows

(i) For the pendulum

Kinetic Energy:

$$T_1=\tfrac{1}{2}J\dot{\theta}^2 + \tfrac{1}{2}\,m\{[\tfrac{d}{dt}(r\,\mathrm{Cos}\theta + l\,\mathrm{Sin}\theta]^2 + [\tfrac{d}{dt}(r\,\mathrm{Sin}\theta + l\,\mathrm{Cos}\theta)]^2 \qquad 3.1.9$$

Potential Energy: $V_1 = m(r\,\mathrm{Sin}\theta + l\,\mathrm{Cos}\theta)g$ 3.1.10

Dissipation Energy: $D_1 = \tfrac{1}{2}\,c\dot{\theta}^2$ 3.1.11

(ii) For the cart

Kinetic Energy: $T_2 = \tfrac{1}{2}m_c\dot{r}^2$ 3.1.12

Potential Energy: $V_2 = m_c(r\,\mathrm{Sin}\theta)g$ 3.1.13

Dissipation Energy: $D_2 = \tfrac{1}{2}F\dot{r}^2$ ... 3.1.14

For the integrated cart-pendulum system, we have

$$\left.\begin{aligned} &\text{Total Kinetic Energy of the system, } T = T_1 + T_2 \\ &\text{Total Potential Energy of the system, } V = V_1 + V_2 \\ &\text{Total Dissipation Energy, } D = D_1 + D_2 \end{aligned}\right\} \qquad 3.1.15$$

Then from the Lagrange's Law, we can write

$$\left.\begin{aligned} \frac{d}{dt}\frac{\partial T}{\partial \dot{r}} - \frac{\partial T}{\partial r} + \frac{\partial D}{\partial \dot{r}} + \frac{\partial V}{\partial r} &= u \\ \frac{d}{dt}\frac{\partial T}{\partial \dot{\theta}} - \frac{\partial T}{\partial \theta} + \frac{\partial D}{\partial \dot{\theta}} + \frac{\partial V}{\partial \theta} &= 0 \end{aligned}\right\} \quad \ldots\ldots \quad 3.1.16$$

where,

u is the force applied to the cart in Newtons.

After substituting the relations 3.1.9 - 3.1.15 into 3.1.16, we will get the following relations

$$\left.\begin{aligned} (m + m_c)\ddot{r} + ml\ddot{\theta}\,\mathrm{Cos}\theta &= -F\dot{r} + ml\dot{\theta}^2\,\mathrm{Sin}\theta + u \\ ml\ddot{r}\,\mathrm{Cos}\theta + (J + ml^2)\ddot{\theta} &= -C\dot{\theta} + mlg\,\mathrm{Sin}\theta \end{aligned}\right\} \quad \ldots\ldots \quad 3.1.17$$

The differential equations given by 3.1.8 are same and are quite nonlinear, since they contain various products and trigonometric functions of the state variables, and they are virtually impossible to solve except with numerical methods Consequently, we need further simplifications Since the object of controlling the system is to keep the pendulum upright, it seems reasonable to assume that $\theta(t)$ and $\dot{\theta}(t)$ will remain close to zero With this assumption, we can linearize the equations by retaining only those terms which are linear in θ and $\dot{\theta}$ and neglecting higher order terms such as θ^2, $\dot{\theta}^2$ and $\theta\dot{\theta}$ on the grounds that they will be insignificantly small.

Applying this process to the trigonometric expansions, we have

$$\left.\begin{aligned} \mathrm{Sin}\theta &= \theta - \frac{\theta^3}{3!} + \frac{\theta^5}{5!} - \ldots\ldots \simeq \theta \\ \mathrm{Cos}\theta &= 1 - \frac{\theta^2}{2!} + \frac{\theta^4}{4!} - \ldots\ldots \simeq 1 \end{aligned}\right\} \quad \ldots\ldots \quad 3.1.18$$

Substituting these into equations 3.1.17 and dropping the higher order terms, we get a set of approximate differential equations for the system,

$$\left.\begin{aligned} (m + m_c)\ddot{r} + ml\ddot{\theta} &= -Fr + u \\ mlr + (J + ml^2)\ddot{\theta} &= -C\dot{\theta} + mlg\theta \end{aligned}\right\} \quad . \qquad 3.1.19$$

The validity of these equations, depends, of course, on the validity of the assumption that $\theta(t)$ and $\dot{\theta}(t)$ are nearly equal to zero. As long as the control force is applied which maintains this condition, our mathematical model will be accurate, otherwise, it will breakdown

The dynamic behavior of this system is completely described by the position and velocity of the cart and the angular position and velocity of the pendulum. So we may define the state vector to be

$$\underline{X}(t) = \begin{bmatrix} r(t) \\ \theta(t) \\ \dot{r}(t) \\ \dot{\theta}(t) \end{bmatrix} \qquad \ldots \qquad 3.1.20$$

Equations 3.1.19 may be solved simultaneously for $\ddot{r}(t)$ and $\ddot{\theta}(t)$ and by selecting a state vector given in 3.1.20 these relations may be expressed in the state-variable form

$$\dot{\underline{X}}(t) = A\underline{X}(t) + Bu(t) \qquad \ldots\ldots \qquad 3.1.21$$

where,

$$A = \begin{bmatrix} 0 & 0 & 1 & 0 \\ 0 & 0 & 0 & 1 \\ 0 & a_{32} & a_{33} & a_{34} \\ 0 & a_{42} & a_{43} & a_{44} \end{bmatrix} \quad B = \begin{bmatrix} 0 \\ 0 \\ b_3 \\ b_4 \end{bmatrix} \qquad \ldots \qquad 3.1.22$$

The a_{ij}'s and b_j's in eqn 3.1.22 are parameters listed in Table 3.2 The characteristic roots of the matrix A are shown in fig.3.3

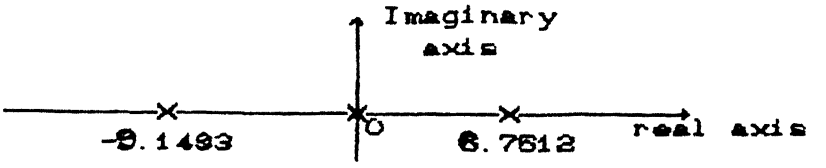

Fig 3.3 Charecteristic roots of the Cart-Pendulum System

To check the controllability of this system, we compute the controllability matrix

$$P_c = [\, B \;\; AB \;\; A^2B \;\; A^3B \,]$$

Since $\det(P_c) \neq 0$, P_c has full rank and, therefore, the system is completely state controllable Thus if the pendulum angle departs from equilibrium by a small amount, a control always exists which will drive it back to zero. Moreover, a control also exists which will drive both θ and r, as well as their derivatives, to zero

Table 3.2 Parameters of the system matrices A and B

a_{32}	$= -N^2 g / N_{01}$	$= -2.0413$
a_{33}	$= -J_1 F / N_{01}$	$= 0$
a_{34}	$= cN / N_{01}$	$= 0.0504$
a_{42}	$= M_{01} Ng / N$	$= 50.1187$
a_{43}	$= FN / N_{01}$	$= 0$
a_{44}	$= -M_{01} c / N_{01}$	$= -1.4604$
b_3	$= J_1 G / N_{01}$	$= 2.2632$
b_4	$= -NG / N_{01}$	$= -11.200$
M_{01}	$= m + m_c$	$= 0.470$
N	$= ml$	$= 0.01173$
J_1	$= J + ml^2$	$= 0.00214$
N_{01}	$= M_{01} J_1 - N^2$	$= 0.00080$

3.2 Design of Servo-Control System

For the linear model given in the previous Section, a controller is designed depending on a chosen performance index of the system. This section sets out to design a servo controller to stabilize the inverted pendulum at the given cart position where the cart is placed on a horizontal rail

To design a controller, which will stabilize the system, instead of seeking a gain matrix to achieve specified closed loop pole locations, we now seek a gain to minimize a specified performance criterion J (or "cost function") expressed as the integral of a quadratic form in the state plus a second quadratic form in the control u, i.e ,

$$J = \int_0^\infty [\underline{X}(\tau)^T Q \underline{X}(\tau) + u(\tau)^T R u(\tau)]\, d\tau \qquad \ldots . \qquad 3.2.1$$

where,

R is a positive definite matrix and Q is a symmetrical positive semidefinite matrix such that the pair $(A,(Q^{1/2})^T)$ is a completely observable pair $(Q^{1/2}(Q^{1/2})^T \triangleq Q)$. Since the system defined by the matrices (A,B) is completely controllable, there exists a unique, positive definite solution P of the matrix Riccatti equation

$$A^T P + PA - PBR^{-1}B^T P + Q = 0 \qquad \ldots\ldots \qquad 3.2.2$$

As it is well known, the feedback law in this case is given by

$$u(t) = -K\underline{X}(t), \qquad \ldots \qquad 3.2.3$$

with

$$K = R^{-1}B^T P \qquad \ldots\ldots \qquad 3.2.4$$

This is a unique optimal feedback law when all the states $\underline{X}(t)$ are accessible.

The main difficulties associated with the use of Linear Quadratic Regulator (LQR) theory are as follows. One is the choice of suitable values for the weighing matrices Q and R in the performance index. In general, the relative magnitudes of the elements of these matrices are determined to some extent by the physical

constraints imposed on the states and the inputs of the system But in practice, we need to *"tune"* these values in order to get suitable responses The selection of these matrices is discussed in the following parts of this section

The second difficulty associated with LQR design is in its implementation. Since the solution of the LQR problem is a linear state variable feedback law, we need to have access to all the states of the system in order to implement the design This is, of course, not possible in general. One way out of this difficulty is to use observers to obtain estimates of the states, as discussed in section 3 3. This has the disadvantage that it introduces a considerable amount of complexity in the feedback loop. Further more, during the transient stage, i.e. before the estimated stage has reached the true state, the behavior of the closed-loop system using an observer is different from that of the system using true state feedback Another possibility is to solve the LQR problem by means of output feedback This problem is considerably more difficult to solve than the standard LQR problem, and is not considered for this thesis This can be found in any book on control theory e g [26].

Selection of the Weighing matrices

As has been said above, the question of concern to the control system designer is the selection of the weighing matrices Q and R. In the performance or cost function defined by 3.2.1 two terms contribute to the integrated cost of the trajectory: the quadratic form $\underline{X}^T Q \underline{X}$ which represents a penalty of the deviation of the state $\underline{X}$ from the origin and the term $u^T Ru$ which represents the "cost of control". The weighing matrix Q specifies the importance of the various components of the state vector relative to each other. For example, if one is interested in the states x_1 and x_2 i.e., deviation of cart and pendulum from the origin, and none of their derivatives are of concern then one might select a state weighing matrix

$$Q = \mathrm{diag}(c_1, c_2, 0, 0) \quad . \quad 3.2.5$$

But the choice of 3.2.5 as a state weighing matrix may lead to a control system in which the velocity of the cart is larger than desired. To limit the velocity, the performance integral might include a velocity penalty i.e.,

$$\underline{X}^T Q \underline{X} = c_1 x_1^2 + c_2 x_2^2 + c_3 \dot{x}_3^2 \quad \ldots \quad 3.2.6$$

which would result in a state weighing matrix

$$Q = \mathrm{diag}(c_1, c_2, c_3, 0) \quad \ldots \quad 3.2.7$$

Another possible situation is one in which we are interested in the state only through its influence on the system output

$$y = H\underline{X} \quad \ldots \quad 3.2.8$$

For a system with this output, a suitable performance criterion might well be

$$y^T y = \underline{X}^T H^T H \underline{X} \quad \ldots \quad 3.2.9(a)$$

So in this case

$$Q = H^T H \quad \ldots \quad 3.2.9(b)$$

It should by now be clear that the choice of the state weighing matrix Q depends on what the system designer is trying to achieve. The considerations alluded to above with regard to Q apply as well to the control weighing matrix R The term $u^T Ru$ in the performance index 3.2.1 is included in an attempt to limit the magnitude of the control signal u Unless a "cost" is imposed for use of control, the design that emerges is liable to generate control signals that cannot be achieved by the actuator - the physical device that produces the control signal i e , the motor driving the cart and the result will be that the control signal will saturate at the maximum signal that can be produced This, in fact, would have been a desired situation, as in most cases, saturation of the control will produce the fastest possible response. But when saturation occurs, the closed loop system

behavior that was predicted on the basis that saturation will not occur, may be very different from the actual system behavior A system that a linear design predicts to be stable may even be unstable when the control signal is saturated Thus in a desire to avoid saturation and its consequences, the control signal weighing matrix is selected large enough to avoid saturation of the control signal under normal conditions of operation.

The relationship between the weighing matrices Q and R and the dynamic behavior of the closed-loop system depend of course on the matrices A and B and are quite complex It is impractical to predict the effect on closed-loop behavior of a given pair of weighing matrices The approach we have taken is solve for the gain matrix K that result from a range of weighing matrices Q and R, and simulate the closed-loop response The gain matrix K that produces the response closest to the required is selected

We have followed the method suggested by [25] and is explained below The equation given in 3 2 2 can be modified to the Kalman equation

$$\Delta_k(-s)\Delta_k(s) = \Delta(-s)\Delta(s) + R^{-1}\Gamma(-s)^T Q\Gamma(s) \quad \ldots\ldots \quad 3.2.10$$

where

$$\left.\begin{aligned} \Delta(s) &= \det(sI - A) \\ \Delta_k(s) &= \det(sI - A + BK) \\ \Gamma(s) &= \mathrm{adj}(sI - A)B \end{aligned}\right\} \quad \ldots\ldots \quad 3.2.11$$

Assume the matrix Q to be a positive definite diagonal matrix

$$Q = \mathrm{diag}(q_1, q_2, q_3, q_4) \quad \ldots\ldots \quad 3.2.12$$

and parameterize q_i's as

$$\left.\begin{aligned} \mu_1 &= \sqrt{q_1/q_3} & \mu_2 &= \sqrt{q_2/q_3} \\ \nu_1 &= b_3^2 q_3 & b_3^2 q_3 + b_4^2 q_4 &= 1 \end{aligned}\right\} \quad \ldots\ldots \quad 3.2.13$$

where b_i's are the parameters listed in Table and ν_i's and μ_i's are any real

numbers. Using the parameters presented in equation 3.2.13, the second term on the right-hand side of 3.2.10 can be written as

$$\Gamma(-s)^T Q \Gamma(s) = \nu_1(s^2 - \mu_1^2)(s^2 - \zeta_1^2)(s^2 - \zeta_2^2) + \nu_2(s^2 - \mu_2^2)s^4 \quad \ldots\ldots \quad 3.2.14$$

where $\nu_2 + \nu_1 = 1$ and ζ_i's are two zeros of the transfer function from u to r

Although the closed-loop poles can be arbitrarily allocated by the selection of K, if the poles are not carefully chosen, some undesirable phenomena may occur. For example, since $(sI - A + BK)^{-1}B = \Gamma(s)/\Delta_k(s)$ is obtained from eqn 3.2.11, if all the roots of $\Delta_k(s) = 0$ are chosen to be too far from the origin in the complex plane aiming at the high-speed response, undesirably large over or undershoot may result due to the unmovable allocation of the zeros, i.e. the roots of $\Gamma(s)$.

On the other hand, in order to avoid the effect of the uncertainty in parameters in the matrix A and of the non-linearity of the system, the positive number of R should be sufficiently small If R is small enough, as seen from eqn. 3.2.10, three of the closed loop poles, i.e. the roots of $\Delta_k(s) = 0$, are very close to the roots which are determined by the choice of the parameters μ_1, μ_2 and ν_1 in eqn 3.2.13 To eliminate the undesirable effect of the weighing matrices, the following procedure is adopted in determining the feedback law [25].

(i) In consideration of the response speed choose μ_1, μ_2 and ν_1 in 3.2.13 so that the roots of the second term in 3.2.10 may not be remote from each root of $\Gamma(s)=0$, i.e., zeros of the system.

(ii) Since the norm of the feedback law K increases as $R \to 0$, determine R so that every element of K is realizable

(iii) Set the parameters of K in the actual stabilizer, and observe the actual performance of the controlled pendulum. If not desirable, select a new triple (μ_1, μ_2, ν_1)

3.3 Design of the Observer

The feedback law given in 3.2 3 can be implemented if the state vector $\underline{X}(t)$ is available for measurement and feedback But in many situations this may not be the case and only few of the state variables are available for measurement To estimate the remaining state variables one has to observe the system using a linear observer The design is described below[11].

We can group the state variables into two sets those that can be measured directly and those that depend on the former The state vector is partitioned accordingly

$$\underline{X}(t) = \begin{bmatrix} X_1 \\ \cdot\ \cdot \\ X_2 \end{bmatrix}$$

with

$$\left.\begin{aligned} \dot{X}_1(t) &= A_{11}X_1 + A_{12}X_2 + B_1u \\ X_2(t) &= A_{21}X_1 + A_{22}X_2 + B_2u \end{aligned}\right\} \quad \ldots \quad 3.3.1$$

The observation is given by

$$Y = C_1X_1 \quad \ldots \quad 3.3.2$$

The standard observer for 3.3 1 and 3.3.2 is

$$\dot{\hat{X}}_1 = A_{12}\hat{X}_1 + A_{12}\hat{X}_2 + B_1u + K_1(Y - C_1\hat{X}_1) \quad \ldots\ldots \quad 3.3.3$$

$$\dot{\hat{X}}_2 = A_{21}\hat{X}_1 + A_{22}\hat{X}_2 + B_2u + K_2(Y - C_1\hat{X}_1) \quad \ldots\ldots \quad 3.3.4$$

But $\hat{X}_1$ can be directly computed from 3.3.2 and is given by

$$X_1(t) = \hat{X}_1(t) = C_1^{-1}Y(t) \quad \ldots \quad 3.3.5$$

In this case the observer 3.3.4 for those states that cannot be measured directly becomes

$$\dot{\hat{X}}_2 = A_{21}C_1^{-1}Y + A_{22}\hat{X}_2 + B_2u \quad \ldots\ldots \quad 3.3.6$$

which is a dynamic system of the same order as the number of state variables that

cannot be measured directly. The dynamic behavior of the reduced-order observer is governed by the eigen values of A_{22} which is a submatrix of the open-loop dynamic matrix A, over which we don't have any control. A more general system for the reconstruction of $\hat{X}_2$ is given by

$$\hat{X}_2 = Ly + z \quad \ldots\ldots \quad 3.3.7$$

where z is the state of a system

$$\dot{z}(t) = Fz + Gy + Hu \quad \ldots\ldots \quad 3.3.8$$

It can be shown that the estimation error

$$e = \underline{X}(t) - \hat{X}(t) = \begin{bmatrix} X_1 - \hat{X}_1 \\ X_2 - \hat{X}_2 \end{bmatrix} = \begin{bmatrix} e_1 \\ e_2 \end{bmatrix} \quad \ldots\ldots \quad 3.3.9$$

will decay to zero following the differential equation

$$\dot{e}_2(t) = F e_2(t) \quad \ldots\ldots \quad 3.3.10$$

if we choose the observer matrices as follows

$$\left.\begin{aligned} F &= A_{22} - LC_1A_{12} \\ H &= B_2 - LC_1B_1 \\ G &= (A_{21} - LC_1A_{11})C_1^{-1} + FL \end{aligned}\right\} \quad \ldots\ldots \quad 3.3.11$$

and see that the eigen values of F lie in the left half of the s-plane. Therefore, for the stability of the observer we have to choose the matrix L properly

3.4 Digital Computer Simulation

The effectiveness of the above aspects were tested by computer simulation of the inverted pendulum incorporating the controller and observer described in the pervious sections of this chapter. Fig. 3.4 shows the simulation block diagram. The objective of the control, as already said, is to bring the pendulum to the vertical position and cart to the center of the rails. The system parameters used

in simulation are given in Table 3.1. The state weighing matrix, Q is chosen as

$$Q = \begin{bmatrix} 3.4437 & 0.1155 & 0.13775 & 0.001155 \end{bmatrix}$$

which results from $\mu_1 = 5$, $\mu_2 = 10$ and $\nu_1 = 0.8$ (eqn 3.2.13)

In performing the simulation studies it is also assumed that only two states are available for measurement. So a second-order observer is designed by selecting the observer-matrix L (eqn 3.3.7) as

$$L = \begin{bmatrix} 10 & 0 \\ 0 & 10 \end{bmatrix}$$

Other observer matrices that correspond to this L-value (eqn 3.3.11) are found as

$$F = \begin{bmatrix} -10 & 0.0587 \\ 0 & -12.3981 \end{bmatrix} \quad H = \begin{bmatrix} 2.4 \\ -13.1586 \end{bmatrix} \quad G = \begin{bmatrix} -100 & -0.9256 \\ 0 & -62.2121 \end{bmatrix}$$

with

$$C = \begin{bmatrix} 1 & 0 \\ 0 & 1 \end{bmatrix}$$

In all these simulation studies, the control is bounded to lie in the region [-5, 5] N-m. The feedback law 3.2.3 together with the observer described, stabilizes the system 3.1.21 and creates a stable zone in the neighborhood of the origin. This is quite natural as one can not expect a controller of eqn 3.2.3 to

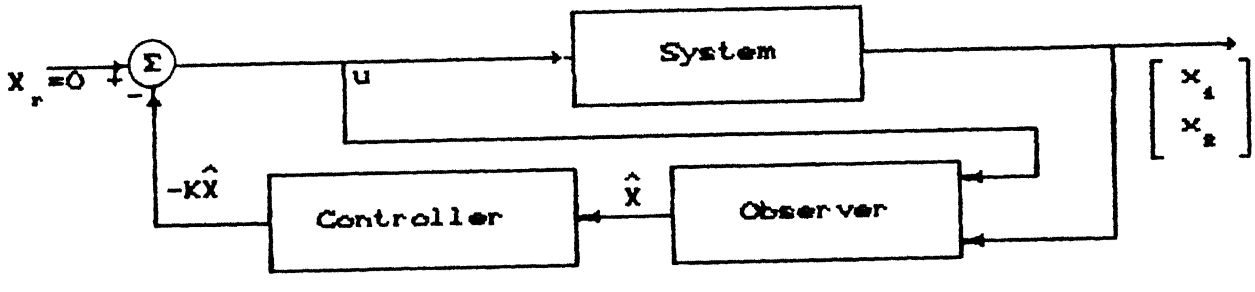

Fig. 3.4. Simulation Block Diagram

bring the pendulum from its pendent position, which is natural stable state, to the vertical position, even if there is no limit on the control input. Of course, there are some controllers in combination with the controller described in this chapter which can achieve this task. This however, is a two-stage process In the first stage, the so called "swinging-up" control discussed by S.mori et al.[25] drives the pendulum from its natural pendent state to the upright position with the cart being in the central position at the end of the control Once it is brought into the vicinity of the upright position, the second stage is, to switch the controller described in this chapter to take over from the swinging-up controller to bring the system's states to the required positions. A border of stable zone is determined by the unstable mode of the constrained value of input To find this zone, first the system given by eqn 3.1.21 is transformed into the following form

$$\dot{Y}(t) = \Lambda Y(t) + \Gamma u(t) \quad \ldots\ldots \quad 3.4.1$$

where,

$$\Lambda = P^{-1}AP \quad \text{and } \Gamma = P^{-1}B \quad \ldots\ldots \quad 3.4.2$$

and P is the matrix given by

$$P = [\, p_1 \quad p_2 \quad p_3 \quad p_4 \,] \quad \ldots\ldots \quad 3.4.3$$

with p_i as the eigen vector associated with eigen value λ_i, i = 1 .. 4

From this canonical form, the unstable zone that can not be stabilized is expressed as

$$|y_l| = |\sigma_l^T x| > \frac{u_0}{\lambda_l} \quad \ldots\ldots \quad 3.4.4$$

where,

u_0 is the maximum control available,

λ_l is the greatest positive root among the characteristic roots of the uncontrolle system, and

σ_l^T is the lth row vector of the coordinate transformation matrix P.

The projection of, y_l, thus obtained from the condition 3.4.4 onto the (r,θ)

plane of the actual stable zone is shown in fig 3.5 The border is obtained from the eqn 3 4.4 Here this stable zone also depends on the length of the rail on which the cart can move.

The transition of the states of the closed-loop system, as the weighting matrix R is varied, is shown in figs 3 6 - 3 10 As R value is reduced, the penalty on control is reduced, and in the limit the behaviour is that of a dead-beat controller. Again as R value is increased, too much of penalty on control is introduced . This will also affect the controller performance. Thus an optmal behavior lies in choosing an R which is not too much high or not too low These are demonstrated in figs 3 6 to 3 10 where the time responses of pendulum position, cart position and control are shown It can be seen for low R values, the system resonse is too oscillatory, for high R values it is too sluggish

From these responses, and the above discussions we see that optium response is obtained for R=0.1 because we see that this does not exhibit either oscillatory or sluggish transient behaviour. Of coure, as said in section 3.2 the criteria for optimality depends on our requirements. For example, if we were

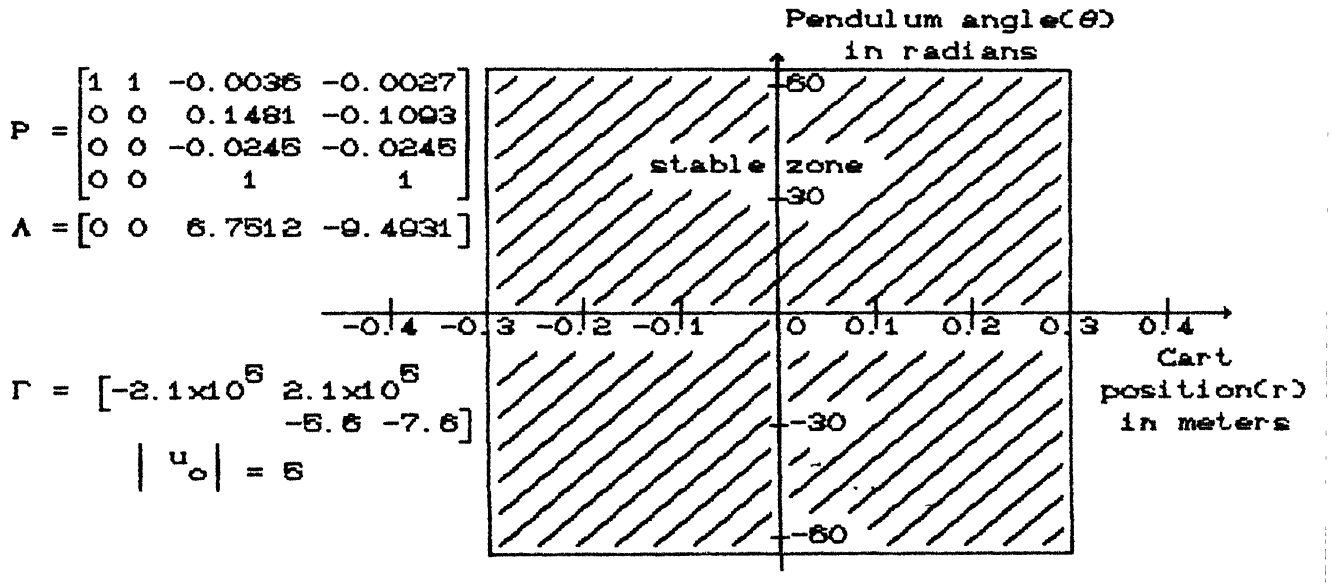

Fig.3.5. Stable zone of the cart-pendulum system

interested in studying the periodic motion generation in bipeds, which was described in Chapter 1, then we would have chosen low values of R which would make the sytem oscillatory Even here, i.e in studying the periodic motion, also we have criterialike generating optimal stride length, minimum time trajectory control, minimum energy control etc Finally, one should note hre that for studying the responses we have chosen a fixed state weighing matrix and different control weighing matrices The sate weighing matrix Q has been chosen after scrutinizing the responses obtained for different values of Q as described in sectin 3.2

3.5 Conclusions

Several aspects for the control of an inverted pendulum have been discussed in this Chapter Many of these aspects will be quite useful in designing most of the practical systems The controller designed can stabilize the system only when the deviations of pendulum from the vertical-axis are small. The simulation studies were performed on a linearized sytem and will be compared with the actual nonlinear system's behaviour in Chapter 5 Hints have been given for providing insight into the study of bipeds with the help of this simple inverted pendlum model

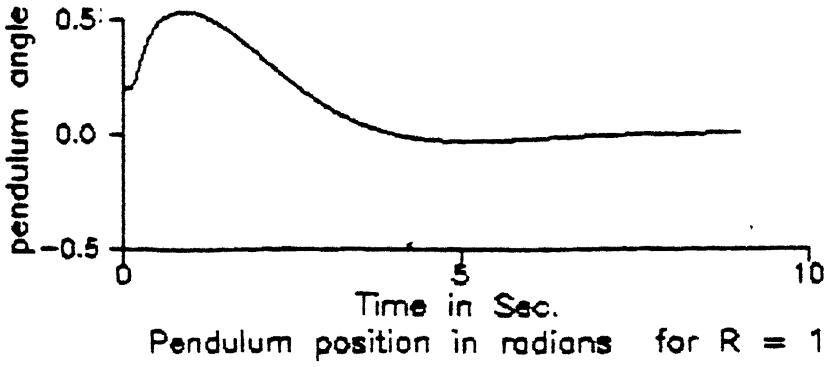

Pendulum position in radians for R = 10

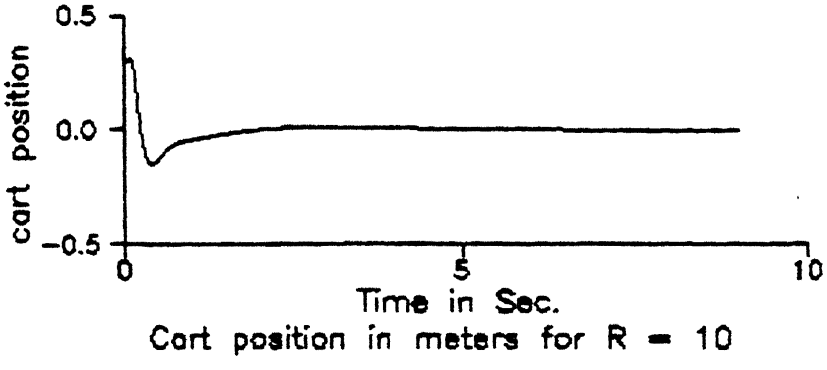

Cart position in meters for R = 10

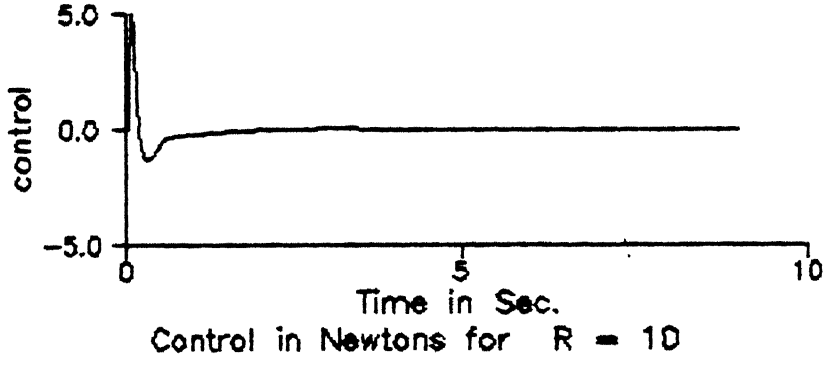

Control in Newtons for R = 10

FIG 3.6 RESPONSES FOR R=10

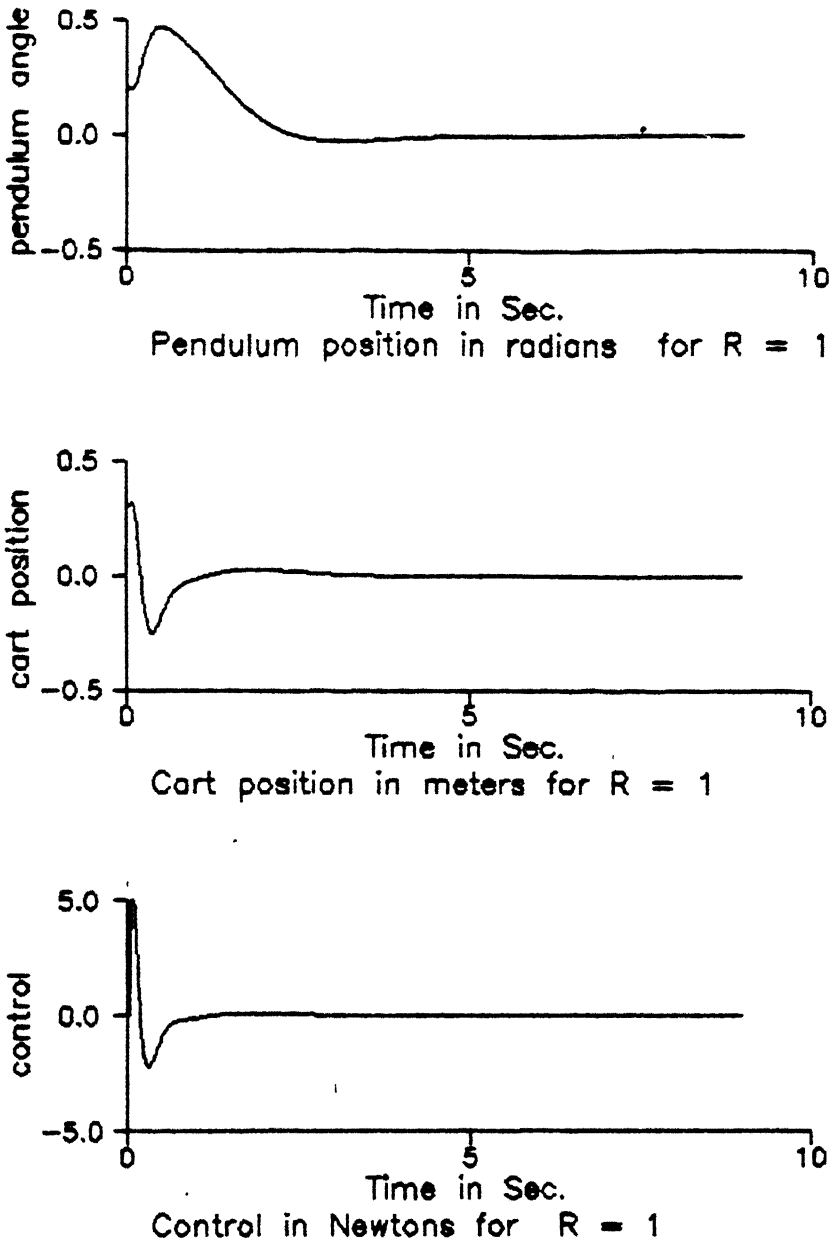

FIG 3 7. RESPNOSES FOR R=1

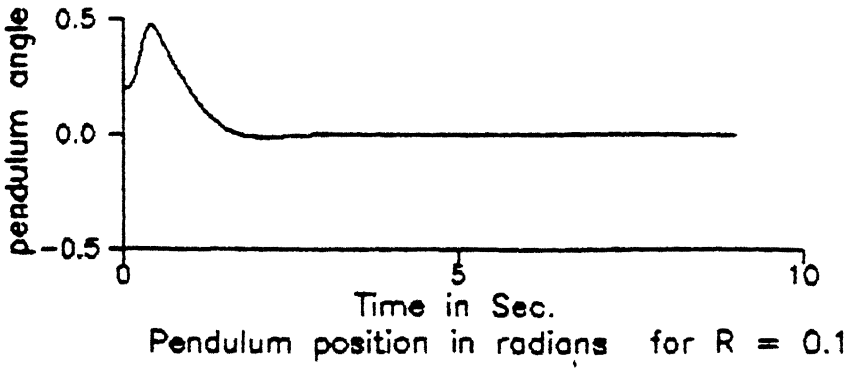

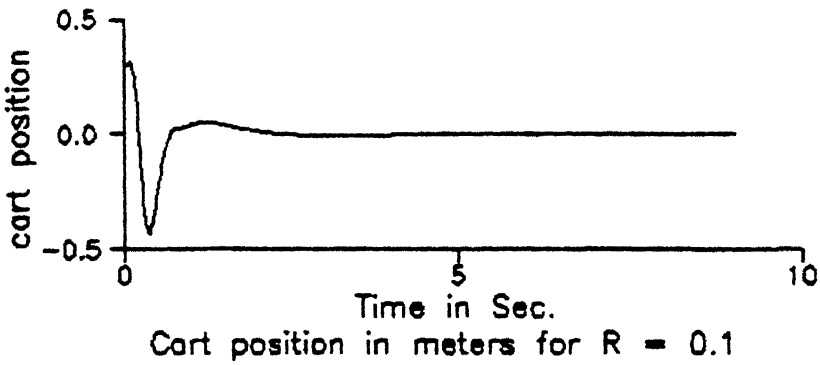

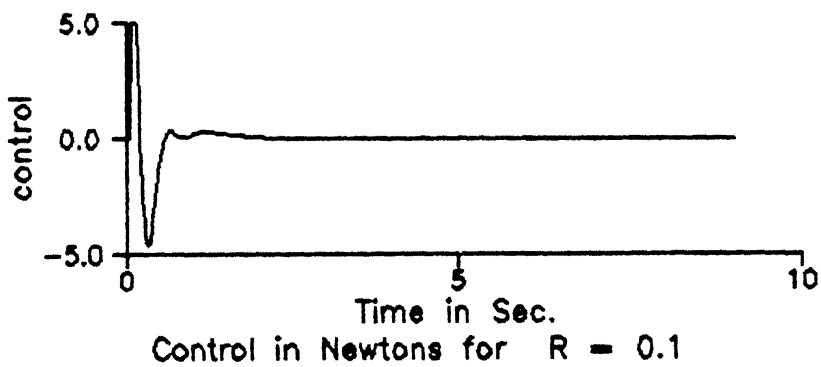

FIG. 3.8. RESPONSES FOR R=0.1

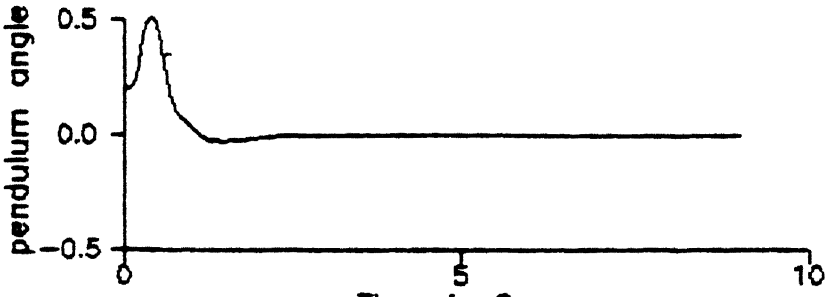

Pendulum position in radians for R = 0.03

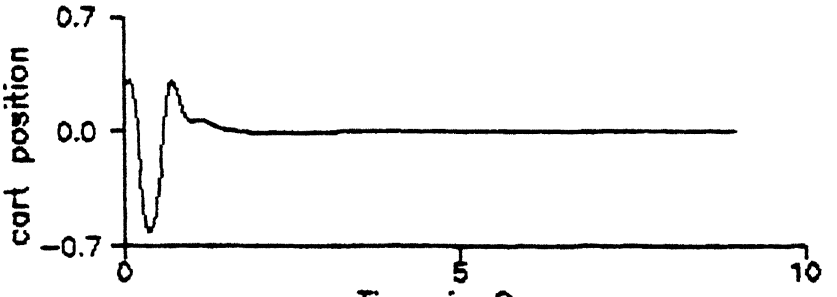

Cart position in meters for R = 0.03

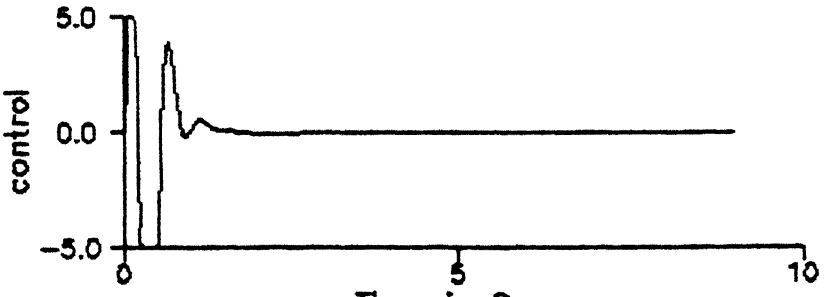

Control in Newtons for R = 0.03

FIG. 3.9 RESPONSES FOR R=0.03

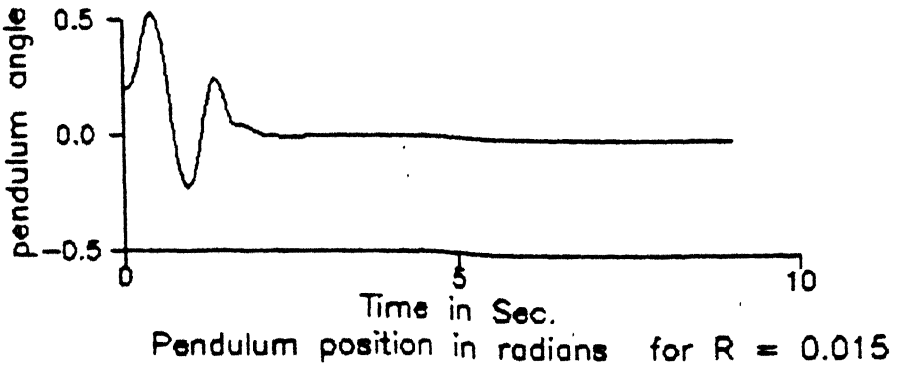

Pendulum position in radians for R = 0.015

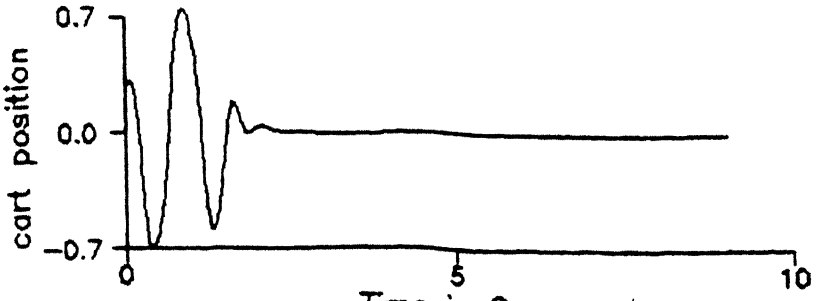

Cart position in meters for R = 0.015

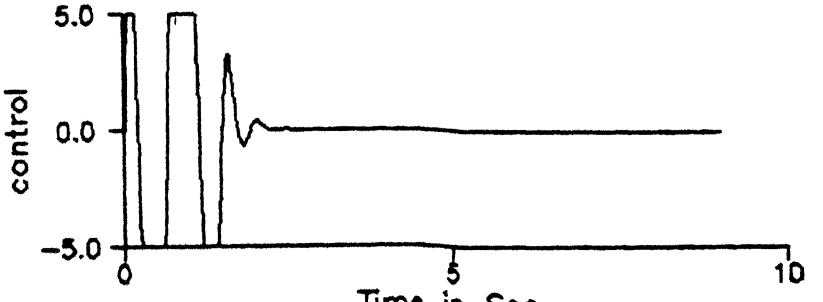

Control in Newtons for R = 0.015

FIG. 3.10. RESPONSES FOR R=0.015

Chapter 4
Experimental Set-up

In this chapter, implementation issues of the cart-pendulum system and the driver for the same are discussed A 230v, 50w separately excited DC Motor is used for driving the cart Four quadrant operation of the motor is required as we need the motor torque movement in forward as well as reverse direction Driving a DC motor by a class A amplifier is a very inefficient operation because of the excessive dissipation in the amplifier[28] In order to avoid the power dissipation in the amplifier, we can operate the amplifier in a class D mode where the transistors constituting the amplifier are turned on and off like a switch When the amplifier is turned on, the voltage across it is negligible, and when it is turned off the current through it is zero. In either case the resulting power dissipation is small. The switching can be performed in various ways One simple method is to switch the amplifier at a constant frequency and vary the on and off phases according to the need Such amplifiers are called pulse-width modulated amplifiers, and can be operated in many modes as described in the following sections

4.1 Experimental setup of the Cart-Pendulum System

The mechanical system developed is schematically shown in fig. 4.1 and the photograph of the realized set-up is shown in fig 4.2. Its main parts are

(i) a cart moving along a line on rails of limited length

(ii) a pendulum hinged to the cart and

(iii) a cart-driving means which contains a D.C.motor, a pulley belt transmission system and a chopper for driving the motor.

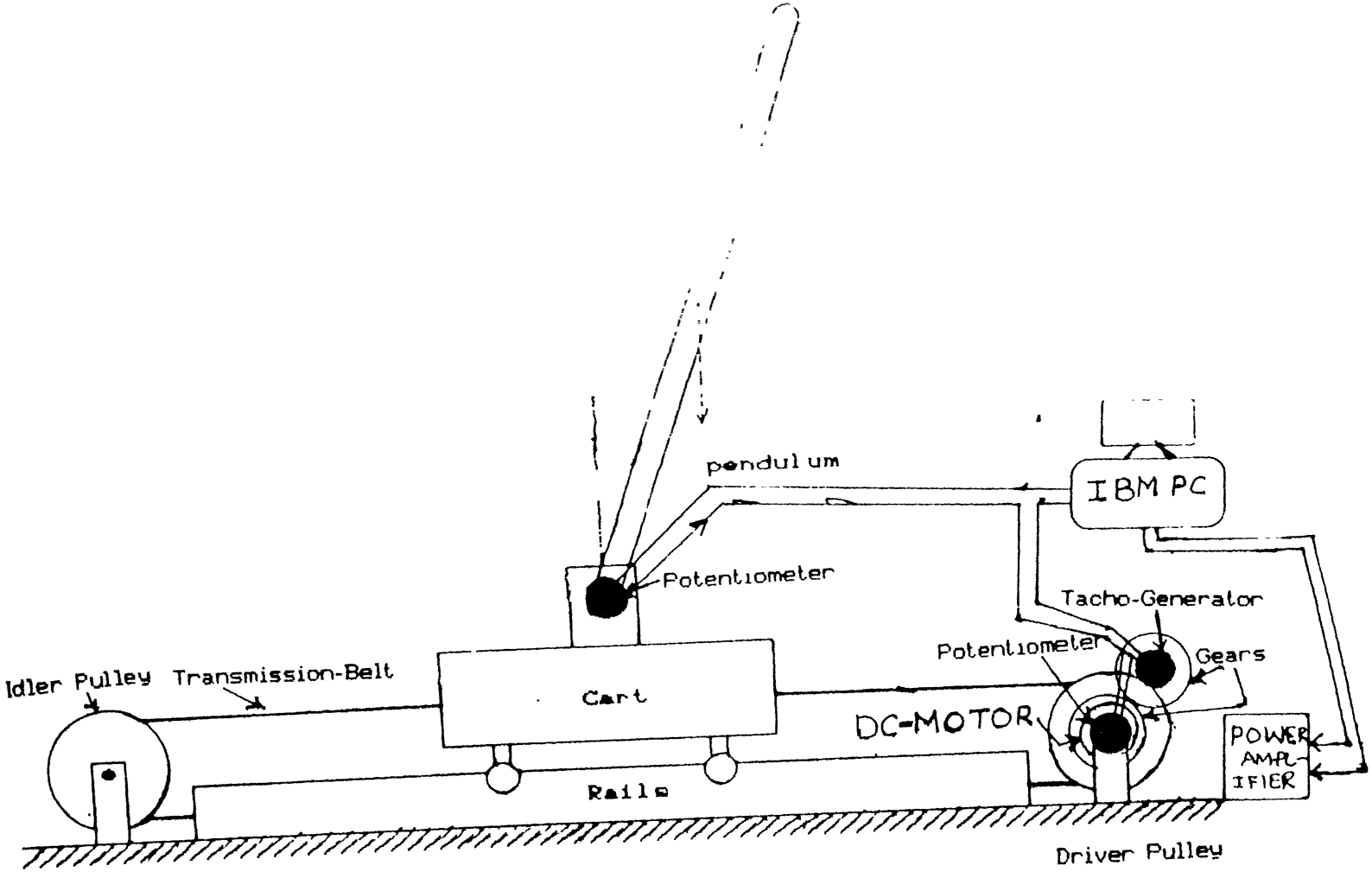

Fig 4 1 Experimental Cart-Pendulum System

The Pendulum

The pendulum made of ebonite is hinged to the cart so that its motion is smooth and restricted to the vertical plane containing the line of the rail Table3 1 gives the dimensions and parameters of the realized system A potentiometer mounted on the cart base measures the pendulum's angular position.

The Cart

The cart is made of perspex, which has got sufficient strength to carry the sensor and other supporting materials required for mounting the pendulum. This cart is supported by four wheels so that it can move freely on rails which are made using an aluminum plate of thickness 3mm The cart is driven from a DC-motor by a pulley-belt transmission mechanism Pulley is connected directly to the motor shaft Position of the cart is measured by using a potentiometer which is also directly coupled to the motor shaft. Cart velocity is measured using the tacho generator which is coupled to the motor shaft using a gear mechanism.

To select a motor for driving the cart, we first calculated the approximate power and speed requirements of the motor These requirements are given below

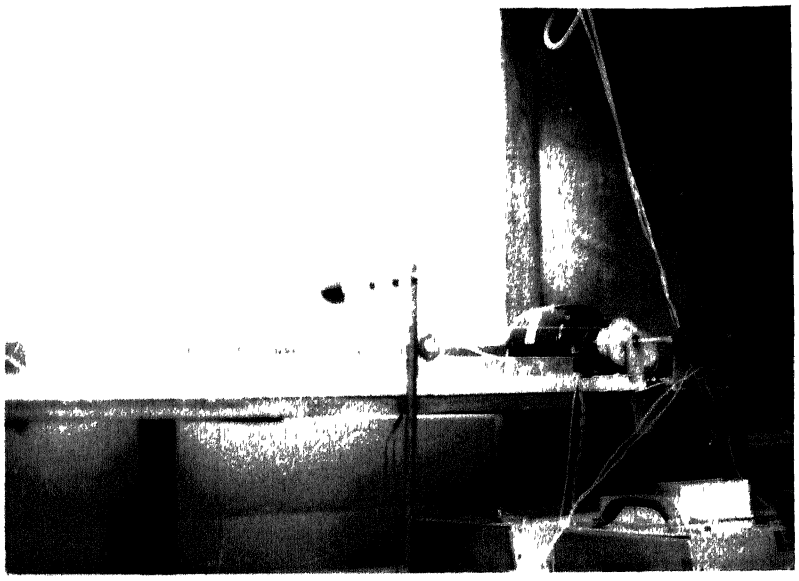

Maximum Speed = 1000rpm

Maximum power = 40watts

Here, for controlling the pendulum, fast reversals, i e, quick acceleration and deceleration in either direction are required For this purpose low inertia servo motors are the ideal choice However, as no such motor is locally available either in our stores or in the local market, a separately excited DC motor with good torque characteristics has been chosen The ratings of this motor are given below

Maximum Voltage = 230 V

Maximum current = 0.4 A

Maximum Speed = 1725 rpm

Maximum power = 1/15 HP

4.2 Switching Schemes

The ideal chopper configuration is shown in fig 4.3(a) Many control strategies for the four-quadrant operation of the DC motor exist. All these control strategies have been discussed by Tal [29] as also by Dewan and

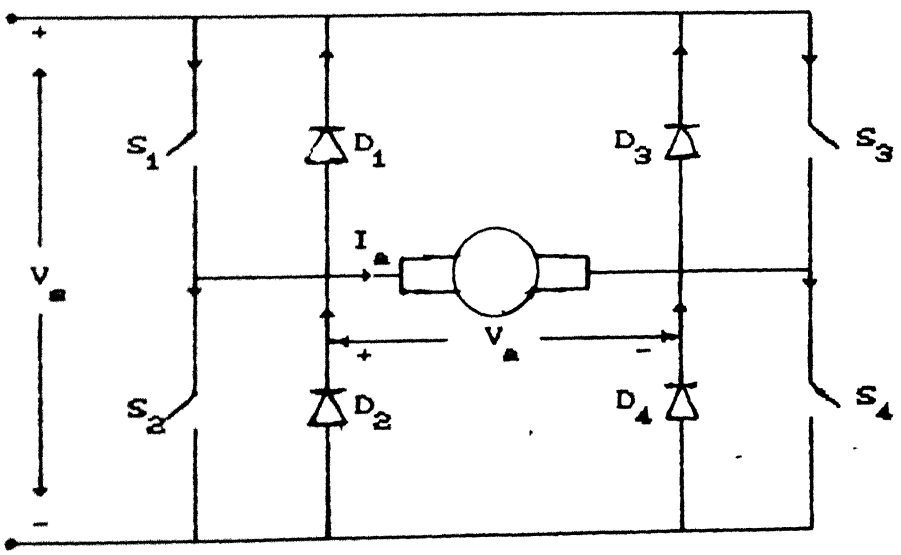

Fig. 4.3 (a). Basic 4-Quadrant Chopper Configuration

Morbid[8] In both these papers, thyristor switches have been considered and the comparisons between various control strategies have been made by keeping this as basis But if the switches are realized using transistors then those comparisons are no longer valid

In the light of above mentioned facts, a very simple and efficient scheme is adopted, as given by the state transition diagram shown in fig. 4.3(b) When switches S_1 and S_4 are ON the current through the motor will be positive and during this time the inductor will store energy. During the remaining part of the cycle no switch is on and so the energy stored in the inductor will cause current to flow through the diodes D_2 and D_3 If the current falls to zero then the state "All-Off" of fig 4.3(b) occurs On the otherhand, if S_1 and S_4 are switched ON again before the current decays to zero, the cycle denoted by "Forward Motoring" results Similarly, switches S_2S_3 and D_1D_4 will provide path for "Reverse Motoring" For transition from one direction to the other all switches are turned

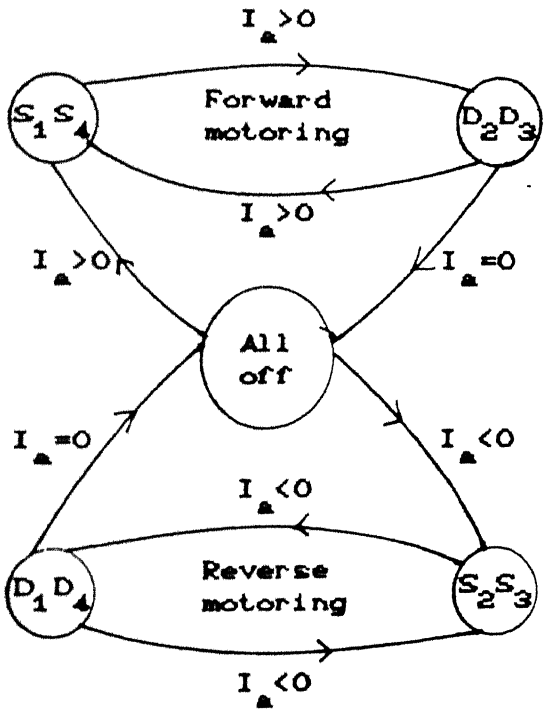

Fig. 4.3 (b). Illustration of Switching Scheme

off for a dead time τ_d so that the motor enters the "All-Off" from which, depending on the requirements, transition from Forward Motoring to Reverse Motoring or vice versa is followed. In order to analyze the current and voltage waveforms, we have to examine the electric equation of the motor

$$V_a = L_a \frac{dI_a}{dt} + I_a R_a + E_b \quad \ldots \quad 4.2.1$$

where,

I_a is the motor armature current,

E_b is the motor Back emf,

L_a is the armature inductance

R_a is the armature resistance

and V_a is the voltage across the motor at a given time t

The solution of 4.2.1 can be simplified by virtue of the facts that

(i) E_b varies with mechanical time constant of the motor for all practical purposes can be treated as constant over a switching period

(ii) $I_a R_a$ is a small term in eqn. 4.2.1 and will also remains essentially constant if the switching period $T \ll \frac{L_a}{R_a}$

Hence, treating E_b as a constant and replacing I_a by its average value I_{AV} in the term $I_a R_a$, the eqn. 4.2.1 can then be modified to the form

$$L_a \frac{dI_a}{dt} = V_a - V_t \quad \ldots \quad 4.2.2$$

where,

$$V_t = I_{AV} R_a + E_b \quad \ldots \quad 4.2.3$$

For our switching strategy the motor voltage $V_a = \pm V_S$ when $|I_a| > 0$.

Therefore, from eqn. 4.2.2 we can say that $\frac{dI_a}{dt}$ is constant and changes according to $V_a = \pm V_S$. This is illustrated in fig. 4.3(c).

From fig. 4.3(c) and eqn. 4.2.2 it can be easily followed that

$$\Delta I_a = I_H - I_L = \frac{V_S - V_t}{L_a} T_{on} = \frac{V_S + V_t}{L_a} T_{off} \quad \ldots \quad 4.2.4$$

$$\Rightarrow \quad (V_S + V_t) T_{off} = (V_S - V_t) T_{on}$$

$$\Rightarrow \quad V_l = V_s \frac{T_{on} - T_{off}}{T_{on} + T_{off}} = V_s\left(\frac{2T_{on}}{T} - 1\right)$$

or

$$V_l = (2\delta - 1)\, V_s \qquad . \qquad 4.2.5$$

where,

$\delta \left(= \frac{T_{on}}{T}\right)$ is the duty cycle

From eqns 4.2.3 and 4.2.5 we can see that, if the drop across the armature resistance is neglected, for getting motoring action in any direction the duty cycle δ must be in the range

$$0.5 < \delta \leq 1 \qquad . \qquad 4.2.6$$

Complete motoring action concepts are illustrated in fig 4.3(d)

From eqns. 4.2.4 and 4.2.6, we can find the relation between the current ripple and duty cycle as

$$\Delta I_a = \frac{2\delta(1 - \delta)}{L_a} V_s T \qquad . \qquad 4.2.7$$

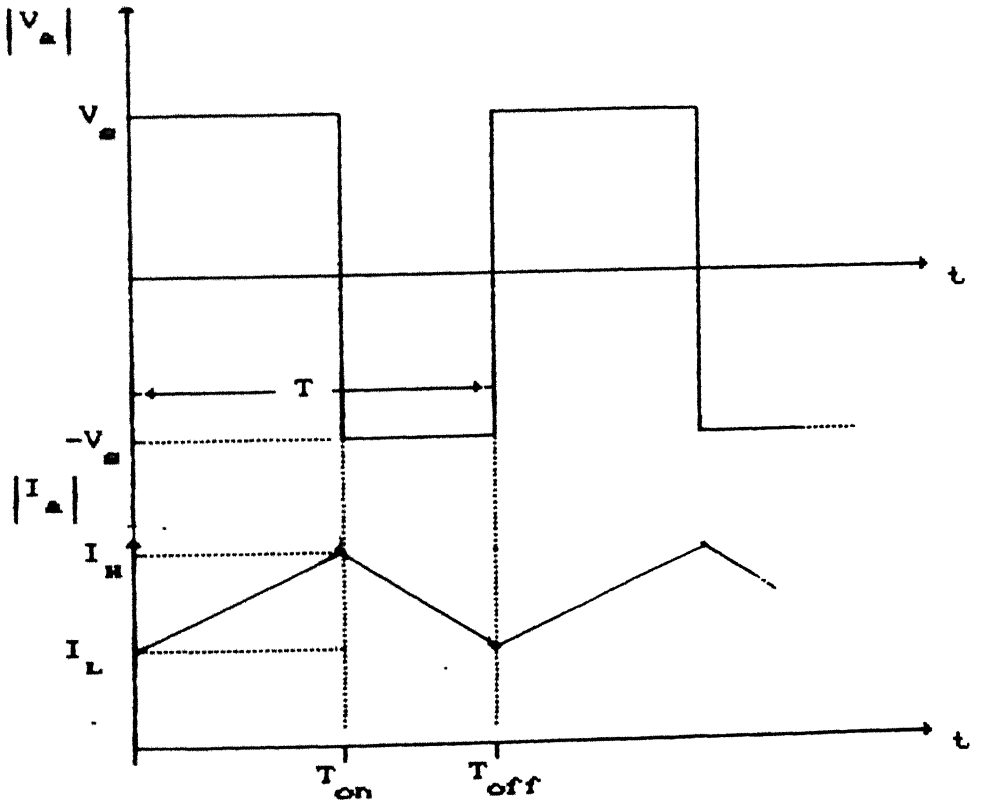

Fig. 4.3 (c) Voltage and Current waveforms

From this eqn we can see that maximum ripple in current results when $\delta = \frac{1}{2}$, which is given by

$$\Delta I_{max} = \frac{V_s T}{2L_a} \qquad \ldots \quad 4.2.8$$

This equation shows the dependence of the current variation on the switching period T, supply voltage V_s and armature inductance L_a. Since for a given motor V_s and L_a are fixed, to reduce the ripple in current we have to choose T properly. For the motor we are using in our experiments

$$(V)_{max} = 230 \text{ V}$$

$$L_a = 70 \text{ mH}$$

$$(I_a)_{max} = 0.4 \text{ A}$$

If we allow a maximum ripple of 40% of $(I_a)_{max}$, we can find from eqn. 4.2.8 that a switching period of 100μs is required. According to this switching period

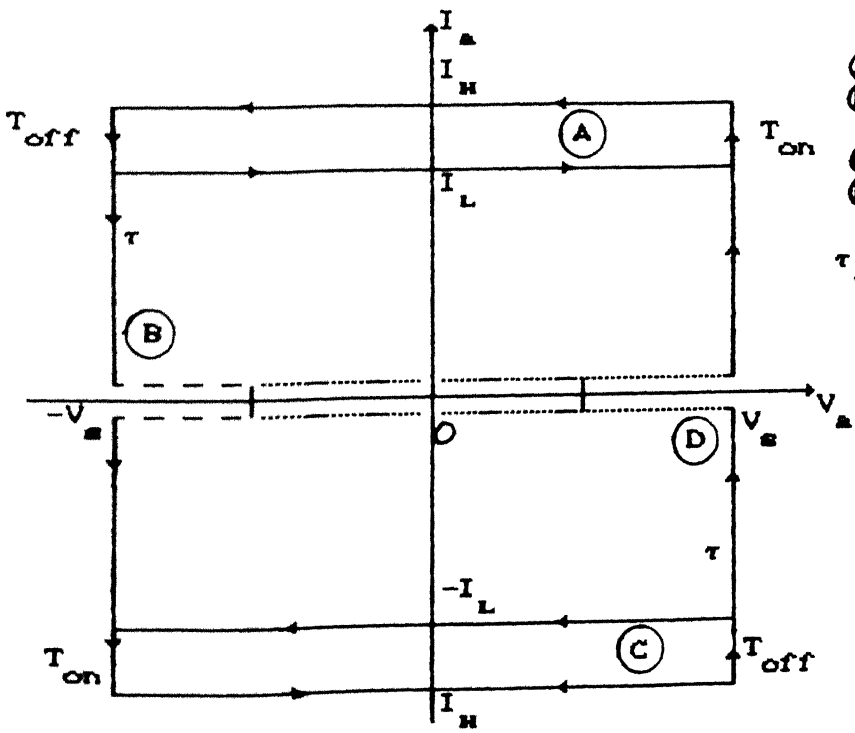

Fig. 4.3 (d). Illustration of the motoring action with the adopted Switching-Scheme

requirements we have chosen a switching frequency of 10 KHz

4.3 Functional Block Diagram of the Motor-Drive Circuit

Fig 4.4 shows the block diagram of the overall scheme that is realized for driving the separately excited DC motor

The control signal from the Master Controller is fed to a Pulse Width Modulator stage, which produces pulses of constant frequency and whose on period changes according to the input signal. The block shown as Current Limiter comes into picture during the transient operations of the motor. Under transient operations such as starting, braking, speed overloads, the current through the motor or the chopper may exceed safe values. The purpose of Current Limiter is to prevent the current from exceeding safe values. If the current I_a through the motor is less than the maximum permissible value, the motor operation is not affected by this limiter.

The operation of the Current Reversing Controller, can be explained as follows The Current Reversing Controller is used to reverse the armature current (so as to reverse the rotation of the motor) by stopping the pulses to the outgoing pair of switches and releasing the pulses to the other pair after a dead time τ_d The dead time is needed to enable the outgoing switches to stop conducting and to let the current fall to zero before it is reversed. At the end of the deadtime the Current Reversing Controller goes out of action.

The Gating Circuit sends the appropriate signals to the Driver Circuit by monitoring all the signals from the blocks, just described, so that no damage occurs in the power circuit.

The purpose of the Driver Circuit is to translate the control signals received from the Gating Circuit to the control signals required to operate the

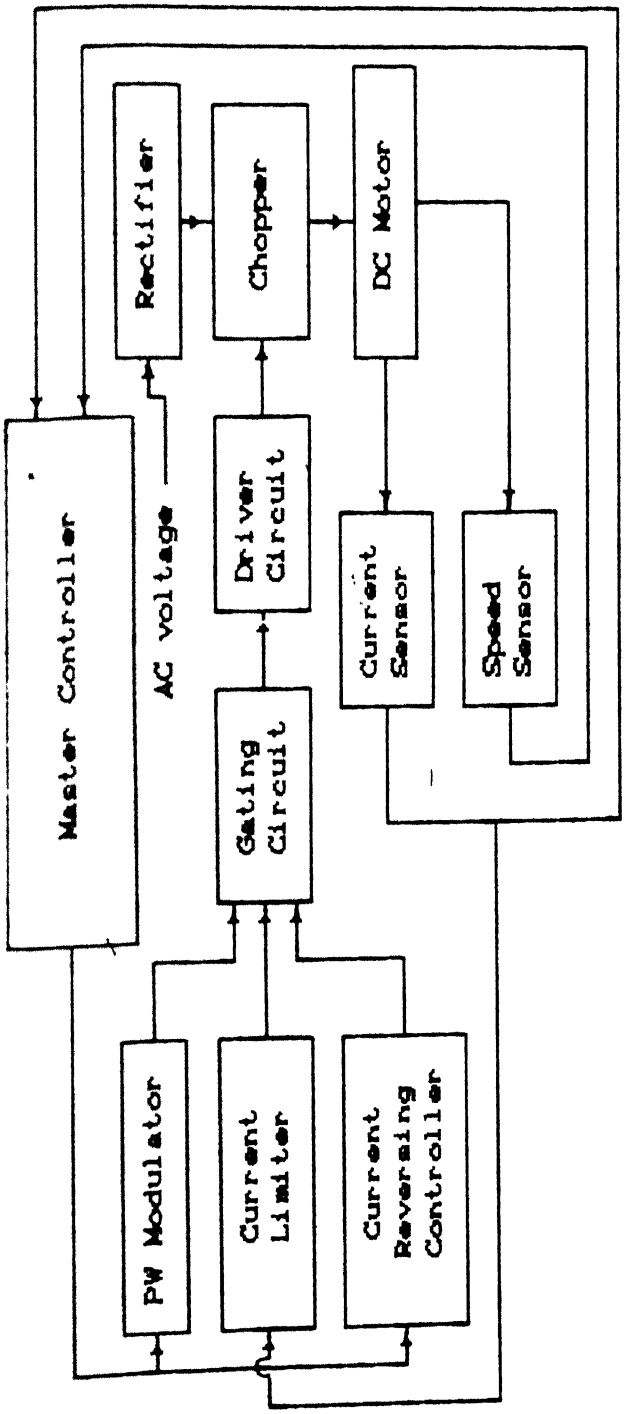

Fig 4.4 Schematic Diagram of the Motor Control

switches properly This is because the minimum current requirements of practical motors are higher than what gate can supply Depending on the size and ratings of the motor, a suitable driver must be selected to take the control signals from the gates and deliver the necessary voltage and current to the motor The Driver design must accommodate the requirements of the inrush currents of the motor during starting as well as during reversal

Another major function provided by the Driver Circuit is isolation between the power ground and the Control circuit. A popular method of coupling the logic circuit to the power circuit is through an opto-coupler or a pulse transformer The advantage of using pulse transformers as isolators is that they do not require any floating supply on the secondary side But the major disadvantage with this is that the duty cycle of the driving pulses must be less than about 70% as the transformers cannot handle DC voltages. On the other hand opto-couplers can handle any signal from DC to very high frequency But they require a floating power supply on the power circuit side.

In order to limit the currents to safe values all closed loop systems are operated either with an inner current control loop or current limit control loop, which is already discussed. Consequently to implement these control loops we require an arrangement for sensing current. Since the current need not be precisely controlled, approximate sensing of current signal is required. Similarly, faulty conditions involving short circuit, overload, switch failure etc can be detected by current sensing. Here also only approximate sensing of the current signal is required. The closed loop current controlled systems designed to supply regulated current may however, require precise sensing of current.

For speed sensing there are two methods. In one method, since the speed is proportional to the back emf at a constant field, speed can be sensed by measuring

the back emf ($V - I_aR_a$), where R_a is the armature resistance. A more direct method of measuring speed, is by using a tachometer driven from the motor shaft, is used in our experiments.

4.4 Chopper and Control Circuits

In this section the actual chopper circuit and the control circuit realized will be discussed.

4.4.1 Chopper Circuit

The Chopper configuration shown in fig. 4.3(a) is realized along with a protection as shown in fig. 4.5. The source for supplying the power to the DC motor is realized using a Bridge Rectifier and a Capacitor Filter as shown. A capacitor of 400 μF. is chosen by keeping the motor current ratings, which are given in section, in view.

Transistors which replace the switches of fig. 4.3(a) are chosen to satisfy the requirements of the motor used. They can handle voltages and currents up to

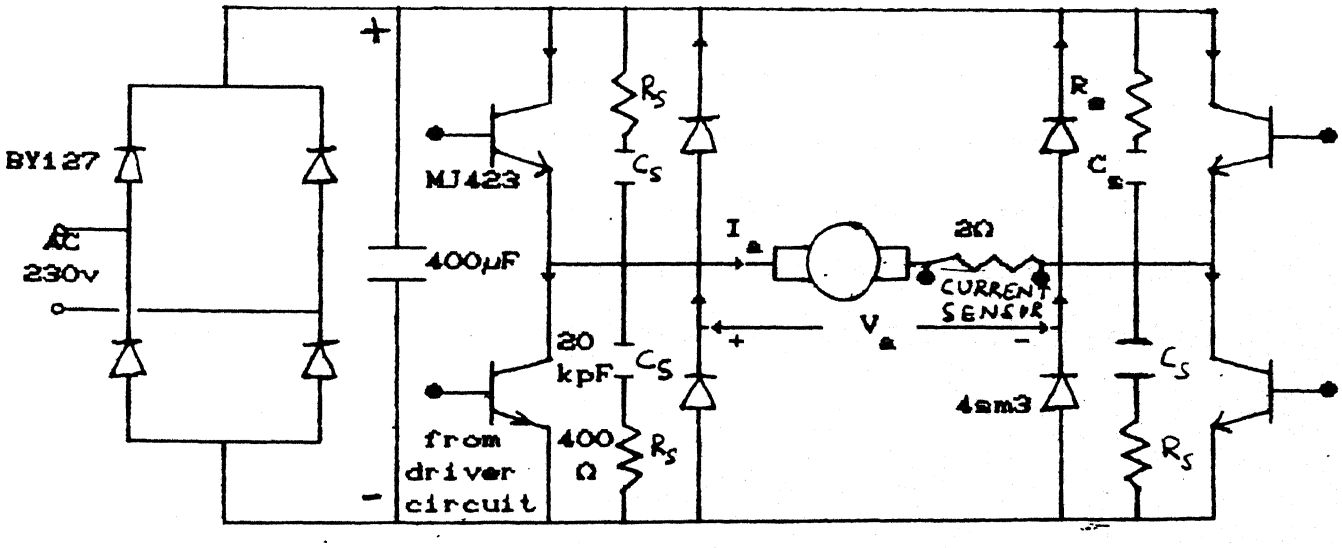

Fig. 4.5. Realized chopper circuit using transistors

400 V and 1 A, respectively Free wheeling diodes should be chosen depending on the requirements of switching-off-times of the transistors The switching of diodes should take place so as to provide path for the motor current as soon as the transistors are turned off.

Each transistor and diode are provided a snubber circuit for over voltage protection The snubber circuit protects these devices against voltage transients due to the reverse recovery. Snubber network values are obtained from the following relations

$$C_S = \frac{I_{Cmax}\, t_1}{V_{CEmax}} \quad \ldots\ldots \quad 4.4.1$$

where,

I_{Cmax} is the maximum collector current of the transistor MJ 423 (= 1 A)

V_{CEmax} is the maximum collector to emitter voltage that can be sustained by MJ 423 (= 400 V)

t_1 is the minimum turn-off time of transistor (= 4 μs)

$$R_S C_S = t_2 \quad \ldots . \quad 4.4.2$$

where,

t_2 is the minimum turn-on time of the transistor (= 2 μs)

According to the specifications (shown in brackets) of the transistors the snubber is realized as shown in figure and the values of snubber capacitor and resistor are chosen as R_S = 400Ω and C_S =20kpF.

The 2Ω resistor in series with the motor shown in fig. 4.5 is used for sensing the motor current. This resistor should be chosen so that it does not affect the electrical time constant of the motor, but at the same time should provide enough sensitivity for current measurement. The two ends of the re are connected to the Current Sensing Circuit, which is explained in the sect follow.

4.4.2 *Driver Circuit*

From the specifications of the motor, we see that at full load a current of 400 mA flows through the motor As the power transistors used can provide a current gain (h_{fe}) of 30, the minimum base current requirement for the power transistor, at full load is about 15 mA. But we shall always provide a over drive of at least 50% for proper functioning of transistors To turn-off the transistors at faster rates it is required to remove the base stored charge, which otherwise cause some short circuit problems. To perform this, we have to force the base of the power transistors to a negative voltage with respect to the emitter Keeping these requirements in view, we have selected a floating supply of ± 6V (fig. 4.6(a)).

The Driver Circuit, which is designed to fulfill the above requirements is shown in fig 4.6(b) The optocoupler 6N136 shown in figure has a Current

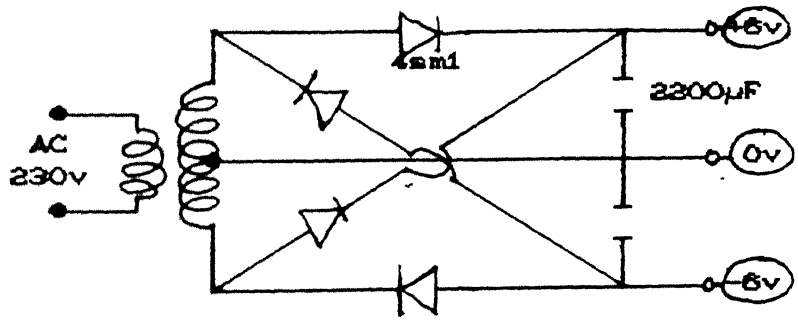

Fig. 4.6 (a) Floating supply for the driver circuit

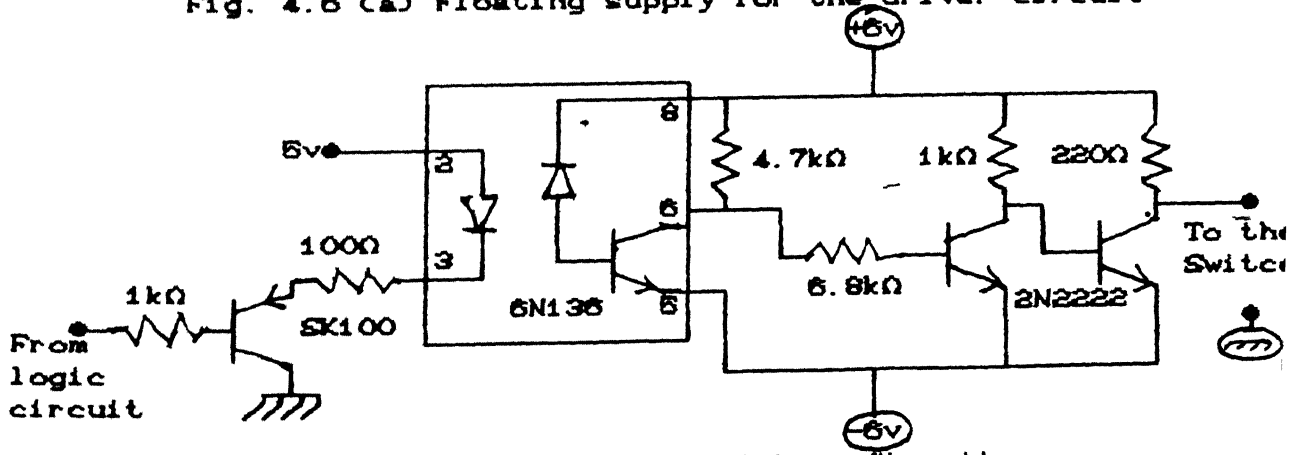

Fig. 4.6 (b) Driver Circuit

Transfer Ratio of 15% which is defined as the ratio of the output current to the input current This can take a maximum input current of 50 mA Therefore, this opto-coupler cannot handle the currents required for driving the power transistor It is, in fact, advisable to operate these opto-couplers at reduced currents rather than at full loads to avoid degradation due to the causes like reduction in efficiency of the emitter, decrease in the transmission of the optical path, reduction in responsivity of the opto-coupler etc Keeping this in view, we have provided some intermediate current gain stages using the transistors 2N2222 and SL100

4.4.3 Pulse Width Modulator (PWM)

The use of pulse width modulation provides an energy efficient method of controlling the motor speed by varying the average voltage applied to the armature winding. For generating Pulse-Width Modulated signals there could basically be three different approaches.

(i) Complete Software to generate pulses

(ii) Programmable Timer Peripheral

(iii) Hardware having DC voltage input through DAC

In an open loop system, the controller spends an insignificant amount of time on controlling the motor. In such a case option (i) could be allright But, in a closed loop system the controller has to continuously monitor the speed and adjust it according to the program and feedback. In this case, the controller may have to spend more time on computations required for the implementation of the closed loop control and therefore, (i) will be a software overhead to the controller. We can avoid this with the options (ii) and (iii). (ii) involves lot of cost and consequently we have adopted the last option which involves simple hardware.

The circuit shown in fig 4 7(a) is the one which gives out a digital pulse ain with the pulse width proportional to the analog input voltage The outputs this are two pulse trains, one for controlling the clockwise rotation of the)tor and the other for the anticlockwise rotation The master controller which

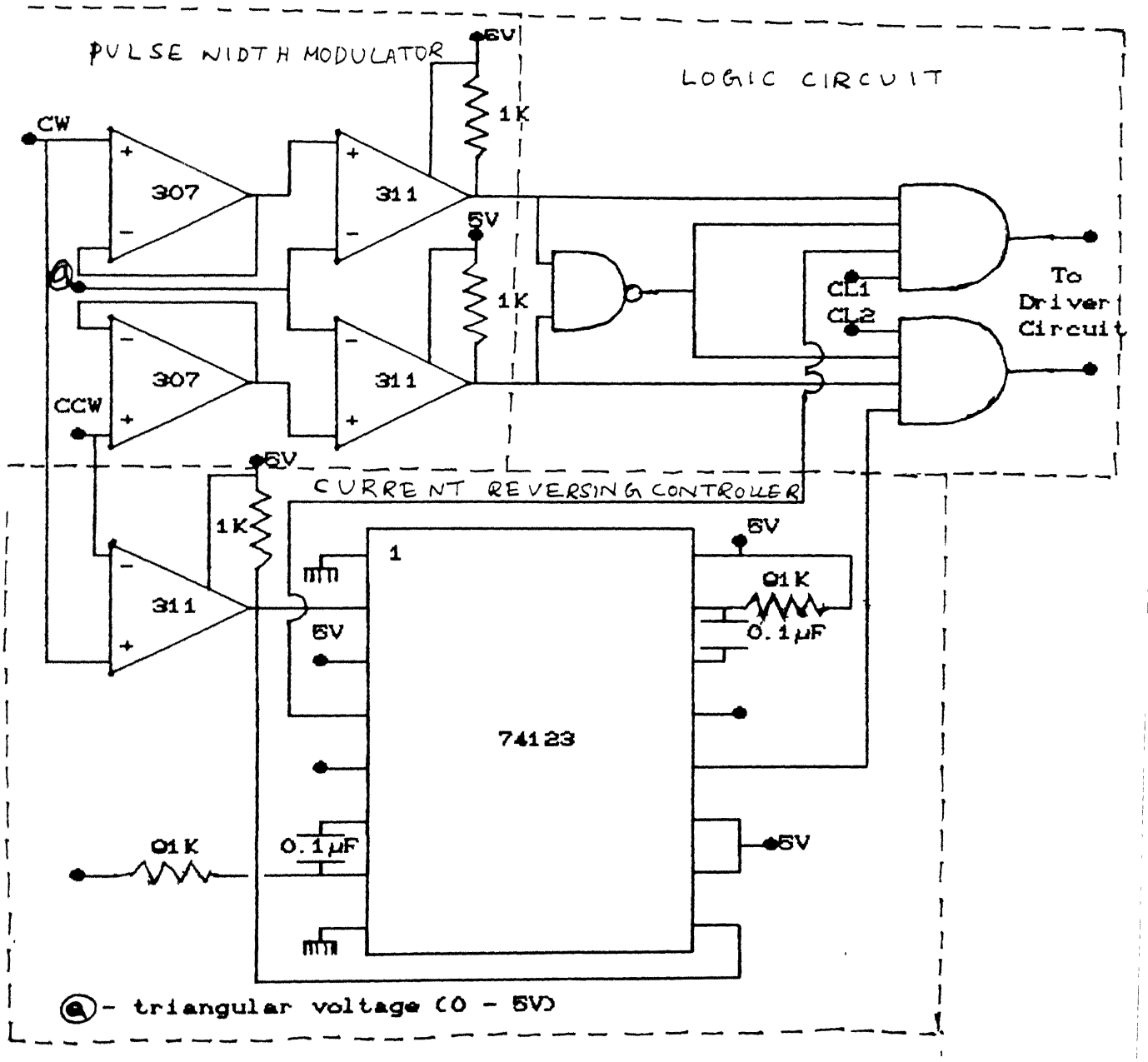

Fig. 4.7(a). CONTROL CIRCUIT

delivers the analog control voltage ensures that at least one signal of the two input signals marked by CW direction and CCW direction will be zero at a given instant so that no over-lapping of the control pulses occur The Pulse Width Modulator compares this analog voltage with a 10 khz triangular voltage to generate the switching pulses The triangular voltage, which eventually controls the chopper operating frequency, is so chosen to keep the ripple in the motor current within acceptable limits

4.4.4 Current Reversing Controller

The circuit diagram of Current Reversing Controller are shown in fig. 4.7(a). This controller continuously monitors the signals from the Master Controller and provides the dead time required for the current reversing operation The two signals from the master controller are compared with each other and whenever it is required to reverse the motor current the comparator produces either a positive going edge or a negative going edge. This output is fed to two monostable multivibrators, one of which is positive edge triggered and the other is negative edge triggered The duration of this monostable output pulse is basically dictated by the electrical time constant of the DC motor that is used The motor we have used has got an electrical time constant of 1 ms So we have selected the monostable period as 3 ms, which will ensure that the current has fallen to zero.

4.4.5 Current Sensor

This sensor continuously monitors the current flowing in the switches and the motor and gives a signal which is proportional to the same. The motor current is converted into a voltage by inserting a small resistor in series with the motor. The output of the shunt is filtered by a low pass RC filter to remove ac components and given to an opto-isolator stage (fig 4.7(b)). The constant current

source biases the LED at 2.6 mA quiescent current. The resistor R can be selected to accommodate any desired input range and this changes the current through the LED of the opto-coupler, which in turn changes the voltage at it's output stage.

4.4.6 Current Limiting Controller

The over-current monitor is designed to prevent the severely overloaded conditions which might occur due to the reasons which are already explained in section 4.3. The circuit used for this purpose is also shown in fig 4.7(b). The signal from the current sensor is fed into one of the two inputs of the comparator, while the other is driven by a presettable reference. During an over-

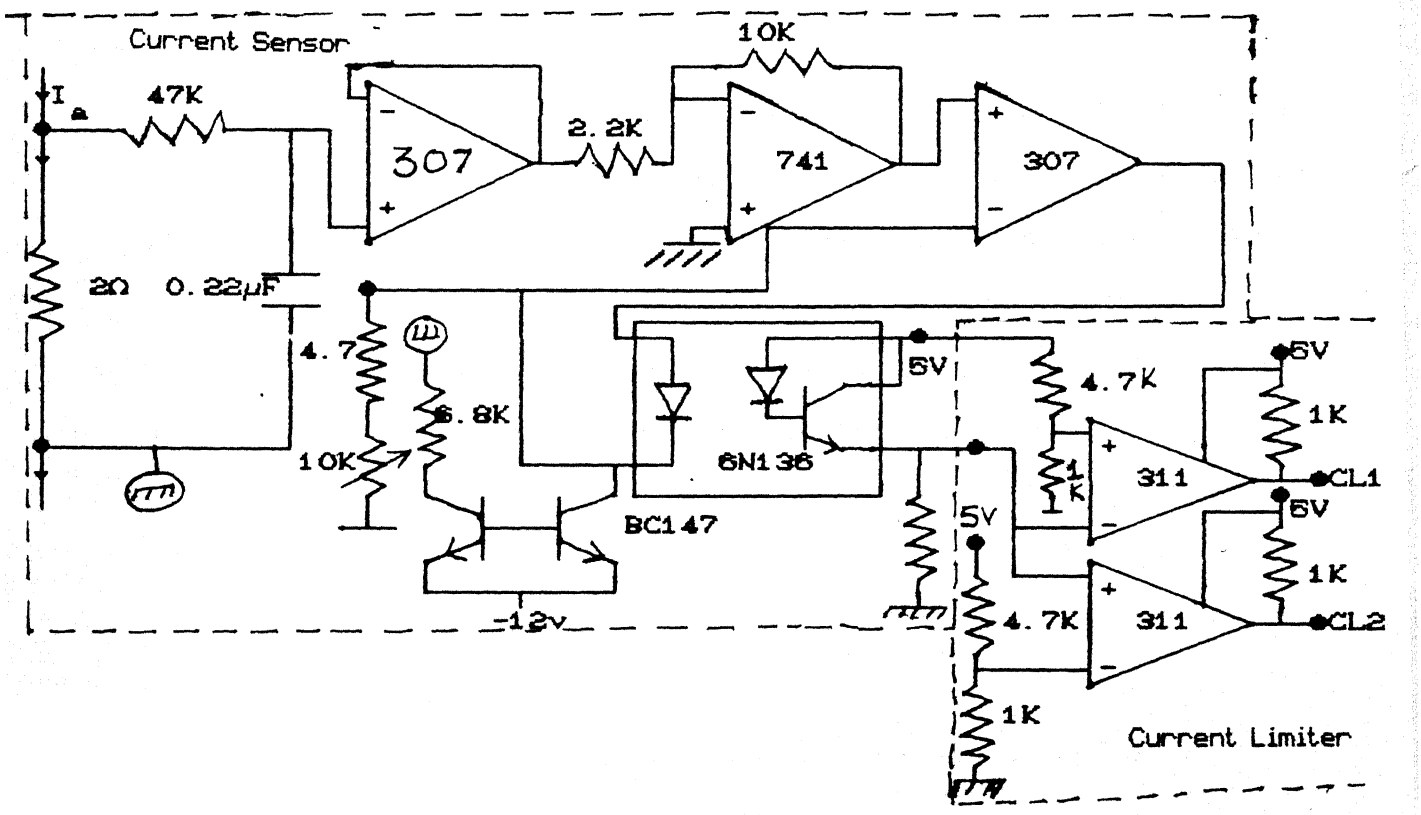

Fig.4.7 (b) Current Sensor and Limiter

current condition, the comparator will turn off and disable the logic circuit that is driven by this Resumption of normal operation will commence when the current falls below the maximum limit

4.4.7 Logic Circuit

The circuit shown by dotted lines in fig 4.7(a) monitors all the control signals and delivers the **actual** control signals required for the ***safe*** operation of the chopper

4.4.8 Tachogenerator Circuit

The tacho signal voltage is proportional to the motor speed A simple RC low-pass filter is added to the tacho-generator to eliminate the ripples in the voltage output. The sensitivity of the tachogenerator is found to be 2.3 V/rpm

4.5 Conclusions:

This chapter described the actual experimental setup used to study the control of inverted pendulum Motor selection is done after calculating the power and speed requirements of the system obtained from the simulation studies. For the selected motor, a 4-Quadrant Chopper, which is quite commonly used for driving high power motors, is designed and vrious design aspects are also given The designed circuit is tested and found to be functioning satisfactorily

Chapter 5
Experimental Results and Conclusions

In the preceding chapters we have discussed the design issues and simulation results. In this chapter practical implementation of the controllers is discussed. Thesis is also concluded in this Chapter with some suggestions for future work.

5.1 Computer control

The controller and observer discussed in Chapter 3, could have been implemented using analog computers which involves few operational amplifiers and passive components like resistors and capacitors. But for doing the friction compensation discussed in Chapter 2, we need to do on-line parameter identification. However, this requires many computations as dictated by the implemented algorithm. To perform these computations, we need to have either a computer or a microprocessor. But implementing adaptive control algorithms using a microprocessor requires assembly language programming which involves lot of software. Of course, as is well known, this would reduce the computation time required for implementing the controller. But if the closed-loop system does not demand a very low sampling period we can afford to write software in high level languages.

For implementing the adaptive controllers, we do not necessarily need a computer. As a matter of fact, these controllers are being implemented using some Digital Signal Processor(DSP) chips also. The advantages of using these chips are improvement in computation time and reduced cost. Intensive research and development work is in progress to develop such chips in VLSI circuits[18].

An IBM PC-XT with 8087 numeric Co-processor and 10 MHz. clock generator is

used to implement the adaptive controllers described in Chapter 2. The numeric co-processor and clock generator were helpful in reducing the computaion time For Data Translation, i.e. for Analog to Digital conversion and Digital Analog conversion, a 12-bit AD-DA Card (PCL-205 manufactured by Dynalog-Micro Systems) is used. This card contains ADC channels for measuring all the three process variables, namely cart position, velocity and pendulum position and as well as DAC channels for sending the appropriate control signals for driving the motor This card is selected because of its low conversion time ($< 30\mu s$) and resolution (12-bit). The software is written in TURBO pascal. During the experiments, the process variables are stored in arrays. This reduces the computation time as the data transfers between system memory and buffer takes more time. Finally, the PCL-205 card just described is connected to the IBM-PC at 220H address. More details of this can be found from IBM-PC/XT and PCL-205 manuals.

5.2 Speed Control of DCMotor

In this section, some implementation aspects and experimental results of the controllers described in Chapter 2 are discussed.

In Chapter 2, we have described a current controller for doing the speed control. However, in practice it is not possible to feed the required current to the motor and usually voltage can be controlled easily. So we should in some way, be able to convert the required current into voltage which can provide the required torque to maintain the desired speed For achieving this task we have adopted the following procedure.

The armature voltage equation of a DC motor is given by

$$V_a = I_a R_a + L_a \frac{dI_a}{dt} + E_b \qquad \ldots\ldots \quad 5.2.1$$

where,

V_a is the voltage applied across the motor

I_a is the current flowing in the armature of the motor

R_a is the armature resistance

L_a is the armature inductance

E_b is the motor back emf

For a separately excited DC-motor, Back emf E_b is proportional to the speed, therefore,

$$E_b = K_b\omega(t) \quad \ldots\ldots \quad 5.2.2$$

Substituting this in eqn 5.2.1, we get

$$V_a = I_aR_a + L_a\frac{dI_a}{dt} + K_b\omega(t) \quad \ldots\ldots \quad 5.2.3$$

This is now discritized using the rectangular rule to obtain

$$V_a(k) = I_a(k)R_a + L_a\frac{I_a(k) - I_a(k-1)}{h} + K_b\omega(k) \quad \ldots\ldots \quad 5.2.4$$

where h is the sampling period and k is the sample number.

This equation suggests that a current $I_a(k)$ will flow in the motor which is running at a speed of $\omega(k)$, if there is an initial current of $I_a(k-1)$, and if we apply a voltage of $V_a(k)$. Or, in other words, to get a current of $I_a(k)$ we shall apply a voltage of $V_a(k)$ with the other conditions as just stated. This is the principle we have used in our experiments. Once we know the voltage to be applied we can control the duty cycle of the chopper described in Chapter 4 accordingly The following relation, which can be deduced from eqn. 5.2.4, is found to be efficient for implementing.

$$V_a(k) = V_a(k-1) + R_a(I_a(k) - I_a(k-1)) + \frac{L_a}{h}(I_a(k) - 2I_a(k-1) + I_a(k-2)) + K_b(\omega(k) - \omega(k-1)) \quad \ldots\ldots \quad 5.2.5$$

From the above discussion, we can summarize the algorithm used for controlling the speed as follows.

step 1: Measure the speed of the motor with the help of tachogenerator

step 2: Compute the current $I_a(k)$ required to get the reference speed $\omega_r(k)$

using the current controller described in section 2.2

step 3. Compute the voltage $V_a(k)$ form eqn. 5.2.5

step 4: Increment k and goto step 1

The parameters of the motor used are given below

R_a = 96 Ω

L_a = 70 mH

K_b = 0.9508 at 30 mA field current

To test the effectiveness of the above mentioned scheme for implementing the controllers of Chapter 2, several experiments were carried out The computation times required for implementing the controllers are different - it is minimum for the PI Controller and maximum for the Self-Tuner. As is known, these time delays encountered in this process may have significant effect on the system response. Therefore, it is important to know the effects of this sampling period on the system response and to know if there are any advantages of using PI Regulator using low high frequency sampling. Another important aspect in the implementation of Controllers on digital computers is the effect of quantization errors. To study the performance of the controllers due to the mentioned problems and to evaluate the controllers of Chapter 2, experiments described below are performed. The design parameters that were varied consisted of the sampling period, proportional and integral gain constants.

Figs. 5.1 to 5.4 show the speed of the motor for various reference signals, ω_r, with PI controller when the above mentioned design parameters are changed. The computation times required for implementing various controllers are given below.

For PI Controller = 3 msec

For friction compensation with constant gain regulator = 16 msec

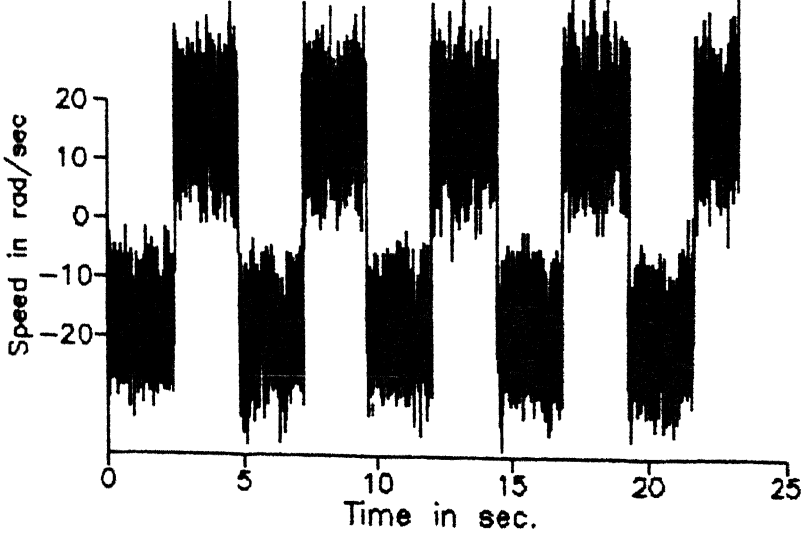

(a) T = 3 msec

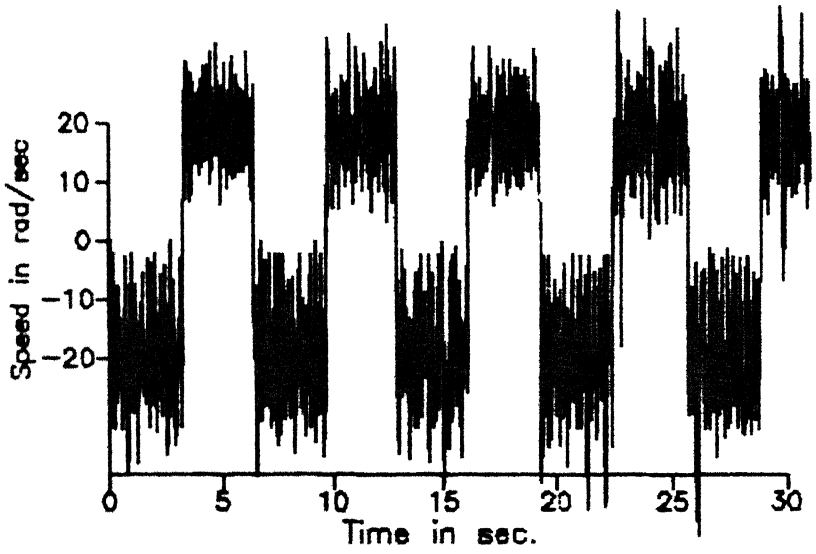

(b) T = 16 msec

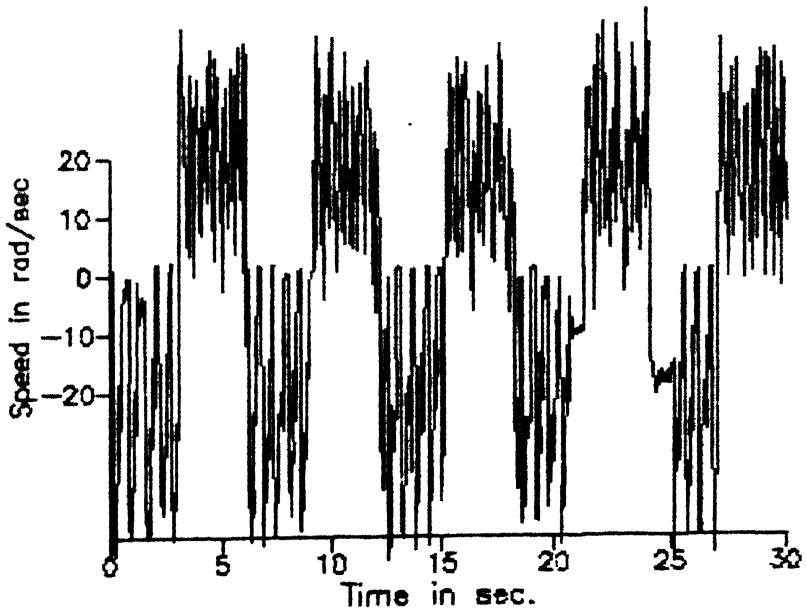

(c) T = 30 msec

Fig. 5.4 SPEED CONTROL WHEN ω_r = ±20

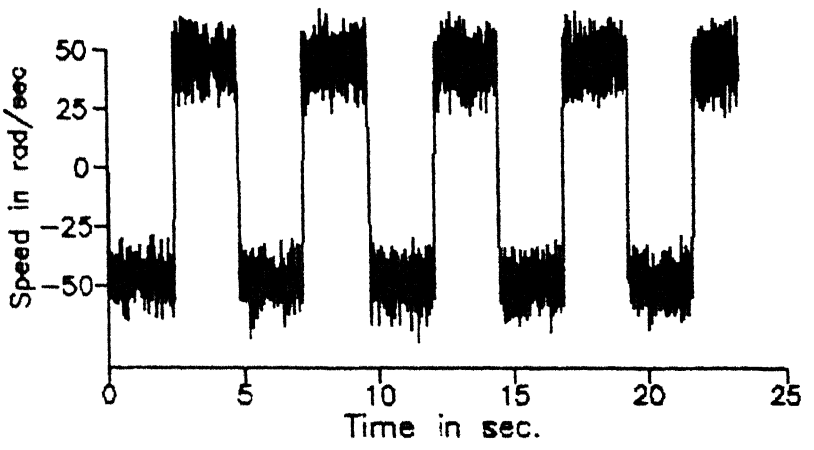

(a) T = 3 msec

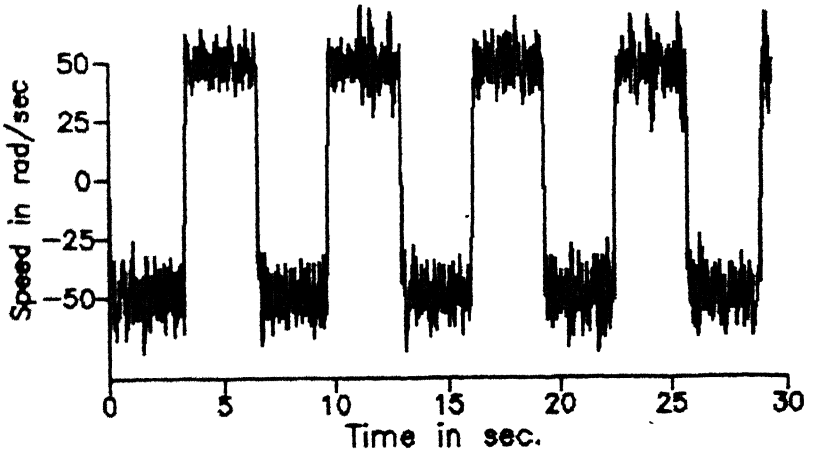

(b) T = 16 msec

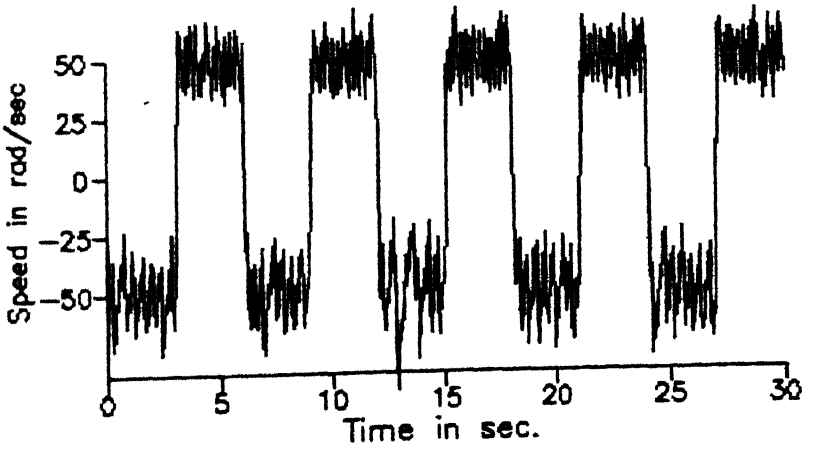

(c) T = 30 msec

Fig. 5.2 SPEED CONTROL WHEN $\omega_r = \pm 50$

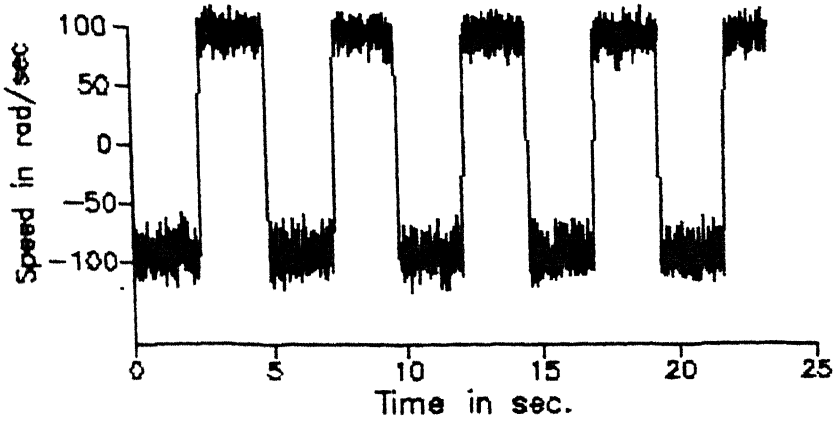

(a) T = 3 msec

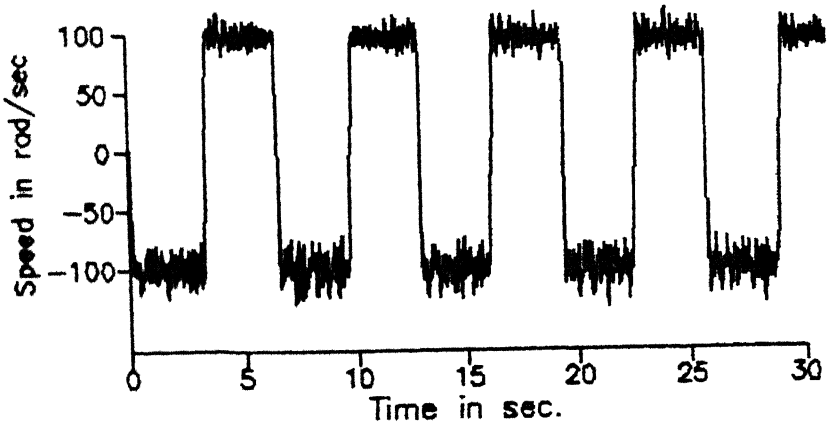

(b) T = 16 msec

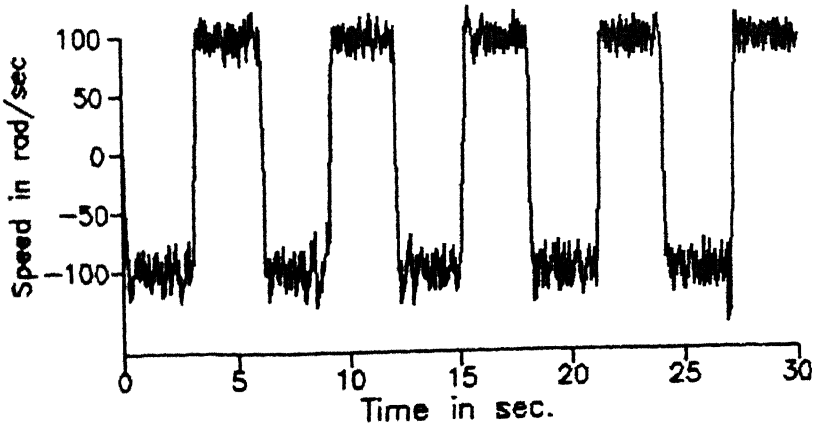

(c) T = 30 msec

Fig. 5.3. SPEED CONTROL WHEN $\omega_r = \pm 100$

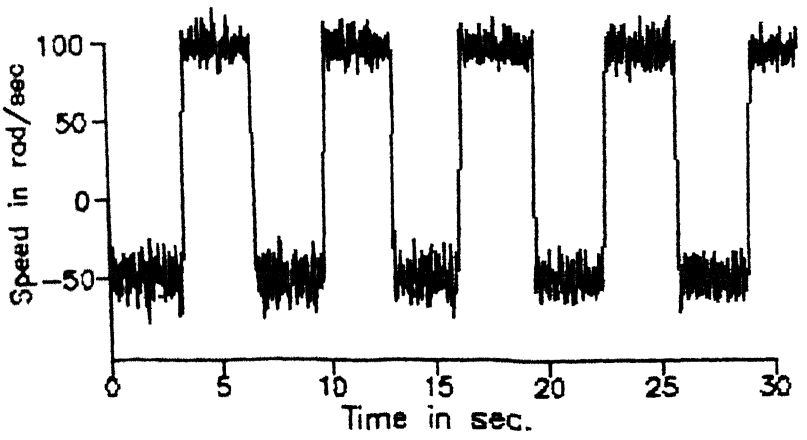

Fig. 5 4. SPEED CONTROL WHEN ω_r = 100 and -50 WITH T = 16 msec

For friction compensation using Self-Tuner = 28 msec

According to these requirements, the sampling periods for carrying the experiments are chosen as 3 msec, 16 msec and 28 msec respectively. These sampling periods along with the parameters given in Table 2.1 are used to compute the remaining controller parameters, from eqns. 2.2.4 and 2.2.5. The results shown in figs. 5.2 to 5.5 demonstrate that the PI Controller performance is consistent at all the sampling periods and there is no special advantage in using a low sampling period. Therefore, the performance can only be improved for the same controller with the help of the adaptive friction compensation control.

From these experiments it is also observed that at low reference signals (figs. 5.1(a), (b) and (c)) the quantization errors have an adverse affect on the performance of the closed-loop control system. The poor performance can also be accounted for the low sensitivity of the tacho-generator used and the friction characteristics at low speeds due to the gears.

Finally, because of the high noise signals present in the speed and current measurements we were unable to perform the adaptive friction compensation experiments. This would require additional experiments on the properties of the noise present, which were not carried out due to the shortage of time. Once we know the properties of the noise present then we can use some noise-canceling filters and eliminate the noise. With this noise elimination, the algorithms developed in Chapter 2 can be used for friction compensation.

5.3 Control of the Inverted Pendulum

This section is concerned with the stability of the developed Inverted Pendulum system. In this section two experiments, one concerning with the control of the inverted pendulum and the other with the control of the Cart position on the rails are discussed. The later is performed to study the effect of feedback

matrix which results from different weighing matrices on the closed loop system. Here also, we were unable to completely study the concepts discussed in Chapter 3, i.e the effect of the feedback matrix on the overall system, because of the poor performance of the motor used. But, nevertheless we have tried to study these effects by controlling the Cart position.

In the first experiments, i.e. in the control of position of the cart, we assumed that the pendulum is in the erect position. The measurements that are available are the position and the velocity of the cart. The control required is obtained from

$$u(t) = k_1x_1(t) + k_2x_2(t) + k_3x_3(t) + k_4x_4(t)$$

where the k_i's are obtained by solving the Riccati eqn. 3.2.2.

Figs 5.5 to 5.9 illustrate the responses obtained for various values of k_i's, which are indicated in the respective plots. From these plots we can see that the responses obtained are essentially similar to those which are obtained from the simulations of Chapter 3.

Finally, for the control of the inverted pendulum we have the available measurements of three states namely pendulum position, cart velocity and position. Therefore, we need an observer of order 1 to estimate the fourth state, i.e. the velocity of the pendulum. The observer is designed from the relations given in section 3.3 and the parameters are given below.

$$L = 10 \quad F = -12.3981 \quad G = 185.651 \quad H = -13.16$$

The sampling period is found out to be equal to 4 msec. The parameters of the system are given in Table 3.2. The maximum torque available from the motor used is 0.3 N-m. Accordingly, we can obtain the stable zone, from 3.4.4, as

$$|\theta| \leq 4 \text{ deg.}$$

$$|r| \leq 0.3 \text{ m}$$

Fig. 5.5 CART POSITION CONTROL WHEN k_1 = -50.86 k_3 = -4.433

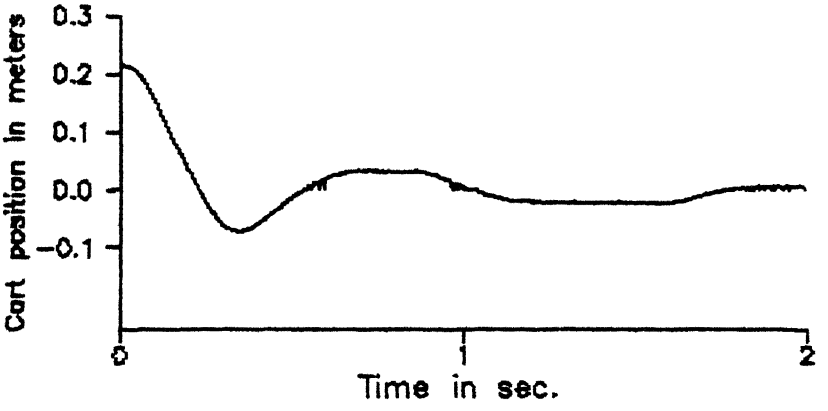

Fig. 5.6 CART POSITION CONTROL WHEN k_1 = -20.6 k_3 = -2.25

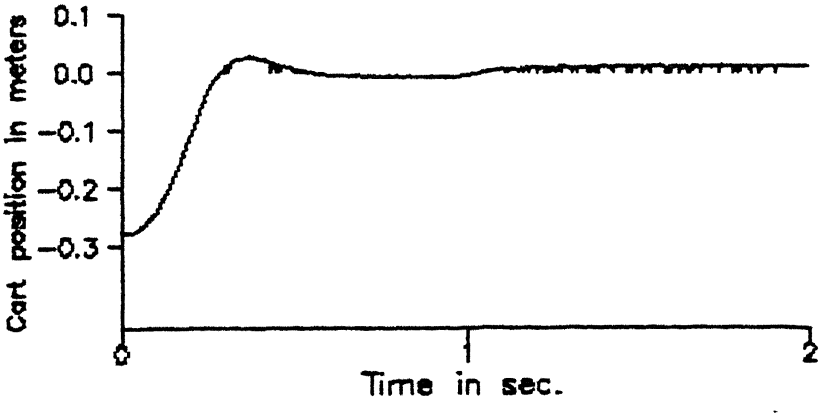

Fig. 5.7 CART POSITION CONTROL WHEN k_1 = -40.86 k_3 = -4.433

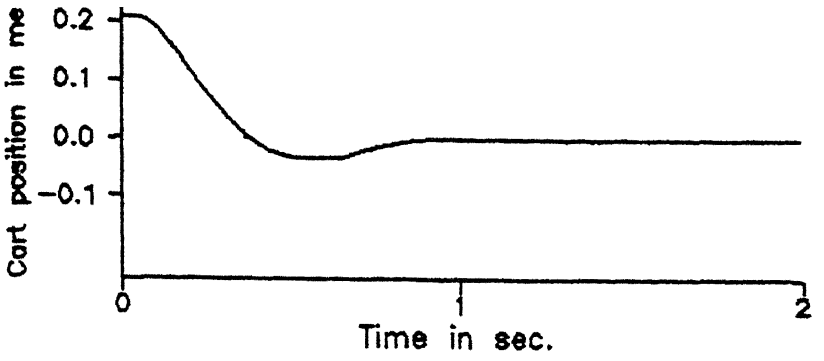

Fig. 5.8 CART POSITION CONTROL WHEN k_1 = -10.86 k_3 = -2.433

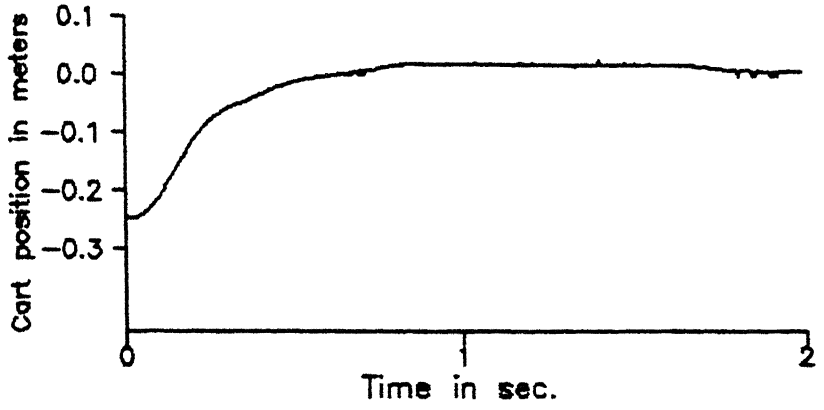

Fig. 5.9 CART POSITION CONTROL WHEN k_1 = -50.86 k_3 = -10.433

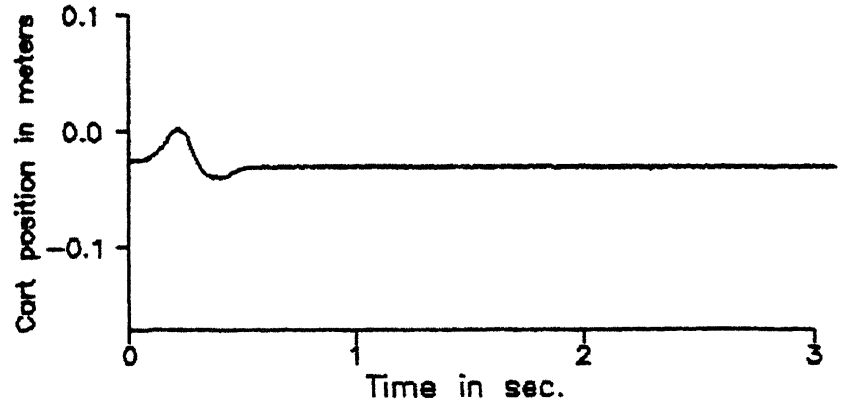

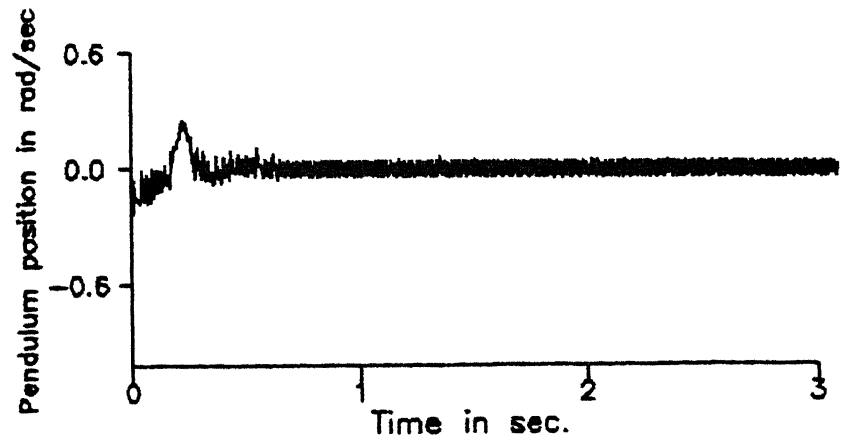

Fig. 5.10 CONTROL OF THE INVERTED PENDULUM
k_1 = -18.56 k_2 = -35.43 k_3 = -11.411 k_4 = -4.102

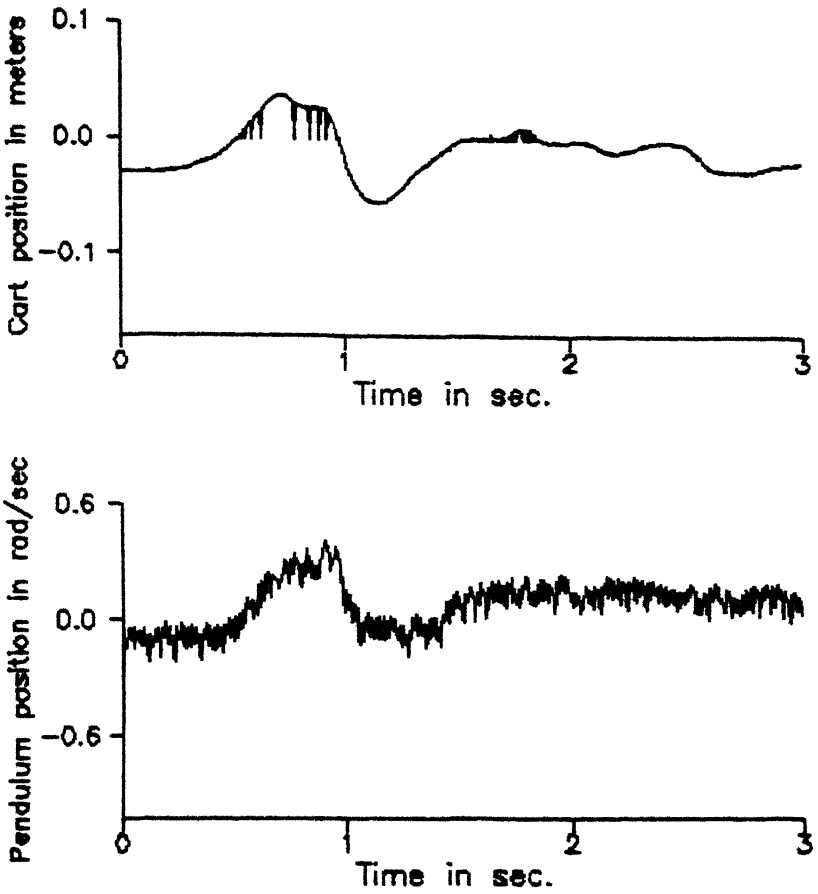

Fig. 5.11 CONTROL OF THE INVERTED PENDULUM
$k_1 = -58.6831$ $k_2 = -82.411$ $k_3 = -32.69$ $k_4 = -9.65$

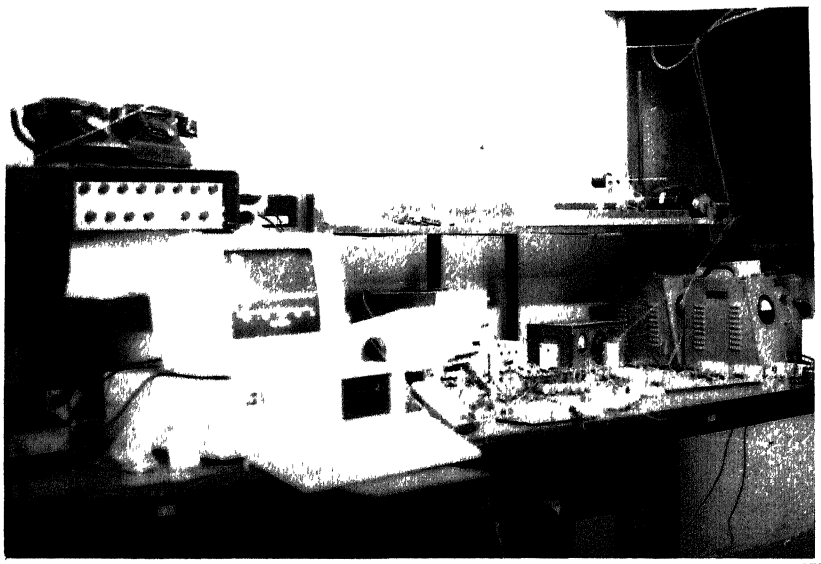

Fig. 5.12. Stabilized Inverted Pendulum

From this stable zone we can see that the pendulum can only be stabilized if it is within this zone. But due to the measurement noises present it is very difficult to achieve this. The stabilization of the inverted pendulum can be done only if the pendulum is restricted to the above mentioned stable zone, which is difficult due to various noises present in the measurement. To keep it in this zone we have tied the pendulum to the vertical using a string so that it can move freely in this zone The results obtained thus are shown in figs. 5.10 to 5.11. The inveted pendulum thus balanced is shown in the photograph (fig. 5.12).

From the experiments we have observed that the errors due to the linearization of the system around the vertical position, the non-linear friction of the gears, and the time constants of the motor play a crucial role in the stabilazation of the inverted pendulum. This non-linear friction can be eliminated with the help of the adaptive friction compensation techniques discussed in Chapter 2.

5.4 Conclusions and Scope for Future work

In this thesis we have developed a control system which is inherently unstable and whose dynamics are basic to study tasks involving the maintenance of balance, such as walking and the control of rocket thrusters. Effects of the non-linear friction present in robots and high-performance servo applications have been studied. Various controllers including a proposed self-tuner for compensating these friction effects are also discussed.

We have discussed some methods to develop the mathematical model of the simple inverted pendulum. It is also reviewed how this simple inverted pendulum model is useful in studying the legged machines, biped locomotion problems etc. Controller is designed for the stabilization of the inverted pendulum based on the LQR theory. The control system developed can also be used to study many other

aspects of the state-space control theory for example design of Kalman-filter for eliminating the noise present in the measurements. Unfortunately, due to the nonavailability of some requirements we couldnot verify all the aspects discussed. But nevertheless simulation results have been provided for explaining various aspects.

Finally, the controllers described in Chapter 3 require considerable knowledge of the system to be controlled, including an accurate model of the dynamics of the system. When this information is not known *"a priori"* then some learning systems must be developed to obtain control, which can stabilize the inverted pendulum.

Neural nets are a typical example of these learning systems. These systems must learn to generate successful action sequences by acquiring the function which maps the current state into control actions. This control, which is known as **Linguistic Control** is expressed by the logic:

If cart is far left and cart is hardly moving and pendulum is hardly leaning and pendulum is swinging to the right then apply force right

Finally, as discussed in Chapter 1, this simple model can be used to study many of the aspects of Biped locomotion. These studies can be further intensified with the help of recent developments in **Neural Net Controllers**.

References

[1] K J Astrom, B Wittenmark, *Self-Tuning Regulators based on pole-zero placement*, **IEE proceedings**, vol 127 120-130, May 1980

[2] K J Astrom, C Canudas, and K Braun, *Adaptive friction compensation in DC-motor drives*, **IEEE journal of Robotics and Automation**, vol RA-3:681-685, December 1987

[3] K.J Astrom and B Wittenmark, **Adaptive Control**, Newyork Addison-Wesley Publishing Company, 1989

[4] B Bavarian, B F Wyman and H Hemami, *Control of the contrained planar simple Inverted Pendulum*, **Int. Jl. of Control**, vol 37:741-753, April 1983

[5] J.J Bongarino and D C Youla, *On Observers in multi-variable Control Systems*, **Int. Jl. of Control**, vol 8:221-243, September 1968

[6] G.K Dubey, **Power Semiconductor Controlled Drives**, New-Jersey : Prentice-Hall inc , 1989

[7] R.H. Cannon, Jr , **Dynamics of Physical Systems**, Newyork McGraw-Hill Book Company, 1967

[8] S.B. Dewan and A. Morbid, *Microprocessor based Optimum Control of Four-Quadrant Chopper*, **IEEE Trans. on Industry Applications**, vol. IA-17.34-40, Jan /Feb. 1981

[9] O.I. Elgerd, **control Systems Theory**, Newyork : McGraw-Hill Book Company, 1967.

[10] T.E. Fortmann and K.L. Hitz, **An introduction to Linear Control Systems**, Newyork : Marcel Dekker inc., 1977.

[11] B. Friedland, **Control System Design : An introduction to state-space methods**, Newyork . McGraw-Hill Book Company, 1987.

[12] K. Furuta and H Kajiwara, *Digital control of Double Inverted Pendulum on an inclined rail*, **Int. Jl. of Control**, vol 32:907-924, November 1980

[13] A Ghosh, **Lecture notes on Digital Control**, I.I.T Kanpur, 1988

[14] J.W Gilbart and G C. Winston, *Adaptive compensation for an optical tracking telescope*, **Automatica**, vol 10:125-131, March 1974.

[15] C.L. Golliday and H Hemami, *An approach to analyzing Biped Locomotion Dynamics and designing Robot Locomotion Controls*, **IEEE Trans. on Automatic Control**, vol AC-22:963-972, December 1977

[16] B Gopinath, *On the Control of Linear Multiple-Input Output Systems*, **Bell System Tech. Journal**, vol. 50:1063-1081, March 1971.

[17] F. Gubina, H. Hemami and R B. McGhee, *On the Dynamic Stability of Biped Locomotion*, **IEEE Trans. on Biomedic[illegible]ing**, vol BME-21:102-108, - 1974.

[18] K H Gurubasavaraj, *Implementation of a Self-Tuning Controller using Digital Signal Processor chips*, **IEEE Control Systems Magazine**, vol 9:38-42, June 1989

[19] H Hemami, F C Weimer, and S H.Koozekanani, *Some aspects of the Inverted Pendulum problem for modeling of Locomotion Systems*, **IEEE Trans. on Automatic Control**, vol AC-18:658-661, December 1973

[20] H Hemami and C L. Golliday, Jr, *The Inverted Pendulum and Biped Stability*, **Mathematical Biosciences**, vol 34 95-110, - 1977.

[21] H Hemami and A Katbab, *Constrained Inverted Pendulum model for evaluating upright Postural Stability*, **Trans. ASME, Jl. Dynamic Systems, Measurement, and Control**, vol.104 343-349, December 1982

[22] B C Kuo, **Digital Control Systems**, Tokyo · Holt-Saunders Japan Ltd, 1980

[23] R B McGhee, *Some finite State aspects of Legged locomotion*, **Mathematical Biosciences**, vol 2:67-84, February 1968

[24] R.B McGhee, *Computer Simulation of human movements* in A Morecki (ed), **Biomechanics of Motion**, Newyork Spriner-Verlag, 1980.

[25] S. Mori, H Nishihara and K Furuta, *Control of Unstable Mechanical System : Control of Pendulum*, **Int. Jl. of Control**, vol.23:673-692, May 1976

[26] R.V. Patel and N. Monro, **Multivariable System Theory and Design**, Oxford · Pergamon press, 1982

[27] M.H Raibert, **Legged Robots that Balance**, Massachussets · MIT Press, 1986

[28] W.W. Seifert and C.W Steeg, Jr., *Models*, in W.W Seifert and C.W. Steeg, Jr.,(eds.) **Control Systems Engineering**, Newyork : McGraw-Hill Book Company, 1960

[29] J. Tal, *Design Analysis of Pulse Width Modulated amplifier for DC-Servo Systems*, **IEEE Trans. on Ind. Electronics, Control and Instrumentation**, vol IECI-23:47-55, Febrauary 1976

[30] M. Vukobratovic and D Juricic, *Contribution to the synthesis of Biped Gait*, **IEEE Trans. on Biomedical Engineering**, vol BME-16:1-6, January 1969

[31] M. Vukobratovic, A A Frank and D. Juricic, *On the Stability of Biped Locomotion*, **IEEE Trans. on Biomedical Engineering**, vol. BME-17:25-36, January 1970.

[32] M. Vukobratovic and J. Stepanenko, *Mathematical models of General Anthromorphic Systems*, **Mathematical Biosciences**, vol.17:191-242, - 1973.

[33] C.D. Walrath, *Adaptive gearing friction compensation based on recent knowledge of dynamic friction*, **Automatica**, vol 20:717-727, November 1984.